NUCLEAR LAMINA PROTEINS IN PLANTS AND THEIR INVOLVEMENT IN PATHOGEN RESPONSE AND DEVELOPMENT

A Dissertation
Presented to the Faculty of the Graduate School
of Cornell University
in Partial Fulfillment of the Requirements for the Degree of
Doctor of Philosophy

by
Junsik Choi
August 2019

NUCLEAR LAMINA PROTEINS IN PLANTS AND THEIR INVOLVEMENT IN PATHOGEN RESPONSE AND DEVELOPMENT

Junsik Choi, Ph.D.

Cornell University 2019

The nuclear lamina is a reticular network of filaments that lie under the inner nuclear membrane in eukaryotic cells. I investigated the roles of the nuclear lamina in plant cells, which were previously implicated in control of nuclear morphology and genome organization. CROWDED NUCLEIs (CRWNs) are *Arabidopsis thaliana* homologs of plant nuclear lamina proteins NUCLEAR MATRIX CONSTITUENT PROTEINs (NMCPs). In this dissertation, I demonstrated that loss of CRWNs induces a wide range of gene expression changes and the spontaneous induction of immunity responses. At least two double mutants, *crwn1 crwn2* and *crwn1 crwn4*, exhibit salicylic acid mediated (SA) defense responses and cell death lesion formation. I further discovered that short-day conditions can partially suppress dwarfism and cell death in *crwn1 crwn2* mutants. I found that long-day conditions are necessary to produce reactive oxygen species (ROS), which contributes to cell death and dwarfism in *crwn1 crwn2* mutants, indicating that CRWNs are necessary to regulate light-mediated ROS generation and cell death. Finally, I examined roles of NMCPs/CRWNs in *Solanum lycopersicum* cv. M82 to check if functional similarities of NMCPs/CRWNs are present among different species. The Richards group found that *nmcp2* single mutants and *nmcp1a nmcp1b* double mutants are not recoverable, demonstrating that *NMCPs* are indispensable for viability of plants. In addition, pollen abortion was found in *NMCP1A/nmcp1a-1*; *nmcp1b-1/nmcp1b-1* mutants, which raised the possibility of NMCPs roles in male fertility. Collectively, these studies shed light on the role of plant nuclear lamina in pathogen response and development.

BIOGRAPHICAL SKETCH

Junsik Choi was born in Seoul, the Republic of Korea in June 1985. He went to Baemyeong High School from March 2001 to February 2004. Afterward, he began studying Applied Life Chemistry at Seoul National University from March 2005, receiving a Bachelor of Science in Agriculture and Life Sciences in February 2009. From March 2009, he served the Republic of Korea Army, stationed in 8th Chemical Company in 8th Corps. He finished the service with a final rank of first lieutenant in June 2011. He came to the U.S. in August 2014 with the support of a Korean Government Fellowship and began studying Arabidopsis nuclear lamina protein CRWNs under the supervision of Dr. Eric J. Richards.

ACKNOWLEDGMENTS

I am deeply obliged to Eric who is not only a great scientist but also a patient teacher and the warmest mentor. It is one of my luckiest event in my life to meet Eric. I also appreciate Wojtek Pawlowski, Jian Hua and Dan Klessig for their participations in my committee and giving me important comments on my research. I want to give my special thanks to Karl Niklas who was my boss for two times of TA classes, which bestowed me an insight into botany and plant evolution. Affable and unrestrained conversations with faculties across School of Integrative Plant Science formulated vital idea. And it was culturally eye-opening experience, which taught me the importance of collaboration and communication in academia.

I cannot be grateful enough to BTI, for providing great environment for my research. Without Suzy, Mamta and Navid, it would be difficult to finish key experiments. Thanks to Brian, Jay, Brittany, Gary, Don and Doug for their works which significantly helps my research. BTI also supported my summer stipend, which was the critical part of my grad life.

In my first year in Cornell, rotating Klaas van Wijk and Jiping Liu's labs was precious experience in that I can search for my interest in various labs. I also appreciate Elden Rowland and Jianyong Li for their kind responses in the labs and comments on my life in Ithaca. And special thanks to my neighbor Alan Bitar who helped me live in comfort in Varna. My cohort - Leiyun, Julia and Joe (and Celine, Fleet and Scully) - is absolutely the unforgettable part of my 5 years in Ithaca. And special thanks to Mike Scanlon, who is not only a great mentor in Plant Biology section but also in baseball.

Finally, my motherland, my family, my Korean mentors and friends were the crucial part of my life in Ithaca, which spurred my research whenever it is stalled. I also appreciate the U.S. and wish the alliance between two countries remain firm.

TABLE OF CONTENTS

Chapter 1. Introduction

Structure of nuclei

The nucleus is the key organelle that defines eukaryotic organisms and one that plays multiple roles. First, nuclei compartmentalize the genome and define the partitioning of the cell into the nucleoplasm and cytoplasm. Transport across this partition is highly regulated through complex structures called nuclear pores. Within the nucleus, more highly ordered processes occur that control proper gene expression, RNA processing and maturation, and proteolysis.

Changes in nuclear size and shape can provide clues to a cell's biological status, specialization, or pathology. For example, normal human neutrophils have lobulated, ring-shaped nuclei that are deformable and allow these immune function cells to move between cells to attack invaders (Hoffmann et al., 2007). In contrast, most human cells have somewhat rigid ovoid nuclei that would resist compression (Davidson and Lammerding, 2014; Kirby and Lammerding, 2018). In cancer cells, changes in nuclear morphology are often correlated to cancer cell function (Dey, 2010). One study suggests that analyzing morphological features of nuclei can make a better prognosis of breast cancer compared to conventional methods (Wolberg et al., 1999). Given the fact that nuclei are places for genome storage, nuclear morphology also reflects genomic status, such as endoreduplication. For example, guard cells in *Arabidopsis thaliana* have 2C nuclei, which exhibit only round nuclei, while highly endopolyploid cells in this species have elongated, non-spherical nuclei (Poulet et al., 2017; Hu et al., 2019). The ploidy level of nuclei is also correlated with the size of nuclei (Jovtchev et al., 2006; Robinson et al., 2018). However, many features of nuclear morphology and dynamics still remain mysteries. For instance, potato cell (*Solanum tuberosum* L. cv. Datura) nuclei move to the invasion site of the fungal pathogen *Phytophthora infestans* (Freytag et al., 1994; Schmelzer, 2002; Griffis et al., 2014) and similar coordinated nuclear movement is observed during fungal-plant symbiont interactions (Skalamera and Heath, 1998; Genre et al., 2005). It

is still elusive how this movement is achieved, but mechanical stimulation of the cell by the fungus appears to be involved (Genre et al., 2009; Jayaraman et al., 2014). These examples of mechanosensing demonstrate how the nucleus is integrated, as an organelle, into cellular responses (Fal et al., 2017).

The nuclear envelope consists of two lipid bilayer membranes, where the outer and inner membranes make a doublet configuration. In addition to the double membrane structure, nuclei have long been thought to possess another structure called the nucleoskeleton. Unlike the cytoskeleton, however, the existence of nucleoskeleton was not fully confirmed, and remained as a hypothesis until the 1970s (Simon and Wilson, 2011; Adam, 2017). A tangible form of nucleoskeleton was first isolated from rat liver nuclei after DNase, RNase and salt treatment and named as the 'nuclear matrix' (Berezney and Coffey, 1977). Researchers also found that proteinases such as trypsin destabilized the spherical shape of the nuclear matrix, suggesting that the structure consists of protein (Berezney and Coffey, 1977). However, the nuclear matrix preparation consists of various proteins and efforts to further characterize constituent proteins led to the discovery of a more defined structure called the nuclear lamina, which is composed of lamin intermediate filament proteins (Gerace et al., 1978; Aebi et al., 1986; Simon and Wilson, 2011). This reticular structure resides under the inner nuclear membrane and interacts with the genome. Thus, the lamina is an important subject for both nuclear structure and the regulation of genomic configurations. In this chapter, I will begin by considering the structure and function of the nuclear lamina in metazoan cells, as they are much better understood compared to their counterparts in fungi and plants. With the animal studies as a context, I will then provide an overview of what is known about the nuclear organization in plants and the plant version of the nuclear lamina. In addition, background information on plant immunity is included at the end of this introductory chapter to lay a foundation for my studies described in Chapter 2 linking the plant nuclear lamina and pathogen defense response.

Lamin proteins and nuclear lamina

Lamins are type V intermediate filament proteins. They are composed of three distinct domains - head, rod and tail. The rod domains contain α-helical coiled-coil domains, which are responsible for homodimerization. Rod domains retain the most highly conserved amino acid sequences shared among different lamins (Stuurman et al., 1998). The tail domains contain a CaaX motif, which is the target site of protein prenylation (reviewed below). Nuclear lamina formation from lamin monomers starts by homodimerization of two individual lamins (Aebi et al., 1986; Ben-Harush et al., 2009). These homodimers in turn interact to each other in head-to-tail manner, making tetrameric units that form long filaments of 3.5 nm thickness. (Heitlinger et al., 1991; Turgay et al., 2016). These filaments interact to each other to form lattice-like structures (Burke and Stewart, 2013). Electron microscopy images of the nuclear lamina in *Xenopus* oocytes show a dense meshwork, into which nuclear pore complexes are incorporated (Aebi et al., 1986).

Lamins are divided into two groups - A-type and B-type. In mammals, A-type lamins include lamin A, lamin C, lamin C2 and lamin AΔ10, all of which are encoded by the single *LMNA* gene through alternative splicing (Andres and Gonzalez, 2009). B-type lamins in humans include lamin B1, lamin B2 and lamin B3. Lamin B1 and Lamin B2 are encoded by *LMNB1* and *LMNB2,* respectively. Lamin B3 is the result of alternative splicing of the *LMNB2* transcript. The expression patterns of specific lamins is also different from each other. While lamin A, lamin C, lamin B1 and lamin B2 are expressed in somatic cells, lamin C2 and lamin B3 are found in testis (Burke and Stewart, 2013).

Linker of nucleoskeleton and cytoskeleton complex (LINC)

Unlike typical diagrams featuring eukaryotic cells in text books, nuclei are not free-floating balls in the cytoplasm. Instead, nuclei are tethered to the cytoskeleton by protein

complexes called LINC (LInker of Nucleoskeleton and Cytoskeleton) in metazoan cells (Crisp et al., 2006). The LINC complex is composed of KASH (Klarsicht, ANC-1 and SYNE Homology) domain-containing proteins and SUN (Sad1 and UNC-84) domain-containing proteins (Simon and Wilson, 2011). The KASH domain-containing proteins SYNE1-4 encode nesprins (nuclear envelope spectrin repeat proteins) 1–4 (Simon and Wilson, 2011). The spectrin-repeat serves as interacting sites with other proteins (Parry et al., 1992; Yan et al., 1993). In addition, the spectrin-repeat family proteins often have N-terminal calponin homology domains, which bind filamentous actins (Rajgor and Shanahan, 2013). These proteins often include other motifs which allow them to interact with other cytoskeleton structures, thereby allowing interconnections among different cytoskeletal elements (Rajgor and Shanahan, 2013). Nesprins are primarily known for this role - bridging among nuclear envelope, cytoskeleton and nuclear lamina. Although KASH domain proteins are known to interact with the cytoskeleton, not all nesprins are localized to the ONM (Tzur et al., 2006; Mejat, 2010; Simon and Wilson, 2011). The nesprin genes are transcribed into various splice variant isoforms that encode different size of proteins (Mejat, 2010; Morris and Randles, 2010). One hypothesis is that 'nesprin giant' proteins interact with the outer nuclear membrane while the smallest nesprins localize to the inner nuclear membrane (Morris and Randles, 2010). There are five human SUN-domain containing proteins, SUN1, SUN2, SUN3, SPAG4 and SUN5 (Tzur et al., 2006; Meinke and Schirmer, 2015). SUN domain proteins are localized to the INM (Meinke and Schirmer, 2015). SUN1 is known to interact with lamins, and preferentially with prelamin A (Crisp et al., 2006). Thus, the LINC complex makes a continuous network throughout the cell by interconnecting the cytoskeleton and nuclear lamina. This connectivity enables the integration of mechanical signals throughout the cell. One example is mechanotransduction mediated by the LINC complex. When forces are exerted on nesprin-1 proteins in isolated nuclei, nuclei become stiff to resist the tension and induces the recruitment of lamin A/C (Guilluy et al., 2014).

SUN1 and SUN2 proteins are involved in other mechanical stimulus phenomena, such as the low-magnitude mechanical signal pathway which suppresses adipocyte formation (Uzer et al., 2015).

Human laminopathies

The nuclear lamina in human cells has become the target of intense interest because severe and sometimes lethal diseases, known as laminopathies, are caused by polymorphisms in lamin genes. It has been reported that mutations in the *LMNA* gene alone can cause more than 10 clinically distinctive syndromes (Worman and Bonne, 2007). Laminopathies are not only clinically important but also critical to understand the aging process because symptoms of several laminopathies are characterized by extremely accelerated aging known as progeroid syndromes. Hutchinson-Gilford progeria syndrome (HGPS) (Hutchinson, 1886; Gilford, 1904; Goldman et al., 2004) is the most prominent progeroid syndrome that is caused by mutations in the *LMNA* gene. Lamin A, which is encoded from *LMNA*, has a C-terminal CaaX motif. The CaaX motif comprises four amino acids - cysteine (C), two aliphatic residues (aa) and one of any amino acid (X). This motif is the target of protein prenylation (addition of hydrophobic prenyl groups). One of the prenylation modifications is called farnesylation where 15 carbons are added to a cysteine residue (Gao et al., 2009). After the addition of farnesyl groups, the CaaX motif undergoes proteolysis and carboxyl methylation. This series of post-translational processing steps are followed by further proteolytic cleavage steps where 18 residues in the C-terminus, including farnesylated cysteine residue, are removed (Weber et al., 1989; Gonzalo et al., 2017). In HGPS cells, however, *LMNA* mutations hinder these post-translational modifications. Although multiple HGPS alleles are known, the mutation on nucleotide at position 1824, C → T (G608G) is the most frequent. This mutation creates a cryptic splice site on exon 11 and encodes abnormal proteins lacking 50 amino acids near the C terminus. The

mutant protein is called as 'progerin' and it does not lose the CaaX motif because the deleted region contains the cleavage site for the endoprotease Zmpste24. As a result, prenylated progerin accumulates within the INM, leading to changes in nuclear morphology and organization.

From gestational period to delivery, HGPS patients generally do not exhibit disease symptoms although fetuses are typically slightly smaller and newborn babies with HGPS often have visible veins across their nasal bridges (Hennekam, 2006). Nonetheless, patients at this early stage usually appear to be healthy. By the time that patients reach 1 year old, however, developmental failure is usually apparent, including loss of hair and loss of subcutaneous fat tissue (Hennekam, 2006). At age around 2 to 3 years old, infant HGPS patients start to exhibit facial characteristics including loss of hair, wide veins over the scalp, prominent eyes, narrow nasal bridges and many more (Hennekam, 2006). In general, these infant patients look very old and their physical development, including height growth and weight increase, are greatly hindered. Life expectancy of HGPS patients is usually around 13 years (Hennekam, 2006). The mechanisms through which changes in the nuclear lamina lead to such severe clinical manifestations is not well understood, but in the next section I will consider some of the leading hypotheses for how nuclear organization changes cause disease and alter phenotypes on both a cellular and whole-organism level.

Mechanisms for nuclear periphery nuclear lamina action

Defective nuclear lamina could mediate phenotypes through a variety of mechanisms, which are not mutually exclusive. The first mechanism invokes the role of the nuclear periphery on gene expression. Studies in metazoan cells found that heterochromatin tends to be found at the nuclear periphery (Francastel et al., 2000; Akhtar and Gasser, 2007; Egecioglu and Brickner, 2011). In addition, many genes at the nuclear periphery can be silenced; for instance, the

immunoglobulin heavy (IgH) and kappa (Igκ) genes are located at the nuclear periphery presumably through interaction with the nuclear lamina, but move into the nuclear interior upon transcription (Kosak et al., 2002). This finding suggests that the nuclear periphery might be the repressive environment of gene expression or be depleted in active transcriptional machinery and that the nuclear lamina plays important roles. Since the lamina resides inside of the inner nuclear membrane, the structure is used as a target for gene positioning studies. Tethering genes to the inner nuclear membrane represses gene expression in both fungal and mammalian nuclei (Akhtar and Gasser, 2007). However, studies also revealed that nuclear periphery is neither always repressive nor irreversible for gene expression. For example, ChIP-on-chip (chromatin immunoprecipitation on microarray 'chip') experiments against nuclear pore proteins showed that many active genes are indeed positioned at the nuclear periphery interacting with the nuclear pore complex (Casolari et al., 2004; Casolari et al., 2005; Akhtar and Gasser, 2007). Thus, nuclear pores might play important roles in controlling gene expression of genes dynamically partitioned close to the inner nuclear membrane (Egecioglu and Brickner, 2011). These results suggest that nuclear subdomains close to nuclear pore complexes are enriched in transcriptional and RNA processing machinery, where access to nuclear export pathways are available. These studies show that nuclear periphery is likely to be a complex genomic environment with different properties with respect to gene expression.

The nuclear lamina and the nuclear periphery can regulate gene expression by several mechanisms. First, the nuclear lamina binds and sequesters transcription factors. One example from animal cells is Oct-1 (octamer transcription factor 1) that binds to Lamin B1 (Guelen et al., 2008; Malhas et al., 2009). Loss of Lamin B1 can alter expression of genes in the oxidative stress response pathway when Oct-1 sequesteration by the lamin at the nuclear periphery is lost (Malhas et al., 2009). Second, laminopathies and nuclear lamina changes can affect epigenetic marks that regulate gene expression. As mentioned above, nuclear periphery is generally

considered as repressive environment for gene expression. In HGPS, the constitutive heterochromatin mark trimethylation at lysine 9 of histone H3 (H3K9me3) is downregulated, which leads to transcription of the pericentric satellite III repeat, whereas another constitutive heterochromatin mark, H4K20me3 (trimethylation at lysine 20 of histone H3) is increased (Shumaker et al., 2006; Arancio et al., 2014). H3K27me3 (trimethylation at lysine 27 of histone H3), a facultative heterochromatin mark is downregulated as well in HGPS (Shumaker et al., 2006). A third mechanism of nuclear lamina control of gene expression involves higher-order organization of the genome. Metazoan cell nuclei have lamin-associated domains (LAD) or regions of the genome that are in physical contact with the nuclear lamina (van Steensel and Belmont, 2017). LADs appear to be critical for both three-dimensional genome organization and epigenetic regulation of large domains of repressed chromatin (van Steensel and Belmont, 2017). These two features support each other because LADs mainly consist of heterochromatin, exhibit low gene density and are enriched for the repressive chromatin marks histone H3 di- and tri-methylation at lysine 9 (H3K9me2 and H3K9me3) (van Steensel and Belmont, 2017). Although there are studies showing that loss of lamins does not necessarily disrupt LADs and/or gene expression (Kim et al., 2011; Amendola and van Steensel, 2015), many studies support that the disruption of lamina leads to upregulation of transcription (van Steensel and Belmont, 2017; Zheng et al., 2018). An example is the case of *Drosophila melanogaster* fat bodies, where immune related genes enriched in LAD are derepressed upon age-related reduction of lamins (Chen et al., 2014).

Defects in the nuclear lamina can exert effects on cell- and organism-level phenotypes through mechanisms that do not involve primary changes in gene expression. One well understood mechanism involves the generation of reactive oxygen species (ROS). It is documented that cells from laminopathy patients accumulate ROS (Sieprath et al., 2012). In fact, both ROS levels and sensitivity to ROS were increased in several laminopathies, including

HGPS (Viteri et al., 2010). The farnesylated prelamin A is thought to trigger increased ROS levels because inhibition of farnesylation of prelamin A prevented oxidative stress (Caron et al., 2007). The confusing relationship between ROS and lamin arises from the fact that lamina structure is also affected by oxidative stress and the resulting defects, in turn, are thought to induce aging (Pekovic et al., 2011). This 'chicken or the egg' conundrum is still unresolved, leaving open the question of whether mutations in lamins make excess oxidative damages or mutated lamins are vulnerable to basal oxidative stress. There are several hypotheses to explain the situation (Sieprath et al., 2012). The first hypothesis posits that aberrant nuclear lamina disorganizes chromatin and in turn mis-regulates gene expression. For example, lamin B1 regulates Oct-1, the loss of which elevates ROS level. Mutations on lamin B1 also recapitulates the elevated ROS symptoms, suggesting that lamin B1 can affect ROS level via Oct-1 (Malhas et al., 2009). The second hypothesis suggests that 'nuclear shielding' might be affected by laminopathies (Fabrini et al., 2010). In this hypothesis, the nuclear shield, a population of protective enzymes including ROS diffusing enzymes near the perinuclear region, is perturbed by laminopathy. Thus, disruptions in lamina can reduce antioxidant machinery and hence increased oxidative damage. The final hypothesis holds that laminopathies cause a breakdown in cellular compartmentalization between the nucleoplasm and cytoplasm. In this case, evidence was provided by a study where mitochondria, sites of massive ROS production, are found in nuclei of laminopathy cells (De Vos et al., 2011).

The plant nuclear lamina

Efforts to find a nuclear matrix or nuclear lamina in plants started in 1980s and 1990s (Moreno Diaz de la Espina, 1995). Several early reports utilized antibodies against animal proteins to detect putative plant lamins and intermediate filament proteins. One representative study published in 1992 used antibodies recognizing animal lamins against extracts from pea

(*Pisum sativum* cv. milk and honey) to precipitate several proteins (Mcnulty and Saunders, 1992). Another work published in the same year used antibodies for intermediate filament proteins and found antigens of size 60 and 65 kDa in carrot (*Daucus carota*), broad bean (*Vicia faba*) and pea, bolstering the possibility of the presence of lamin-like proteins in plants (Frederick et al., 1992). Similar results were also reported in onion (*Allium cepa*) (Minguez and Delaespina, 1993). Whether these antigens are true intermediate filaments or lamins has never been resolved, but the lack of genes encoding proteins related to lamins in subsequently characterized plant genomes suggests that these cross-reacting proteins are artifactual. Nonetheless, the existence of plant nuclear matrices has been demonstrated by several groups, and proteomics study of isolated nuclear matrix preparations showed a composition comparable to that of their animal counterpart (Calikowski et al., 2003; Pendle et al., 2005). Another key study showing that plants might have a true nuclear lamina came from cytological studies in *Nicotiana tabacum* (tobacco) BY-2 cells (Fiserova et al., 2009). This study revealed that an organized filamentous layer is present under the inner nuclear membrane, raising strong physical evidence of plant nuclear lamina.

A key advance in the study of the plant nuclear lamina grew from characterization of nuclear matrix fractions in carrot conducted by Masuda's group. As reported in 1997, they identified a monoclonal antibody that detected the protein Nuclear Matrix Constituent Protein1 (NMCP1), which localizes to nuclear periphery and has alpha-helices, similar to filament-forming proteins (Masuda et al., 1993; Masuda et al., 1997). The same group subsequently discovered a closely related protein, which they named NMCP2 (Kimura et al., 2010). These two proteins define two phylogenetically distinct clades present in land plants. These two subclasses of NMCP proteins are both present at nuclear periphery during interphase, but a study in *Apium graveolens* (celery) and onion, showed that NMCP1 and NMCP2 show different

localization patterns during metaphase and anaphase in mitotic cell divisions (Kimura et al., 2010; Ciska et al., 2018).

Proper nuclear morphology and organization requires NMCPs

Defining the roles of these phylogenetically distinct NMCP proteins has relied on functional studies in Arabidopsis. The Arabidopsis genome encodes four NMCP homologs, which were originally named as LITTLE NUCLEI (LINC) proteins (Dittmer et al., 2007) and then later renamed as CROWDED NUCLEI (CRWN) to avoid confusion with components of the LINC complex (Wang et al., 2013). CRWN1, CRWN2 and CRWN3 have coiled-coil domains and the highly conserved C-terminal motif shared with NMCP1 (Dittmer et al., 2007) (Fig. 1.1). In constrast, CRWN4 is NMCP2-type protein that lacks this C-terminal motif. Not all CRWNs are targeted to the nuclear periphery (Fig. 1.1). Expression of fluorescent proteins tagged versions of CRWNs under *35S* promoters showed that while CRWN1 and CRWN4 localize to the nuclear rim, and that CRWN2 and CRWN3 are distributed throughout the nucleoplasm (Sakamoto and Takagi, 2013). Furthermore, CRWN3 and CRWN4 forms punctuate structures within the nucleus in these over-expression lines (Dittmer et al., 2007; Sakamoto and Takagi, 2013). CRWN1 and CRWN4 remain insoluble after high salt extraction of nuclear preparation (unpublished work from Haiyi Wang). Further, CRWN3 is found in Arabidopsis nucleolar proteome (Pendle et al., 2005). These biochemical fractionation studies combined with subcellular localization indicate that CRWN proteins are part of the plant nucleoskeleton and that CRWN1 and CRWN4 are good candidates for components of the plant nuclear lamina.

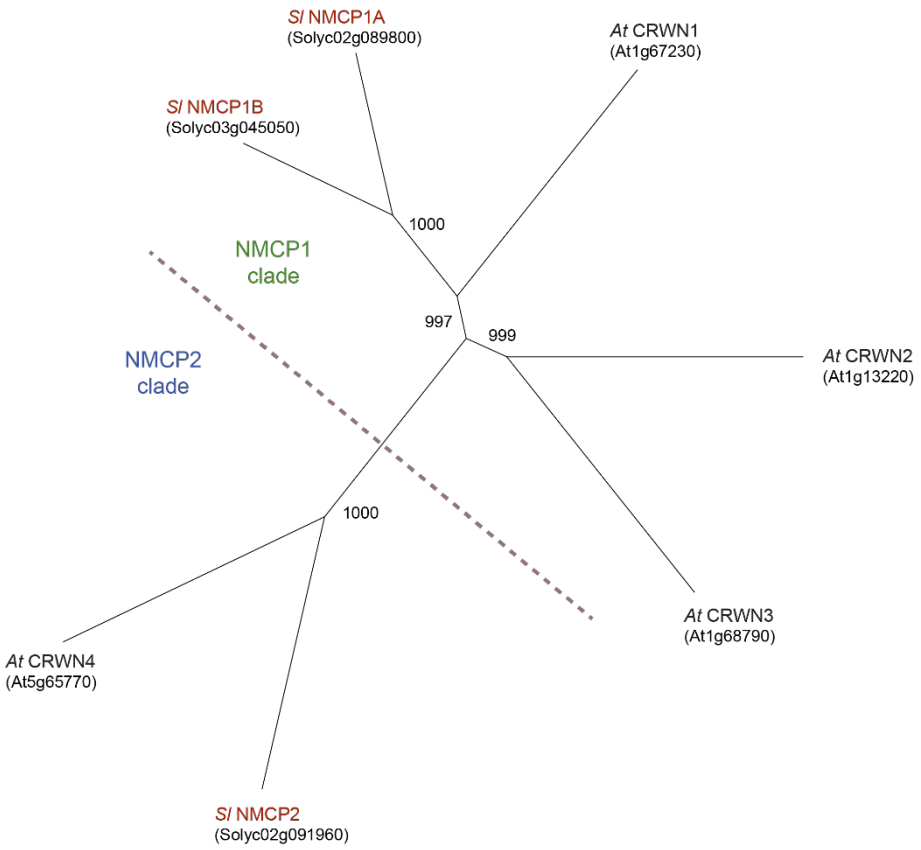

Figure 1.1 Phylogenetic tree of *NMCP*/*CRWN* genes. Alignments of tomato NMCP and Arabidopsis CRWN protein sequences were performed using the ClustalX (version 2.1). The alignments were limited to the coiled-coil regions. A distance phylogenetic tree (phylogram) was generated from the .phb output file from ClustalX. Bootstrap values (out of 1000) are shown.

Phenotypic analysis of Arabidopsis *crwn* mutants demonstrates the importance of these proteins in specification and/or maintenance of nuclear structure. Most notably, nuclei in *crwn1* and *crwn4* mutants are reduced in size and fail to elongate but remain spherical in enlarged endopolyploid cells (Dittmer et al., 2007; Sakamoto and Takagi, 2013; Wang et al., 2013). In contrast, *crwn2* and *crwn3* mutant nuclei are similar in size and shape when compared to wild-type nuclei (Sakamoto and Takagi, 2013; Wang et al., 2013). This lack of an effect in *crwn2* and *crwn3* single mutants might reflect the fact that these proteins, which are localized throughout the nucleoplasm, are not part of the nuclear lamina. However, these mutations when combined with *crwn1*, but not *crwn4*, lead to a further reduction in nuclear size (Dittmer et al.,

2007; Wang et al., 2013). These synthetic genetic interactions argue that CRWN2 and CRWN3 are functionally redundant with their NMCP1-type paralog, CRWN1. Combining *crwn1* and *crwn4* mutation also lead to more severe nuclear phenotypes, and triple mutants (only two of the possible four are viable & the quadruple mutant is inviable) exhibit even smaller nuclei (Wang et al., 2013). These results using loss-of-function mutations are corroborated by overexpression studies; when CRWN4-GFP is overexpressed, nuclei in pavement cells become enlarged and further elongated (Sakamoto and Takagi, 2013). Taken together, these findings demonstrate that NMCP proteins are important to specify or maintain proper nuclear size and shape. The phenotypes of these plant nucleoskeletal mutants parallel the effects of lamin defects that alter nuclear morphology in animals, although it must be emphasized that lamin mutants show irregular nuclear shapes while plant *nmcp* mutants contain more regularly shaped, spherical nuclei. These differences are likely a reflection of the differences in the wild type state of nuclei in these two kingdom; plant nuclei remodel their shape dynamically in wild-type cells whereas animal nuclei in most cell types show some rigidity and resist deformation (Kirby and Lammerding, 2018).

Other nuclear morphology mutants in plants

In addition to *crwn* mutants, there are other nuclear morphology mutants in Arabidopsis. Like metazoan cells, Arabidopsis cells have SUN-domain and KASH-domain proteins (Meier et al., 2016). Arabidopsis has two C-terminal SUN domain proteins, SUN1 and SUN2, and three mid-SUN domain proteins, SUN3, SUN4 and SUN5 (Meier et al., 2016). There are four KASH domain proteins: WIP1, WIP2, WIP3 and AtTIK (Meier et al., 2016). In addition, a family of proteins including WIT1 and WIT2 are in the outer nuclear membrane (Meier et al., 2016). Collectively, SUN-WIP-WIT forms Arabidopsis LINC complex (Meier et al., 2016). Mutations in LINC complex proteins can affect nuclear morphology. *sun1* null mutants exhibit round

nuclei in trichomes and root hair cells, whereas *sun2* mutants show elongated nuclei similar to wild type in the same cell types (Zhou et al., 2015). *sun3* mutants have spherical nuclei in root epidermal cells (Graumann et al., 2014). Neither *sun4* nor *sun5* single mutants have distinct nuclear phenotypes but combination of the two mutations gives smaller nuclei (Graumann et al., 2014). Among KASH-domain proteins, Arabidopsis *tik* mutants display smaller nuclei (Graumann et al., 2014). *wip1 wip2 wip3* mutants exhibit round nuclei in trichome and root hair cells in which *wit1* and *wit1 wit2* also have spherical nuclei (Zhou et al., 2015).

In addition to LINC complex members, there are also other proteins affecting nuclear morphology, including the Myosin XI family protein MyoXI-I (KAKU1), nucleoporin CPR5, another nucleoporin NUP1/NUP136 (Nucleoporin1/Nucleoporin136), KAKU4, and PWO1 (Pro-Trp-Trp-Pro INTERACTOR OF POLYCOMBS1). Of the 13 Arabidopsis Myosin XIs, only *myoxi-i* mutants exhibit round nuclei (Tamura et al., 2013). GFP-tagged MyoXi-i without its motor domain localizes to nuclear membrane, showing that MyoXi-i can anchor to the nuclear envelope (Tamura et al., 2013). NUP1/NUP136 is a plant-specific nucleoporin, loss of which leads to round nuclei in leaf epidermal cells (Lu et al., 2010; Tamura et al., 2010). *cpr5* mutants, known for their spontaneous immunity phenotypes, have small and round nuclei (Gu et al., 2016). KAKU4 is a putative nuclear lamina protein that interacts with CRWN1, and loss of KAKU4 leads to smaller, rounder nuclei. Similarly, PWO1 interacts with CRWN1, as well as PRC2 (Polycomb Repressive Complex 2); and *pwo1* mutants exhibit small and round nuclei (Mikulski et al., 2019). These results demonstrate that many different types of perturbations can result in rounder or smaller nuclei in Arabidopsis, suggesting that nuclear morphology is tied to multiple processes, not simply defects in the nucleoskeleton.

Plant nuclear structure and epigenetics

As reviewed above, the nuclear lamina in metazoan cells interacts specifically with the genome and altered gene expression results from disruption of the animal nuclear lamina, prompting research into whether or not plant nuclear lamina proteins play similar roles in the epigenetic regulation of gene transcription. Investigation of nuclear organization provided some hints about the possible role of CRWNs in epigenetic regulation. The Richards group found that the number of chromocenters is significantly reduced in *crwn1 crwn2* mutants (Dittmer et al., 2007; Wang et al., 2013). Poulet et al. subsequently showed that these chromocenters in *crwn1 crwn2* mutants have increased volume and also exhibit more condensed chromocenters (Poulet et al., 2017). In addition, *crwn1 crwn2* mutants tend to have fewer decondensed 180 bp centromeric repeats (Wang et al., 2013; Poulet et al., 2017), although transcription of 180 bp centromeric repeats in *crwn1 crwn2* mutants is not significantly altered (Poulet et al., 2017). Chromocenters are also affected in *crwn4* mutants but, in this case, the heterochromatin aggregates are more dispersed (Wang et al., 2013). These finding suggest that CRWN proteins have complex and potential antagonistic effects on higher-order chromatin organization.

Recent evidence provides more molecular details to explain how the nuclear lamina affects genomic organization in plants. Hu et al. showed that tethering of chromatin to the nuclear periphery is altered in *crwn1* and *crwn4* mutants (Hu et al., 2019). This conclusion derives from their FISH experiments that show that hybridization probes separately localized to the nuclear periphery versus non-nuclear periphery regions are not differentially localized in *crwn1* and *crwn4* mutants (Hu et al., 2019). Similarly, compartmentalization of chromosome 1 in the mutants is also affected in that interactions normally not seen in WT are increased in the mutants, suggesting chromatin organization is less compartmentalized compared to WT (Hu et al., 2019). Previously, Grob et al. also showed that *crwn1* and *crwn4* mutants exhibit increased inter-chromosomal interactions at the expense of intra-chromosomal contacts (Grob et al., 2014), suggesting loss of CRWNs affect both nuclear morphology and genome organization.

In addition, the Hu et al. defined PLADs (plant lamina-associated domains) using ChIP-seq in transgenic plants expressing CRWN1:2HA to define CRWN1-associated chromatin (Hu et al., 2019). PLADs consist of transcriptionally inert regions in which repressive chromatin marks and lowly expressed genes are enriched. Hence, plant LADs resemble LADs in metazoans in being mainly composed of repressive chromatin regions with lowly expressed genes.

Another clue about how the nuclear lamina helps organize epigenetic compartmentalization of the genome comes from the identification of CRWN-interacting proteins. Recently, Mikulski et al. reported that CRWN1 interacts with PWO1, which interacts with PRC2 (Polycomb Repressive Complex 2). This complex methylates histone H3 at lysine 27 (H3K27me3) and therefore connecting the nuclear lamina to the deposition of this repressive chromatin mark (Mikulski et al., 2019). Hohenstatt et al. previously found that PWO1 interacts with histone H3 (Hohenstatt et al., 2018). Hu et al. also showed H3K27me3 is enriched in PLADs (Hu et al., 2019). Collectively, these results indicate that the nuclear lamina in plants might establish a transcriptionally repressive region at the nuclear periphery via H3K27 trimethylation.

Plant nuclear structure and immune response

One important unresolved question is whether or not plant nuclear morphology mutants alter developmental or physiological phenotypes. Several studies have highlighted interesting correlations between plant defense and nuclear morphology mutants. Some of these examples come from the study of nuclear pore complex (NPC) components - nucleoporins. NUP136 was first discovered through proteomics approaches using immunoprecipitation coupled to mass spectrometry (IP-MS) (Tamura et al., 2010) and was one of 30 nucleoporins precipitated via a GFP-tagged RAE1 (RNA export factor 1) nucleoporin. Mutations in *NUP136* cause a reduced

number of rosette leaves, shorter silique size and shrunken pollen grains. Also, Tamura et al. found that *nup136* mutants exhibit small and round nuclei. In 2017, the same group found that NUP136 is not only involved in nuclear morphology but also regulate salicylic acid-dependent defense responses in Arabidopsis (Tamura et al., 2017). Tamura et al. showed that *nup136* mutants express lower levels of Arabidopsis immune-related genes, including *PR1* (*PATHOGENESIS-RELATED 1*), suggesting NUP136 is specifically required for robust immune responses. When combined with mutations in a gene encoing another nucleoporin NUP82 that interacts with NUP136, the resulting *nup136 nup82* mutants showed even more compromised immune gene expression. This trend was also observed when assessing bacterial pathogenesis: *nup136 nup82* mutants exhibit higher levels of *Pseudomonas syringae* pv. *tomato* DC3000 (DC3000) growth compared to wild type, while either single mutant shows intermediate levels of the pathogen growth. Finally, *nup136 nup82* mutants have compromised sensitivity in SA-induced gene expression, showing that these two nucleoporins positively regulate the SA pathway. In 2016, Gu et al. found that *cpr5* mutants have small and round nuclei like *nup136* mutants (Gu et al., 2016). The *cpr5* mutant has long been known for its spontaneous immune responses (Bowling et al., 1997). Gu et al. showed that CPR5 is a nucleoporin, which undergoes conformational changes to release cyclin-dependent kinase inhibitors (CKIs) that can mediate effector triggered immunity (ETI). This event also allows the influx of immune signaling complexes into the nucleoplasm.

In accordance with the above studies, recent publications exploring the role of CRWNs found that *crwn* mutants also exhibit stress-related responses. Guo et al. showed that *crwn* mutants exhibit abnormally enhanced defense response against bacterial pathogens (Guo et al., 2017). They also showed that YFP-tagged CRWN1 protein is degraded upon bacterial pathogen infection and SA treatment, indicating that CRWNs are required to suppress uncontrolled defense responses. In their yeast-two-hybrid assay, CRWN1 interacts with NTL9 (NAC WITH

TRANSMEMBRANE MOTIF1-LIKE 9). The NTL9 is involved in various defense responses and it is known to interact with the SNI1, the HopD1 type III effector and the *ICS1* (*ISOCHORISMATE SYNTHASE 1*) promoter (Kim et al., 2012; Block et al., 2014; Zheng et al., 2015). Guo et al. concluded that binding of NTL9 to *PR1* promoter is enhanced by CRWN1, which prevents *PR1* expression.

Another study regarding CRWNs and whole-plant phenotypes found that *crwn* mutants exhibit hypersensitivity to abscisic acid (ABA) by suppressing the degradation of ABA INSENSITIVE 5 (ABI5) (Zhao et al., 2016). Mutations in *ABI5* make plants insensitive to ABA (Skubacz et al., 2016). Zhao et al. showed that degradation of ABI5 is hindered in *crwn1 crwn3* mutants. This effect makes *crwn1 crwn3* mutants hypersensitive to ABA, leading to low germination rate of *crwn1 crwn3* seeds compared to wild type when exposed to exogenous ABA. These authors also showed that ABI5 co-localizes with CRWN3 in the nucleus, and they hypothesized that CRWN3 is involved in shuttling ABI5 to the proteasome in nuclear bodies. From all of these studies, it becomes more obvious that CRWNs are involved in stress signaling pathways, suggesting that aberrant nuclear structure could trigger plant resistance against both biotic and abiotic stresses.

Salicylic acid, ROS and programmed cell death

Salicylic acid (SA) is a phytohormone best known for its roles in plant defense (Dempsey and Klessig, 2017). Biosynthesis of salicylic acid is thought to be largely regulated by two important enzymes. One is the phenylalanine ammonia lyase (PAL) and the other is isochorismate synthase (ICS). PAL, known to be induced by both biotic and abiotic stresses, regulates the phenylpropanoid pathway where phenylalanine is converted to cinnamate and then to SA (Coquoz et al., 1998). There are two *ICS* genes in Arabidopsis (Wildermuth et al., 2001). A mutation in the *ICS1/SID2* gene leads to 90 - 95% decrease of total SA accumulation after

infection of pathogens in Arabidopsis, suggesting that the isochorismate pathway contributes most to SA biosynthesis (Wildermuth et al., 2001). In accordance with the higher contribution of *ICS1/SID2* in SA biosynthesis, it was also reported that *PAL* family is responsible for low level of SA biosynthesis (Huang et al., 2010; Dempsey and Klessig, 2017).

Reactive oxygen species (ROS) have various roles in cellular signaling and responses. It was first thought that ROS are merely by-products of aerobic respiration. ROS can be classified by their reactivity and chemical structure and all of them are capable of inflicting damage on cellular components, including DNA and protein (Apel and Hirt, 2004). Plants have four main ROS: singlet oxygen, superoxide anion, hydrogen peroxide and hydroxyl radical, the reactivity and lifetime of which are distinct (Waszczak et al., 2018). Among these ROS, hydrogen peroxide (H_2O_2) is relatively moderate in its activity and has a longer lifetime (milli-seconds to seconds) compared to the more highly active and short-lived (nano-second) hydroxyl radical ($^{\bullet}OH$). The superoxide anion ($O_2^{\bullet-}$) has an activity comparable with hydrogen peroxide but has a shorter lifetime (milli-seconds) (Waszczak et al., 2018). Damage on genomic DNA can be induced by hydroxyl radicals, superoxide and nitric oxide (Demple and Harrison, 1994). However, various roles of ROS in plant defense showed that ROS act not only as mere waste but also as signaling molecules (Waszczak et al., 2018). In plants, both photosynthesis and aerobic respiration continuously generate ROS, which are maintained at basal levels in the absence of environmental perturbations (Apel and Hirt, 2004). This steady state could be agitated by outer stimuli, which dramatically increases ROS level, a phenomenon called oxidative burst (Apostol et al., 1989). ROS can directly inhibit pathogens as antimicrobial agents (Shetty et al., 2008). They are also involved in signal transduction, gene expression, cell wall cross-linking and induction of the hypersensitive response (HR) (Shetty et al., 2008).

In plant immunity study, SA, ROS, DNA damage and HR have complicated relationships, where simple induction - inhibition correlation is often hard to be determined

because of dosage dependency and looping/feedback signaling. This situation is further entangled by the existence of chloroplasts, which produce ROS through light-reactions (Waszczak et al., 2018), whereas animal cells have only mitochondria which are main source of ROS.

Like many positive regulating roles of SA in plant defense response, it was first reported that SA can induce H_2O_2 in tobacco leaves (Chen et al., 1993). However, it was unclear whether SA acts upstream or downstream of H_2O_2 induction to express *PR1* gene (Neuenschwander et al., 1995; Chamnongpol et al., 1996). After many years, the interplay of SA and ROS are understood as a non-hierarchical model where SA can act both upstream and downstream of ROS (Herrera-Vasquez et al., 2015). It has also been shown that SA can act in anti-oxidant signaling, counterintuitive to the initial observation where SA induces ROS signaling. Despite this complication, the interplay between SA and ROS tells us that both agents regulate many overlapping pathways.

One of the important plant immune processes regulated by both SA and ROS is HR. HR is defined as a mechanism used in plants to inhibit the growth of infected pathogen. In plants, HR is treated as being equivalent to programmed cell death (PCD) in defense response, although programmed cell death is more general term used in animal science. If HR is triggered, PCD occurs and a spreading lesion develops, thereby hindering growth of biotrophic pathogens. Lesions initiated by HR, however, cannot slow the invasion of the necrotrophic pathogens, such as *Botrytis cinera* as these pathogens exploit dead cells for their growth (Govrin and Levine, 2000).

The complicated relationship among SA, ROS and HR is well depicted in one study by Straus et al (Straus et al., 2010). They showed that SA can act as anti-oxidant agent by promoting conversion of $O_2^{\bullet-}$ to H_2O_2 as well as limiting the cell death rather than promoting it. In the study, the mutant *nudt7-1* which lacks NUDT7 limiting oxidative stress (McLennan, 2006) develops

even more cell death when the *sid2* mutation is introduced, suggesting a role for SA in alleviating cell death. In addition, *nudt7 sid2* mutants develop less H_2O_2 but higher $O_2^{\bullet-}$ levels compared to *nudt7* mutants, showing SA's role in limiting superoxide anion level. The study also showed that *nudt7 sid2* mutants develop more lesions with less H_2O_2 level compared to *nudt7* mutants, counter-intuitive to the role of H_2O_2 in an earlier study where H_2O_2 from either oxidative burst triggered by microbial elicitors or exogenous injection can initiate PCD (Levine et al., 1994). It should be also noted that ROS from different subcellular compartments could have different roles in downstream pathways as signal molecules (Straus et al., 2010; Waszczak et al., 2018).

REFERENCES

Adam SA (2017) The Nucleoskeleton. Cold Spring Harbor Perspectives in Biology **9**

Aebi U, Cohn J, Buhle L, Gerace L (1986) The nuclear lamina is a meshwork of intermediate-type filaments. Nature **323:** 560-564

Akhtar A, Gasser SM (2007) The nuclear envelope and transcriptional control. Nat Rev Genet **8:** 507-517

Amendola M, van Steensel B (2015) Nuclear lamins are not required for lamina-associated domain organization in mouse embryonic stem cells. Embo Reports **16:** 610-617

Andres V, Gonzalez JM (2009) Role of A-type lamins in signaling, transcription, and chromatin organization. J Cell Biol **187:** 945-957

Apel K, Hirt H (2004) Reactive oxygen species: Metabolism, oxidative stress, and signal transduction. Annual Review of Plant Biology **55:** 373-399

Apostol I, Heinstein PF, Low PS (1989) Rapid stimulation of an oxidative burst during elicitation of cultured plant cells - Role in defense and signal transduction. Plant Physiology **90:** 109-116

Arancio W, Pizzolanti G, Genovese SI, Pitrone M, Giordano C (2014) Epigenetic involvement in Hutchinson-Gilford Progeria Syndrome: A mini-review. Gerontology **60:** 197-203

Ben-Harush K, Wiesel N, Frenkiel-Krispin D, Moeller D, Soreq E, Aebi U, Herrmann H, Gruenbaum Y, Medalia O (2009) The supramolecular organization of the *C. elegans* nuclear lamin filament. Journal of Molecular Biology **386:** 1392-1402

Berezney R, Coffey DS (1977) Nuclear matrix. Isolation and characterization of a framework structure from rat liver nuclei. J Cell Biol **73:** 616-637

Block A, Toruno TY, Elowsky CG, Zhang C, Steinbrenner J, Beynon J, Alfano JR (2014) The Pseudomonas syringae type III effector HopD1 suppresses effector-triggered immunity, localizes to the endoplasmic reticulum, and targets the Arabidopsis transcription factor NTL9. New Phytologist **201:** 1358-1370

Bowling SA, Clarke JD, Liu YD, Klessig DF, Dong XN (1997) The cpr5 mutant of Arabidopsis expresses both NPR1-dependent and NPR1-independent resistance. Plant Cell **9:** 1573-1584

Burke B, Stewart CL (2013) The nuclear lamins: flexibility in function. Nature Reviews Molecular Cell Biology **14:** 13-24

Calikowski TT, Meulia T, Meier I (2003) A proteomic study of the Arabidopsis nuclear matrix. Journal of Cellular Biochemistry **90:** 361-378

Caron M, Auclair M, Donadille B, Bereziat V, Guerci B, Laville M, Narbonne H, Bodemer C, Lascols O, Capeau J, Vigouroux C (2007) Human lipodystrophies linked to mutations in A-type lamins and to HIV protease inhibitor therapy are both associated with prelamin A accumulation, oxidative stress and premature cellular senescence. Cell Death and Differentiation **14:** 1759-1767

Casolari JM, Brown CR, Drubin DA, Rando OJ, Silver PA (2005) Developmentally induced changes in transcriptional program alter spatial organization across chromosomes. Genes Dev **19:** 1188-1198

Casolari JM, Brown CR, Komili S, West J, Hieronymus H, Silver PA (2004) Genome-wide localization of the nuclear transport machinery couples transcriptional status and nuclear organization. Cell **117:** 427-439

Chamnongpol S, Willekens H, Langebartels C, VanMontagu M, Inze D, VanCamp W (1996) Transgenic tobacco with a reduced catalase activity develops necrotic lesions and induces pathogenesis-related expression under high light. Plant Journal **10:** 491-503

Chen HY, Zheng XB, Zheng YX (2014) Age-Associated Loss of Lamin-B Leads to Systemic Inflammation and Gut Hyperplasia. Cell **159:** 829-843

Chen ZX, Silva H, Klessig DF (1993) Active Oxygen Species in the Induction of Plant Systemic Acquired-Resistance by Salicylic-Acid. Science **262:** 1883-1886

Ciska M, Masuda K, Moreno Diaz de la Espina S (2018) Characterization of the lamin analogue NMCP2 in the monocot Allium cepa. Chromosoma **127:** 103-113

Coquoz JL, Buchala A, Metraux JP (1998) The biosynthesis of salicylic acid in potato plants. Plant Physiology **117:** 1095-1101

Crisp M, Liu Q, Roux K, Rattner JB, Shanahan C, Burke B, Stahl PD, Hodzic D (2006) Coupling of the nucleus and cytoplasm: role of the LINC complex. J Cell Biol **172:** 41-53

Davidson PM, Lammerding J (2014) Broken nuclei - lamins, nuclear mechanics, and disease. Trends in Cell Biology **24:** 247-256

De Vos WH, Houben F, Kamps M, Malhas A, Verheyen F, Cox J, Manders EMM, Verstraeten VLRM, van Steensel MAM, Marcelis CLM, van den Wijngaard A, Vaux DJ, Ramaekers FCS, Broers JLV (2011) Repetitive disruptions of the nuclear envelope invoke temporary loss of cellular compartmentalization in laminopathies. Human Molecular Genetics **20:** 4175-4186

Demple B, Harrison L (1994) Repair of Oxidative Damage to DNA - Enzymology and Biology. Annual Review of Biochemistry **63:** 915-948

Dempsey DA, Klessig DF (2017) How does the multifaceted plant hormone salicylic acid combat disease in plants and are similar mechanisms utilized in humans? Bmc Biology **15**

Dey P (2010) Cancer Nucleus: Morphology and Beyond. Diagnostic Cytopathology **38:** 382-390

Dittmer TA, Stacey NJ, Sugimoto-Shirasu K, Richards EJ (2007) LITTLE NUCLEI genes affecting nuclear morphology in Arabidopsis thaliana. Plant Cell **19:** 2793-2803

Egecioglu D, Brickner JH (2011) Gene positioning and expression. Curr Opin Cell Biol **23:** 338-345

Fabrini R, Bocedi A, Pallottini V, Canuti L, De Canio M, Urbani A, Marzano V, Cornetta T, Stano P, Giovanetti A, Stella L, Canini A, Federici G, Ricci G (2010) Nuclear Shield: A Multi-Enzyme Task-Force for Nucleus Protection. Plos One **5**

Fal K, Asnacios A, Chaboute ME, Hamant O (2017) Nuclear envelope: a new frontier in plant mechanosensing? Biophys Rev **9:** 389-403

Fiserova J, Kiseleva E, Goldberg MW (2009) Nuclear envelope and nuclear pore complex structure and organization in tobacco BY-2 cells. Plant J **59:** 243-255

Francastel C, Schubeler D, Martin DI, Groudine M (2000) Nuclear compartmentalization and gene activity. Nat Rev Mol Cell Biol **1:** 137-143

Frederick SE, Mangan ME, Carey JB, Gruber PJ (1992) Intermediate Filament Antigens of 60 and 65 Kda in the Nuclear Matrix of Plants - Their Detection and Localization. Experimental Cell Research **199:** 213-222

Freytag S, Arabatzis N, Hahlbrock K, Schmelzer E (1994) Reversible Cytoplasmic Rearrangements Precede Wall Apposition, Hypersensitive Cell-Death and Defense-Related Gene Activation in Potato Phytophthora-Infestans Interactions. Planta **194:** 123-135

Gao J, Liao J, Yang GY (2009) CAAX-box protein, prenylation process and carcinogenesis. Am J Transl Res **1:** 312-325

Genre A, Chabaud M, Timmers T, Bonfante P, Barker DG (2005) Arbuscular mycorrhizal fungi elicit a novel intracellular apparatus in Medicago truncatula root epidermal cells before infection. Plant Cell **17:** 3489-3499

Genre A, Ortu G, Bertoldo C, Martino E, Bonfante P (2009) Biotic and Abiotic Stimulation of Root Epidermal Cells Reveals Common and Specific Responses to Arbuscular Mycorrhizal Fungi. Plant Physiology **149:** 1424-1434

Gerace L, Blum A, Blobel G (1978) Immunocytochemical localization of the major polypeptides of the nuclear pore complex-lamina fraction. Interphase and mitotic distribution. J Cell Biol **79:** 546-566

Gilford H (1904) Progeria: A form of senilism. Practitioner **73**

Goldman RD, Shumaker DK, Erdos MR, Eriksson M, Goldman AE, Gordon LB, Gruenbaum Y, Khuon S, Mendez M, Varga R, Collins FS (2004) Accumulation of mutant lamin A causes progressive changes in nuclear architecture in Hutchinson-Gilford progeria syndrome. Proc Natl Acad Sci U S A **101:** 8963-8968

Gonzalo S, Kreienkamp R, Askjaer P (2017) Hutchinson-Gilford Progeria Syndrome: A premature aging disease caused by LMNA gene mutations. Ageing Res Rev **33:** 18-29

Graumann K, Vanrobays E, Tutois S, Probst AV, Evans DE, Tatout C (2014) Characterization of two distinct subfamilies of SUN-domain proteins in Arabidopsis and their interactions with the novel KASH-domain protein AtTIK. Journal of Experimental Botany **65:** 6499-6512

Griffis AHN, Groves NR, Zhou X, Meier I (2014) Nuclei in motion: movement and positioning of plant nuclei in development, signaling, symbiosis, and disease. Frontiers in Plant Science **5**

Grob S, Schmid MW, Grossniklaus U (2014) Hi-C Analysis in Arabidopsis Identifies the KNOT, a Structure with Similarities to the flamenco Locus of Drosophila. Molecular Cell **55:** 678-693

Gu YN, Zebell SG, Liang ZZ, Wang S, Kang BH, Dong XN (2016) Nuclear Pore Permeabilization Is a Convergent Signaling Event in Effector-Triggered Immunity. Cell **166:** 1526-+

Guelen L, Pagie L, Brasset E, Meuleman W, Faza MB, Talhout W, Eussen BH, de Klein A, Wessels L, de Laat W, van Steensel B (2008) Domain organization of human chromosomes revealed by mapping of nuclear lamina interactions. Nature **453:** 948-U983

Guilluy C, Osborne LD, Van Landeghem L, Sharek L, Superfine R, Garcia-Mata R, Burridge K (2014) Isolated nuclei adapt to force and reveal a mechanotransduction pathway in the nucleus. Nature Cell Biology **16:** 376-+

Guo TT, Mao XG, Zhang H, Zhang Y, Fu MD, Sun ZF, Kuai P, Lou YG, Fang YD (2017) Lamin-like Proteins Negatively Regulate Plant Immunity through NAC WITH TRANSMEMBRANE MOTIF1-LIKE9 and NONEXPRESSOR OF PR GENES1 in Arabidopsis thaliana. Molecular Plant **10:** 1334-1348

Heitlinger E, Peter M, Haner M, Lustig A, Aebi U, Nigg EA (1991) Expression of Chicken Lamin-B2 in Escherichia-Coli - Characterization of Its Structure, Assembly, and Molecular-Interactions. Journal of Cell Biology **113:** 485-495

Hennekam RC (2006) Hutchinson-Gilford progeria syndrome: review of the phenotype. Am J Med Genet A **140:** 2603-2624

Herrera-Vasquez A, Salinas P, Holuigue L (2015) Salicylic acid and reactive oxygen species interplay in the transcriptional control of defense genes expression. Frontiers in Plant Science **6**

Hoffmann K, Sperling K, Olins AL, Olins DE (2007) The granulocyte nucleus and lamin B receptor: avoiding the ovoid. Chromosoma **116:** 227-235

Hohenstatt ML, Mikulski P, Komarynets O, Klose C, Kycia I, Jeltsch A, Farrona S, Schubert D (2018) PWWP-DOMAIN INTERACTOR OF POLYCOMBS1 Interacts with Polycomb-Group Proteins and Histones and Regulates Arabidopsis Flowering and Development. Plant Cell **30:** 117-133

Hu B, Wang N, Bi X, Karaaslan ES, Weber AL, Zhu W, Berendzen KW, Liu C (2019) Plant lamin-like proteins mediate chromatin tethering at the nuclear periphery. Genome Biol **20:** 87

Huang JL, Gu M, Lai ZB, Fan BF, Shi K, Zhou YH, Yu JQ, Chen ZX (2010) Functional Analysis of the Arabidopsis PAL Gene Family in Plant Growth, Development, and Response to Environmental Stress. Plant Physiology **153:** 1526-1538

Hutchinson J (1886) Congenital Absence of Hair and Mammary Glands with Atrophic Condition of the Skin and its Appendages, in a Boy whose Mother had been almost wholly Bald from Alopecia Areata from the age of Six. Med Chir Trans **69:** 473-477

Jayaraman D, Gilroy S, Ane JM (2014) Staying in touch: mechanical signals in plant-microbe interactions. Current Opinion in Plant Biology **20:** 104-109

Jovtchev G, Schubert V, Meister A, Barow M, Schubert I (2006) Nuclear DNA content and nuclear and cell volume are positively correlated in angiosperms. Cytogenetic and Genome Research **114:** 77-82

Kim HS, Park HC, Kim KE, Jung MS, Han HJ, Kim SH, Kwon YS, Bahk S, An J, Bae DW, Yun DJ, Kwak SS, Chung WS (2012) A NAC transcription factor and SNI1 cooperatively suppress basal pathogen resistance in Arabidopsis thaliana. Nucleic Acids Research **40:** 9182-9192

Kim Y, Sharov AA, McDole K, Cheng M, Hao H, Fan CM, Gaiano N, Ko MSH, Zheng Y (2011) Mouse B-Type Lamins Are Required for Proper Organogenesis But Not by Embryonic Stem Cells. Science **334:** 1706-1710

Kimura Y, Kuroda C, Masuda K (2010) Differential nuclear envelope assembly at the end of mitosis in suspension-cultured Apium graveolens cells. Chromosoma **119:** 195-204

Kirby TJ, Lammerding J (2018) Emerging views of the nucleus as a cellular mechanosensor. Nature Cell Biology **20:** 373-381

Kosak ST, Skok JA, Medina KL, Riblet R, Le Beau MM, Fisher AG, Singh H (2002) Subnuclear compartmentalization of immunoglobulin loci during lymphocyte development. Science **296:** 158-162

Levine A, Tenhaken R, Dixon R, Lamb C (1994) H2o2 from the Oxidative Burst Orchestrates the Plant Hypersensitive Disease Resistance Response. Cell **79:** 583-593

Lu Q, Tang XR, Tian G, Wang F, Liu KD, Nguyen V, Kohalmi SE, Keller WA, Tsang EWT, Harada JJ, Rothstein SJ, Cui YH (2010) Arabidopsis homolog of the yeast TREX-2 mRNA export complex: components and anchoring nucleoporin. Plant Journal **61:** 259-270

Malhas AN, Lee CF, Vaux DJ (2009) Lamin B1 controls oxidative stress responses via Oct-1. Journal of Cell Biology **184:** 45-55

Masuda K, Takahashi S, Nomura K, Arimoto M, Inoue M (1993) Residual Structure and Constituent Proteins of the Peripheral Framework of the Cell-Nucleus in Somatic Embryos from Daucus-Carota L. Planta **191:** 532-540

Masuda K, Xu ZJ, Takahashi S, Ito A, Ono M, Nomura K, Inoue M (1997) Peripheral framework of carrot cell nucleus contains a novel protein predicted to exhibit a long alpha-helical domain. Experimental Cell Research **232:** 173-181

Mcnulty AK, Saunders MJ (1992) Purification and Immunological Detection of Pea Nuclear Intermediate Filaments - Evidence for Plant Nuclear Lamins. Journal of Cell Science **103:** 407-414

Meier I, Griffis AHN, Groves NR, Wagner A (2016) Regulation of nuclear shape and size in plants. Current Opinion in Cell Biology **40:** 114-123

Meinke P, Schirmer EC (2015) LINC'ing form and function at the nuclear envelope. FEBS Lett **589:** 2514-2521

Mejat A (2010) LINC complexes in health and disease. Nucleus **1:** 40-52

Mikulski P, Hohenstatt ML, Farrona S, Smaczniak C, Stahl Y, Kalyanikrishna K, Kaufmann K, Angenent GC, Schubert D (2019) The chromatin-associated protein PWO1 interacts with plant nuclear lamin-like components to regulate nuclear size. Plant Cell

Minguez A, Delaespina SMD (1993) Immunological Characterization of Lamins in the Nuclear Matrix of Onion Cells. Journal of Cell Science **106:** 431-439

Moreno Diaz de la Espina SM (1995) Nuclear matrix isolated from plant cells. Int Rev Cytol **162B:** 75-139

Morris GE, Randles KN (2010) Nesprin isoforms: are they inside or outside the nucleus? Biochem Soc Trans **38:** 278-280

Neuenschwander U, Vernooij B, Friedrich L, Uknes S, Kessmann H, Ryals J (1995) Is Hydrogen-Peroxide a 2nd-Messenger of Salicylic-Acid in Systemic Acquired-Resistance. Plant Journal **8:** 227-233

Parry DA, Dixon TW, Cohen C (1992) Analysis of the three-alpha-helix motif in the spectrin superfamily of proteins. Biophys J **61:** 858-867

Pekovic V, Gibbs-Seymour I, Markiewicz E, Alzoghaibi F, Benham AM, Edwards R, Wenhert M, von Zglinicki T, Hutchison CJ (2011) Conserved cysteine residues in the mammalian lamin A tail are essential for cellular responses to ROS generation. Aging Cell **10:** 1067-1079

Pendle AF, Clark GP, Boon R, Lewandowska D, Lam YW, Andersen J, Mann M, Lamond AI, Brown JW, Shaw PJ (2005) Proteomic analysis of the Arabidopsis nucleolus suggests novel nucleolar functions. Mol Biol Cell **16:** 260-269

Poulet A, Duc C, Voisin M, Desset S, Tutois S, Vanrobays E, Benoit M, Evans DE, Probst AV, Tatout C (2017) The LINC complex contributes to heterochromatin organisation and transcriptional gene silencing in plants. Journal of Cell Science **130:** 590-601

Rajgor D, Shanahan CM (2013) Nesprins: from the nuclear envelope and beyond. Expert Reviews in Molecular Medicine **15**

Robinson DO, Coate JE, Singh A, Hong LL, Bush M, Doyle JJ, Roeder AHK (2018) Ploidy and Size at Multiple Scales in the Arabidopsis Sepal. Plant Cell **30:** 2308-2329

Sakamoto Y, Takagi S (2013) LITTLE NUCLEI 1 and 4 regulate nuclear morphology in Arabidopsis thaliana. Plant Cell Physiol **54:** 622-633

Schmelzer E (2002) Cell polarization, a crucial process in fungal defence. Trends in Plant Science **7:** 411-415

Shetty NP, Jorgensen HJL, Jensen JD, Collinge DB, Shetty HS (2008) Roles of reactive oxygen species in interactions between plants and pathogens. European Journal of Plant Pathology **121:** 267-280

Shumaker DK, Dechat T, Kohlmaier A, Adam SA, Bozovsky MR, Erdos MR, Eriksson M, Goldman AE, Khuon S, Collins FS, Jenuwein T, Goldman RD (2006) Mutant nuclear lamin A leads to progressive alterations of epigenetic control in premature aging. Proceedings of the National Academy of Sciences of the United States of America **103:** 8703-8708

Sieprath T, Darwiche R, De Vos WH (2012) Lamins as mediators of oxidative stress. Biochemical and Biophysical Research Communications **421:** 635-639

Simon DN, Wilson KL (2011) The nucleoskeleton as a genome-associated dynamic 'network of networks'. Nat Rev Mol Cell Biol **12:** 695-708

Skalamera D, Heath MC (1998) Changes in the cytoskeleton accompanying infection-induced nuclear movements and the hypersensitive response in plant cells invaded by rust fungi. Plant Journal **16:** 191-200

Skubacz A, Daszkowska-Golec A, Szarejko L (2016) The Role and Regulation of ABI5 (ABA-Insensitive 5) in Plant Development, Abiotic Stress Responses and Phytohormone Crosstalk. Frontiers in Plant Science **7**

Straus MR, Rietz S, van Themaat EVL, Bartsch M, Parker JE (2010) Salicylic acid antagonism of EDS1-driven cell death is important for immune and oxidative stress responses in Arabidopsis. Plant Journal **62:** 628-640

Stuurman N, Heins S, Aebi U (1998) Nuclear lamins: their structure, assembly, and interactions. J Struct Biol **122:** 42-66

Tamura K, Fukao Y, Hatsugai N, Katagiri F, Hara-Nishimura I (2017) Nup82 functions redundantly with Nup136 in a salicylic acid-dependent defense response of Arabidopsis thaliana. Nucleus **8:** 301-311

Tamura K, Fukao Y, Iwamoto M, Haraguchi T, Hara-Nishimura I (2010) Identification and Characterization of Nuclear Pore Complex Components in Arabidopsis thaliana. Plant Cell **22:** 4084-4097

Tamura K, Iwabuchi K, Fukao Y, Kondo M, Okamoto K, Ueda H, Nishimura M, Hara-Nishimura I (2013) Myosin XI-i Links the Nuclear Membrane to the Cytoskeleton to Control Nuclear Movement and Shape in Arabidopsis. Current Biology **23:** 1776-1781

Turgay Y, Eibauer M, Goldman AE, Shimi T, Khayat M, Ben-Harush K, Sapra K, Goldman RD, Medalia O (2016) The molecular architecture of lamins in somatic cells. Molecular Biology of the Cell **27**

Tzur YB, Wilson KL, Gruenbaum Y (2006) SUN-domain proteins: 'Velcro' that links the nucleoskeleton to the cytoskeleton. Nat Rev Mol Cell Biol **7:** 782-788

Uzer G, Thompson WR, Sen B, Xie ZH, Yen SS, Miller S, Bas G, Styner M, Rubin CT, Judex S, Burridge K, Rubin J (2015) Cell Mechanosensitivity to Extremely Low-Magnitude Signals Is Enabled by a LINCed Nucleus. Stem Cells **33:** 2063-2076

van Steensel B, Belmont AS (2017) Lamina-Associated Domains: Links with Chromosome Architecture, Heterochromatin, and Gene Repression. Cell **169:** 780-791

Viteri G, Chung YW, Stadtman ER (2010) Effect of progerin on the accumulation of oxidized proteins in fibroblasts from Hutchinson Gilford progeria patients. Mechanisms of Ageing and Development **131:** 2-8

Wang H, Dittmer TA, Richards EJ (2013) Arabidopsis CROWDED NUCLEI (CRWN) proteins are required for nuclear size control and heterochromatin organization. BMC Plant Biol **13:** 200

Waszczak C, Carmody M, Kangasjarvi J (2018) Reactive Oxygen Species in Plant Signaling. Annual Review of Plant Biology, Vol 69 **69:** 209-236

Weber K, Plessmann U, Traub P (1989) Maturation of nuclear lamin A involves a specific carboxy-terminal trimming, which removes the polyisoprenylation site from the precursor; implications for the structure of the nuclear lamina. FEBS Lett **257:** 411-414

Wildermuth MC, Dewdney J, Wu G, Ausubel FM (2001) Isochorismate synthase is required to synthesize salicylic acid for plant defence. Nature **414:** 562-565

Wolberg WH, Street WN, Mangasarian OL (1999) Importance of nuclear morphology in breast cancer prognosis. Clinical Cancer Research **5:** 3542-3548

Worman HJ, Bonne G (2007) "Laminopathies": a wide spectrum of human diseases. Exp Cell Res **313:** 2121-2133

Yan Y, Winograd E, Viel A, Cronin T, Harrison SC, Branton D (1993) Crystal-Structure of the Repetitive Segments of Spectrin. Science **262:** 2027-2030

Zhao WM, Guan CM, Feng J, Liang Y, Zhan N, Zuo JR, Ren B (2016) The Arabidopsis CROWDED NUCLEI genes regulate seed germination by modulating degradation of ABI5 protein. Journal of Integrative Plant Biology **58:** 669-678

Zheng X, Hu J, Yue S, Kristiani L, Kim M, Sauria M, Taylor J, Kim Y, Zheng Y (2018) Lamins Organize the Global Three-Dimensional Genome from the Nuclear Periphery. Mol Cell **71:** 802-815 e807

Zheng XY, Zhou M, Yoo H, Pruneda-Paz JL, Spivey NW, Kay SA, Dong XNA (2015) Spatial and temporal regulation of biosynthesis of the plant immune signal salicylic acid. Proceedings of the National Academy of Sciences of the United States of America **112:** 9166-9173

Zhou X, Groves NR, Meier I (2015) Plant nuclear shape is independently determined by the SUN-WIP-WIT2-myosin XI-i complex and CRWN1. Nucleus **6:** 144-153

Zhou X, Groves NR, Meier I (2015) SUN anchors pollen WIP-WIT complexes at the vegetative nuclear envelope and is necessary for pollen tube targeting and fertility. Journal of Experimental Botany **66:** 7299-7307

Chapter 2. Loss of CRWN nuclear proteins induces cell death and salicylic acid defense signaling

Junsik Choi [a,b], Susan R. Strickler [b], and Eric J. Richards [b]

[a] Section of Plant Biology, School of Integrative Plant Science, Cornell University, Ithaca, New York 14853

[b] Boyce Thompson Institute, Ithaca, New York 14853

ABSTRACT

Defects in the nuclear lamina of animal cell nuclei have dramatic effects on nuclear structure and gene expression as well as diverse physiological manifestations. We report that deficiencies in CROWDED NUCLEI (CRWN), which are candidate nuclear lamina proteins in Arabidopsis (*Arabidopsis thaliana*), trigger widespread changes in transcript levels and whole-plant phenotypes, including dwarfing and spontaneous cell death lesions. These phenotypes are caused in part by ectopic induction of plant defense responses via the salicylic acid pathway. Loss of CRWN proteins induces the expression of the salicylic acid biosynthetic gene *ISOCHORISMATE SYNTHASE1* (*ICS1/SID2*), which leads to spontaneous defense responses in *crwn1 crwn2* and *crwn1 crwn4* mutants, which are deficient in two of the four CRWN paralogs. The symptoms of ectopic defense response, including pathogenesis marker gene expression and cell death, increase in older *crwn* double mutants. These age-dependent effects are postulated to reflect an increase in nuclear dysfunction or damage over time, a phenomenon reminiscent of aging effects seen in animal nuclei and in some human laminopathy patients.

INTRODUCTION

The morphology of cellular organelles is closely related to their function and physiological state. For example, mitochondrial cristae result from a complex corrugation of the inner membrane required to accommodate enzymes for cellular respiration. Mitochondria in skeletal or heart muscle, which require high amounts of energy, have stacked cristae, while

tissues with lower energy demands, such as liver or kidney, contain mitochondria with less stacked cristae (Kuhlbrandt, 2015). This relationship implies that structural components, which provide physical support and define organellar structure, are intimately involved in organelle function. In nuclei, the relationship between morphology and function is particularly important, as nuclei possess genetic information whose expression can be influenced by changes in nuclear structure and organization (Reddy et al., 2008; Schreiber and Kennedy, 2013; Davidson and Lammerding, 2014).

Eukaryotic nuclei are wrapped in a nuclear envelope, a double leaflet consisting of outer and inner nuclear membranes. There are various proteins associated with the envelope essential for nuclear function and morphology. Examples include nucleoporins, which form nuclear pores, Linker of Nucleoskeleton and Cytoskeleton (LINC) complex proteins, which span the nuclear envelope (Lombardi and Lammerding, 2011; Tapley and Starr, 2013; Tatout et al., 2014; Meier, 2016), and a nuclear lamina (NL) structure underlying the inner nuclear envelope (Aebi et al., 1986). Among these, the NL is a key architectural feature that affects both the morphology and the function of nuclei. In animals, the NL is a reticular structure under the inner nuclear membrane. The animal NL is mainly composed of intermediate filament-like proteins called lamins, which polymerize to form fibrillar networks (Aebi et al., 1986). This structure provides docking sites for chromatin and serves as a physical support for the organelle (Gruenbaum and Foisner, 2015). Most heterochromatin resides near or at the nuclear periphery, which is typically a repressive environment for gene expression (Egecioglu and Brickner, 2011). Studies have demonstrated that tethering genes to the NL results in transcriptional repression in mammalian cells (Reddy et al., 2008). Genomic profiling approaches have defined lamina-associated domains (LADs), characterized by repressive chromatin and genes with low expression levels (Pickersgill et al., 2006; Guelen et al., 2008; Ikegami et al., 2010; Peric-Hupkes et al., 2010; van Steensel and Belmont, 2017). This interaction between the genome and NL can link alterations

in NL structure to genomic instability as well as modifications in nuclear morphology. In a well-documented example, certain dominant mutations in the human lamin A gene lead to abnormal nuclear shape, chromatin organization defects, and clinical syndromes, such as premature aging (e.g. Hutchinson-Gilford progeria syndrome) (Hutchinson, 1886; Gilford, 1904; Goldman et al., 2004). Also, fibroblasts cultured from Hutchinson-Gilford progeria syndrome patients exhibit repositioned chromosomes within the nucleus and transcriptional misregulation (Csoka et al., 2004). These findings indicate that the NL is essential for proper gene expression (Zheng et al., 2018).

Although plants lack intermediate filaments and lamin orthologs, different classes of nuclear coiled-coil proteins have been identified as putative NL components, based on pioneering studies by Masuda and colleagues on carrot (*Daucus carota*) Nuclear Matrix Constituent Proteins (NMCPs) (Masuda et al., 1993; Masuda et al., 1997). In Arabidopsis (*Arabidopsis thaliana*), NMCP orthologs, called CROWDED NUCLEI (CRWN) proteins, are candidates for the major structural component of a plant NL. The Arabidopsis genome contains four CRWN genes, which are expressed broadly at the transcript level without obvious tissue specificity. The proteins partition into two distinct clades: one containing the CRWN1, CRWN2, and CRWN3 paralogs (NMCP1 clade), and a distinct one including CRWN4 (NMCP2 clade). Among these paralogs, CRWN1 and CRWN4 proteins localize to the nuclear periphery and are therefore the best candidates for NL components, while CRWN2 and CRWN3 are distributed throughout the nucleoplasm (Dittmer et al., 2007; Dittmer and Richards, 2008; Sakamoto and Takagi, 2013). CRWN genes are essential, as a loss of all four genes leads to inviability. CRWN proteins are important for maintenance of nuclear structure and morphology, as many *crwn* mutants have small and round nuclei (Dittmer et al., 2007; Sakamoto and Takagi, 2013; Wang et al., 2013) compared with wild-type Arabidopsis nuclei, which are elongated in many differentiated cell types (Chytilova et al., 2000; Meier et al., 2016; Meier et al., 2017). Our group

previously reported that CRWN genes have roles in specifying the structure of heterochromatin aggregates in interphase (chromocenters), implying that CRWN proteins not only control nuclear morphology but are also able to regulate higher order genome organization (Dittmer et al., 2007; Wang et al., 2013). Whole-plant phenotypes of *crwn* mutants show that many double and triple *crwn* mutants are smaller in size and have wrinkled leaves, demonstrating that altered plant nuclear structure can ultimately lead to abnormal growth.

Here, we investigate the effects of *crwn* mutations on gene expression and elucidate a mechanism through which loss of CRWN proteins causes dwarfism. We show that mutants lacking the full complement of CRWN genes show altered gene expression patterns, characterized by overexpression of transcripts associated with biotic pathogen response. Plants lacking both CRWN1 and CRWN2, or CRWN1 and CRWN4, exhibit ectopic defense responses, including partial resistance against the virulent bacterial pathogen, *Pseudomonas syringae* pv. *tomato* (strain DC3000). In addition, these *crwn* genotypes exhibit spontaneous cell death, which is associated with the up-regulation of the salicylic acid (SA)-biosynthesis gene, *ISOCHORISMATE SYNTHASE1* (*ICS1/SID2*), and subsequent SA-dependent defense signaling. Our results demonstrate that nuclear periphery defects in plants, like similar changes in animal cells, can lead to premature cell death.

RESULTS

Three *crwn* single mutants show altered transcriptional profiles in the absence of whole-plant phenotypes

We reasoned that the alterations in nuclear size and shape in the *crwn* mutants could have an effect on transcriptional regulation and/or posttranscriptional processing. To test this prediction, we assessed the effect of *crwn* mutations on steady-state transcript levels using RNA sequencing (RNA-seq). Four-week-old rosette leaves from five mutants (*crwn1*, *crwn2*, *crwn4*, *crwn1 crwn2*, and *crwn1 crwn4*) were used as tissue for the RNA purification and transcriptomic analysis. These five mutants encompass the range of phenotypes displayed by *crwn* family mutants and involve both the NMCP1 and NMCP2 clades of CRWN paralogs. Mutants lacking

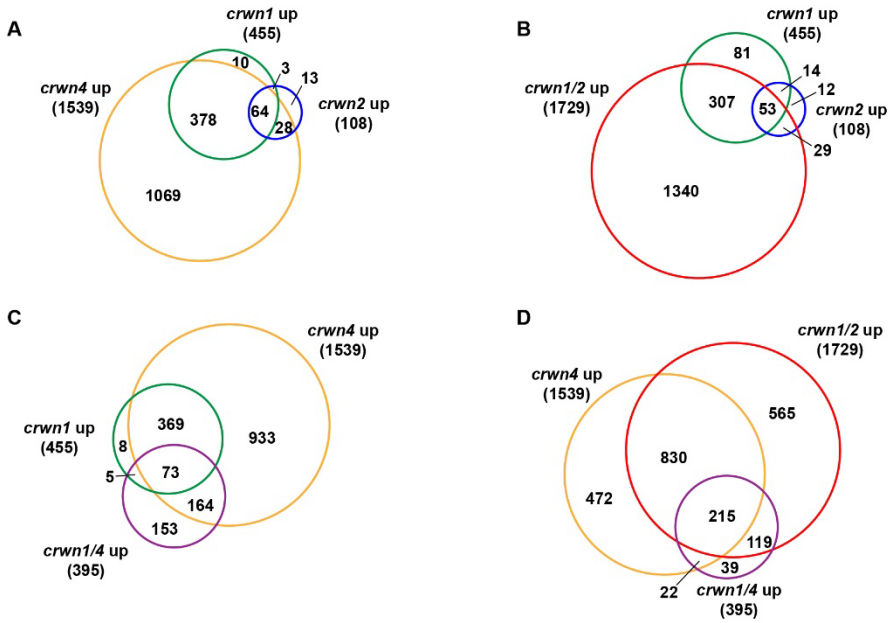

Figure 2.1. The patterns of up-regulated genes in *crwn* mutants demonstrate both synergistic and antagonistic relationships among *crwn* mutations. The sizes of each circle in the Venn diagrams are proportional to the number of genes up-regulated at least two fold in our RNA-seq data ($q < 0.01$). A, up-regulated genes in three *crwn* single mutants, *crwn1*, *crwn2* and *crwn4*, showing shared transcriptomic alterations. B, up-regulated genes in the double mutant *crwn1 crwn2* and corresponding single mutants, *crwn1* and *crwn2*, showing the synergistic effects of the *crwn1* and *crwn2* mutations. C, up-regulated genes in the double mutant *crwn1 crwn4* and corresponding single mutants, *crwn1* and *crwn4*, showing the antagonistic effects of these mutations. D, up-regulated genes in two double mutants, *crwn1 crwn2* and *crwn1 crwn4*, and one single mutant, *crwn4*, illustrating overlapping profiles. Note that *PR1* and *PR2* fell in the overlap between *crwn1 crwn2* and *crwn1 crwn4* mutants (this overlap contains 119 genes) and *PR5* was found only in the sector corresponding to the *crwn1 crwn2* mutant (region with 565 genes).

either CRWN1 or CRWN4 show abnormal nuclei that fail to elongate in differentiated cells and are reduced in size. The *crwn2* mutation by itself does not alter nuclear morphology, but it was included in our analysis because *crwn1 crwn2* double mutants have much smaller nuclei and display dwarf phenotypes (Dittmer et al., 2007; Wang et al., 2013), indicating that CRWN1 and CRWN2 have at least partially overlapping function. Similarly, *crwn1 crwn4* double mutants are smaller than the wild type or either *crwn1* or *crwn4* single mutant.

We first compared misregulated genes among the three single mutants using a threshold for misregulation of 2-fold or greater increase or decrease compared with the wild type, with $q < 0.01$. We discovered that *crwn4* mutants displayed the largest number of up-regulated loci, with 1,539 genes, compared to 455 for *crwn1* mutants and 108 for *crwn2* mutants (Fig. 1A). The number of genes with altered expression scaled with the severity of the abnormal nuclei phenotypes in leaf cells. That is, *crwn2* plants have normally shaped nuclei and the least number of up-regulated genes, while *crwn1* mutants exhibit smaller, round nuclei and a moderate alteration in transcription (Fig. 1A). The most severe misregulation was seen in the *crwn4* mutant (Fig. 1A), which has a more severe effect on nuclear organization, evidenced by a disruption in chromocenter organization and an abnormal nuclear boundary. These results indicate that loss of a single CRWN protein is enough to elicit transcriptomic alterations. The absence of morphological defects on the whole-plant level in *crwn* single mutants indicates that the changes in steady-state transcript levels are tied directly to alterations in nuclear structure, rather than a result of secondary effects from abnormal growth and development.

Complex Interactions among *crwn* mutations are revealed by transcriptomic profiling

The genes misregulated in each *crwn* mutant formed sets with a high degree of overlap, suggesting shared functions among CRWN proteins. For example, many of the genes that were up-regulated genes in the *crwn1* and *crwn2* single mutants were also up-regulated in the *crwn4*

mutants (Fig. 1A). A similar pattern was observed in the Venn diagrams of down-regulated genes as well as for all misregulated genes (Supplemental Fig. S1).

We explored the overlap of function among CRWN proteins further by analyzing the transcriptomic profiles of the two *crwn* double mutants, *crwn1 crwn2* and *crwn1 crwn4*, which display dwarf phenotypes. Of the two, *crwn1 crwn2* mutants showed more extensive transcriptomic misregulation, exceeding the sum of the transcriptomic profiles of *crwn1* and *crwn2* single mutants (Fig. 1B). Thus, loss of CRWN1 and CRWN2 leads to a synergistic effect on transcription (Supplemental Fig. S2). This result is consistent with the synergistic phenotypes of *crwn1 crwn2* double mutants, which have smaller nuclei and suffer from stunted growth, compared with the wild type and *crwn1* or *crwn2* single mutants. The transcriptomic patterns reinforce our previous conclusion that CRWN1 and CRWN2 have overlapping functions, but CRWN1, which is more highly expressed than CRWN2 (~3-fold in wild-type plants in our RNA-seq data set), is sufficient to cover for the loss of its close paralog in *crwn2* mutants.

Given the overlap of misregulated genes in *crwn1* and *crwn4* single mutants, it was surprising to observe that the combination of *crwn1* and *crwn4* mutations resulted in a smaller perturbation of gene expression compared with *crwn4* mutants (Fig. 1C; Supplemental Fig. S2). This result was also unexpected because *crwn1 crwn4* mutants have intermediate whole-plant phenotypes and a nuclear size reduction between that of the single mutants and the *crwn1 crwn2* double mutant. However, the transcriptomic data demonstrating that *crwn1* suppresses the *crwn4* mutation are consistent with our previous observations that CRWN1 and CRWN4 have opposing effects on chromocenter aggregation (Wang et al., 2013).

To summarize, our transcriptomic profiling uncovered a complex set of interactions among *CRWN* genes. On one hand, the gene expression results confirm that *CRWN1* and *CRWN2*, close paralogs in the same clade, have overlapping functions. In contrast, *CRWN1* and *CRWN4*, which lie in distinct clades, appear to have at least partially antagonistic functions.

Misregulated transcripts in *crwn* mutants are evenly distributed on chromosome arms but depleted from pericentromeric regions

Next, we determined if genes misregulated in *crwn* mutants have a nonrandom distribution across the genome. Plant genomes make nonrandom contacts with the nuclear periphery (Bi et al., 2017), as is the case in animals, where a subset of the genome is partitioned into LADs (van Steensel and Belmont, 2017). Therefore, we investigated whether or not particular regions of the folded genome were preferentially affected in *crwn* mutants. An uneven distribution of misregulated genes could also reflect differential effects on distinct epigenetic compartments in the genome. To investigate these possibilities, we drew chromosomal maps marking the positions of misexpressed transcripts. As shown in Supplemental Figure S3, misregulated loci were evenly distributed across each chromosome arm but significantly depleted from pericentromeric regions. The lack of differentially expressed genes in these regions could indicate that transposable elements (TEs), which are concentrated in heterochromatic regions flanking the centromere, are not derepressed in *crwn* mutants. However, the paucity of TEs detected might result from a bias in our RNA-seq analysis based on uniquely mapped reads and a gene-based annotation. Accordingly, we used TEtranscripts, an independent program designed to analyze differential expression of TEs, allowing transcripts to be mapped to families of elements (Jin et al., 2015). This supplemental analysis determined that only a small number of TE families showed modest expression changes (Supplemental Tables S1 and S2), and, in most cases, the detected differences reflected changes in transcript levels from genes that contain an embedded TE. For example, transcripts from AT2TE56040, an element in the VANDAL5A subfamily, were ~16-fold higher in *crwn1 crwn2* mutants compared with the wild type (Supplemental Table S1), with no significant overexpression in *crwn1* or *crwn2*. However, inspection of the RNA-seq reads indicated that this apparent overexpression was due to longer transcripts corresponding to AT2G30020, which contains the element within an exon. Taken as

a whole, our results indicate that epigenetic silencing of TEs is not significantly reduced in any of the *crwn* mutants, despite the significant dispersion of chromocenters observed in *crwn4* nuclei (Wang et al., 2013).

We then characterized the chromatin states of misregulated genes in *crwn* mutants to determine if certain epigenetic signatures were overrepresented or underrepresented. For this analysis, we used the nine chromatin categories established by Sequeira-Mendes et al. to define the landscape of the Arabidopsis epigenome (Sequeira-Mendes et al., 2014). We found that up-regulated genes in *crwn* mutants showed a higher proportion of genes in chromatin state 2 compared with either the whole Arabidopsis gene list or the genes that were tested for differential expression (Supplemental Fig. S4). Chromatin state 2 is characterized by active marks (e.g. histone H3K4me2 and H3K4me3) associated with transcription as well as a high level of the repressive nucleosome modification, histone H3K27me3. The overrepresentation of chromatin state 2 coincided with an underrepresentation of states 1 and 3, which are associated with actively expressed genes and transcriptional elongation, respectively. The shift in representation of chromatin states among up-regulated targets suggests that CRWNs might contribute to the modulation of H3K27me-associated chromatin or differentially affect inducible genes that are packaged in chromatin state 2.

Analysis of gene ontology of misregulated genes shows ectopic defense responses in *crwn* mutants

Next, we asked what kind of genes are misregulated in the RNA-seq profiles of *crwn* mutants. We found two patterns in this analysis. First, up-regulated genes were characterized by stress-associated Gene Ontology (GO) terms (Table 1). Although we found that both biotic and abiotic stress-related GO terms were identified, we focused on biotic stress because the GO terms with the highest fold enrichment were those related to plant defense (e.g. response to

chitin and response to molecule of bacterial origins). The second pattern was an enrichment of genes associated with metabolism and other stress pathways among the down-regulated loci (Supplemental Table S3). Examples of these down-regulated pathways include glucosinolate biosynthesis, wax biosynthesis, and cell wall biogenesis. Together, these two observations suggest that a loss of CRWN1 or CRWN4, or a combination of CRWN paralogs, leads to an induction of defense-related genes and a down-regulation of a subset of metabolic processes.

Two *crwn* double mutants exhibit DC3000 resistance and elevated *PR* gene expression

Our analysis of transcriptomic data uncovered an ectopic induction of defense responses in *crwn* mutants, prompting us to test if there are any defense phenotypes in these mutants. We infected an array of *crwn* mutants with two commonly studied Arabidopsis pathogens representing both fungi and bacteria: the necrotrophic fungal pathogen *Botrytis cinerea* or the hemibiotrophic bacterial pathogen *P. syringae* (DC3000). We did not detect differences among the mutants challenged with *B. cinerea*; however, we found that the *crwn1 crwn2* mutant significantly suppressed DC3000 growth in leaf tissue, compared with the wild type and single *crwn* mutants (Fig. 2A), while the *crwn1 crwn4* mutant exhibited an intermediate phenotype. These graded disease phenotypes paralleled the expression of *Pathogenesis Related* (*PR*) marker genes in uninfected *crwn* mutants. Reverse transcription quantitative PCR (RT-qPCR) assays showed that *PR1*, *PR2*, and *PR5* were highly expressed in both *crwn1 crwn2* and *crwn1 crwn4* double mutants (Fig. 2B), but to a more extreme degree in *crwn1 crwn2* mutants. Furthermore, despite showing widespread transcriptional changes, single *crwn1* and *crwn4* mutants did not show significant up-regulation of *PR* genes, nor did these genotypes suppress

Table 2.1. *Statistical overrepresentation test for up-regulated genes in crwn mutants*

Input	GO Terms (Biological Process Complete)	Total no. of Arabidopsis genes in the term	Input genes #	Expected no. of genes	Fold enrichment	*P* value
Up-regulated genes in *crwn1* mutants (444 genes mapped)	Response (rsp.) to chitin	108x	19	1.76	10.76	1.19E-10
	Rsp. to jasmonic acid	174	18	2.84	6.33	2.68E-06
	Rsp. to wounding	179	17	2.93	5.81	2.66E-05
	Ethylene-activated signaling pathway	135	11	2.21	4.99	4.08E-02
	Rsp. to SA	164	13	2.68	4.85	9.72E-03
	Rsp. to abscisic acid	413	25	6.75	3.70	8.24E-05
	Rsp. to salt stress	417	24	6.81	3.52	3.82E-04
	Protein phosphorylation	828	47	13.53	3.47	6.30E-10
	Rsp. to bac.	353	20	5.77	3.47	5.12E-03
	Cellular rsp. to acid chemical	346	19	5.65	3.36	1.41E-02
Up-regulated genes in *crwn2* mutants (107 genes mapped)	Rsp. to organonitrogen compound	133	6	0.52	11.53	3.42E-02
	Rsp. to cold	281	9	1.1	8.19	4.02E-03
	Rsp. to salt stress	417	10	1.63	6.13	1.35E-02
	Rsp. to acid chemical	896	21	3.51	5.99	9.39E-08
	Rsp. to oxygen-containing compound	1156	22	4.52	4.86	1.51E-06
	Rsp. to inorganic substance	690	12	2.7	4.45	3.88E-02
	Rsp. to hormone	1218	18	4.76	3.78	2.65E-03
Up-regulated genes in *crwn4* mutants (1510 genes mapped)	Rsp. to chitin	108	57	5.98	9.53	1.22E-32
	Rsp. to molecule of bac. origin	20	8	1.11	7.22	4.54E-02
	Defense rsp. to fungus, incompatible interaction	37	14	2.05	6.83	8.20E-05
	Defense rsp. to bac., incompatible interaction	40	11	2.22	4.96	4.48E-02
	Rsp. to wounding	179	46	9.91	4.64	1.09E-13
	Plant-type hypersensitive rsp.	67	17	3.71	4.58	8.54E-04
	Rsp. to SA	164	39	9.08	4.29	2.75E-10
	Protein autophosphorylation	115	27	6.37	4.24	1.98E-06
	Cellular rsp. to jasmonic acid stimulus	61	14	3.38	4.14	2.67E-02
	Ethylene-activated signaling pathway	135	29	7.48	3.88	3.47E-06
Up-regulated genes in *crwn1 crwn2* mutants (1686 genes mapped)	Rsp. to chitin	108	62	6.68	9.27	5.61E-35
	Rsp. to molecule of bac. origin	20	9	1.24	7.27	1.33E-02
	SA mediated signaling pathway	35	14	2.17	6.46	1.61E-04
	Defense rsp. to bac., incompatible interaction	40	15	2.48	6.06	1.27E-04
	Plant-type hypersensitive rsp.	67	24	4.15	5.79	3.97E-08
	Systemic acquired resistance	44	15	2.72	5.51	4.24E-04
	Regulation of cell death	58	16	3.59	4.46	2.64E-03
	Regulation of rsp. to biotic stimulus	49	13	3.03	4.29	3.82E-02
	Regulation of rsp. to external stimulus	53	14	3.28	4.27	1.94E-02
	Positive regulation of defense rsp.	64	16	3.96	4.04	9.07E-03
Up-regulated genes in *crwn1 crwn4* mutants (382 genes mapped)	Toxin metabolic process	54	8	0.76	10.53	2.89E-03
	Cellular rsp. to SA stimulus	50	7	0.7	9.95	1.91E-02
	Defense rsp. to bac.	281	29	3.96	7.33	5.01E-13
	Rsp. to organonitrogen compound	133	13	1.87	6.94	1.85E-04
	Innate immune rsp.	239	16	3.36	4.76	9.87E-04
	Secondary metabolite biosynthetic process	256	14	3.6	3.89	4.85E-02
	Rsp. to abscisic acid	413	22	5.81	3.78	3.62E-04
	Rsp. to fungus	490	26	6.9	3.77	2.90E-05
	Rsp. to oxidative stress	364	17	5.12	3.32	4.89E-02
	Protein phosphorylation	828	29	11.65	2.49	1.97E-02

the growth of DC3000. These RT-qPCR results were consistent with our RNA-seq data, which indicated that *PR* genes are up-regulated in *crwn1 crwn2* and *crwn1 crwn4* plants but not in

crwn single mutants (Fig. 1D). Thus, the *PR* gene expression pattern indicates that *crwn* single mutants fail to induce defense responses fully, while the *crwn1 crwn2* and *crwn1 crwn4* double mutants induce defense responses above a threshold necessary to interfere with pathogen growth.

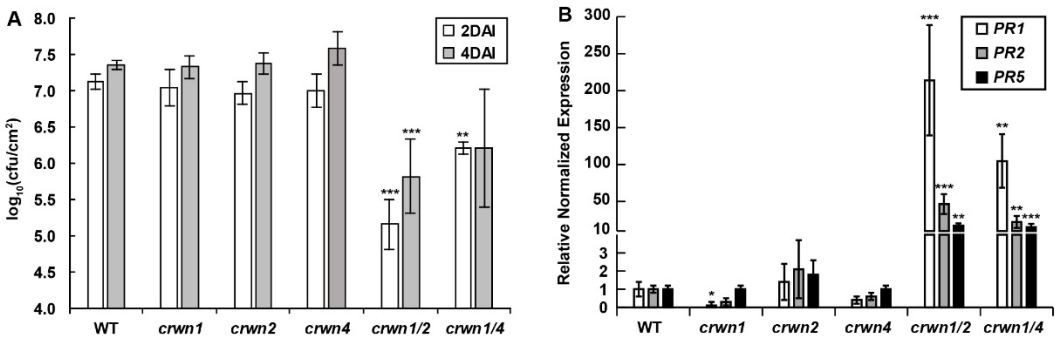

Figure 2.2. *crwn1 crwn2* and *crwn1 crwn4* mutants exhibit spontaneous defense responses. A, DC3000 growth in rosette leaves of 22-d-old plants. The two double mutants have elevated resistance against DC3000. Log_{10} values of colony forming units (cfu) from each mutant were calculated 2 d and 4 d after infection (DAI). Error bars indicate *SD* ($n = 4$). Each mutant was compared to wild type (WT) using the Student's *t*-test (**, $P < 0.01$ and ***, $P < 0.001$). B, RT-qPCR data showing expression of three *PR* genes in 27-d-old plants. Transcript levels of the marker genes are significantly higher in the two double mutants, consistent with their DC3000 resistance phenotype. Error bars indicate *SE* ($n = 3$). Student's *t*-tests were performed based on delta-C_t values (*, $P < 0.05$; **, $P < 0.01$; and ***, $P < 0.001$).

crwn Double Mutants Exhibit Cell Death Lesions

Spontaneous defense responses, such as those observed in *crwn* double mutants, are also characteristic of lesion-mimic mutants (LMMs), which develop ectopic cell death foci similar to hypersensitive response lesions (Moeder and Yoshioka, 2008). As LMMs trigger premature and prolonged defense responses, they also show many growth phenotypes, such as slower growth and dwarfism (Bowling et al., 1997; Bruggeman et al., 2015). We assayed cell death in the *crwn* mutants because *crwn* double mutants display both autonomous defense responses and dwarfism. We found that both *crwn1 crwn2* and *crwn1 crwn4* double mutants exhibited dead cells in rosette leaves stained with Trypan Blue (Fig. 3A). Consistent with the expression level of the *PR* genes and the resistance against DC3000, *crwn1 crwn2* mutants showed a higher incidence of cell death compared with *crwn1 crwn4* plants. Almost no cell death was found in matched tissues from either single *crwn* mutants or wild-type control

samples.

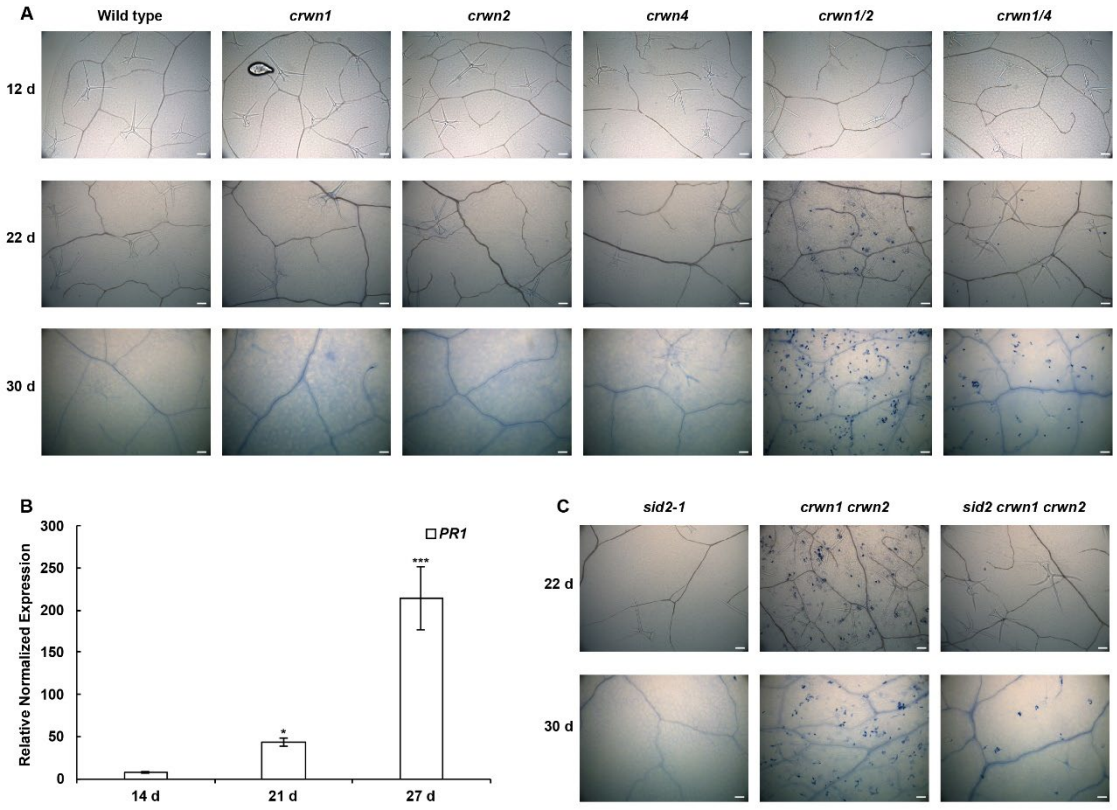

Figure 2.3. *crwn* double mutants exhibit cell death and *PR* gene expression, which are exacerbated with aging. A, Trypan blue staining showed that *crwn1 crwn2* and *crwn1 crwn4* mutants form spontaneous lesions. As plants matured, cell death was more apparent and more frequent. B, *PR1* expression in leaves from *crwn1 crwn2* mutants of different ages. Expression of *PR1* is higher in chronologically older leaves of *crwn1 crwn2* mutants, consistent with our observation that older plants develop more lesions. *PR1* expression at each stage was normalized to transcript levels in wild-type samples for the housekeeping gene *ROC1*. Error bars indicate *SE* ($n = 3$). Student's *t*-tests were performed based on delta-C_t values (*, $P < 0.05$; and ***, $P < 0.001$). C, the *sid2-1* mutation suppressed cell death in 22-d-old *crwn1 crwn2* mutants; however, 30-d-old plants still exhibited some lesion formation. Bars = 100 µm.

We checked if spontaneous defense phenotypes intensify over time, because young seedlings of *crwn1 crwn2* mutants have less wrinkled leaves than older plants. We found no cell death in 12-d-old *crwn1 crwn2* mutants but lesions were frequent in 22-d-old *crwn1 crwn2* leaves (Fig. 3A). Moreover, cell death was more widespread in 30-d-old *crwn1 crwn2* plants (Fig. 3A). A similar age-dependent increase in cell death was observed in *crwn1 crwn4* mutants.

Paralleling the increased incidence of cell death, *PR1* expression was relatively low in leaves from younger 14- and 21-d-old *crwn1 crwn2* plants but increased dramatically in 27-d-

old plants (Fig. 3B). These results show that perturbation of the nuclear periphery in plant cells leads to age-dependent effects on the whole-plant level, manifested here in the form of cell death and gene expression changes.

crwn1 crwn2 and *crwn1 crwn4* double mutants show high levels of total SA

Next, we sought to understand the connection among the diverse responses displayed by the *crwn* double mutants. SA is a prominent regulator of plant defense responses, including the hypersensitive response, systemic acquired resistance, and reactive oxygen species production (Vlot et al., 2009). Consequently, we investigated the causal connection between the phenotypes of *crwn* mutants and SA. First, we measured SA abundance in *crwn* mutants using mass spectrometry coupled with HPLC (HPLC/MS). SA can exist as several derivatives, including SA glucoside and salicylate glucose ester. The glucosylation of SA is known to reduce its toxicity and allows storage of large quantities of the hormone (Dempsey et al., 2011). The level of free SA was more than 2-fold higher in *crwn1 crwn2* mutants compared with the wild type or *crwn1*, *crwn2*, and *crwn4* single mutants (Fig. 4A). For glucosylated SA, the fold change was much higher than that for free SA: we recorded a 14-fold increase of glucosylated SA in *crwn1 crwn2* mutants and a more than 6-fold increase in *crwn1 crwn4* mutants (Fig. 4B). Thus, we found that both free SA and glucosylated SA are elevated in *crwn1 crwn2* mutants, while only glucosylated SA is highly abundant in *crwn1 crwn4* mutants. These results are consistent with the intermediate defense phenotypes in *crwn1 crwn4* plants compared with *crwn1 crwn2* mutants and the lack of significant defense phenotypes in *crwn* single mutants. These findings suggest that SA is an important mediator of the abnormal gene expression and defense responses exhibited by *crwn* mutants.

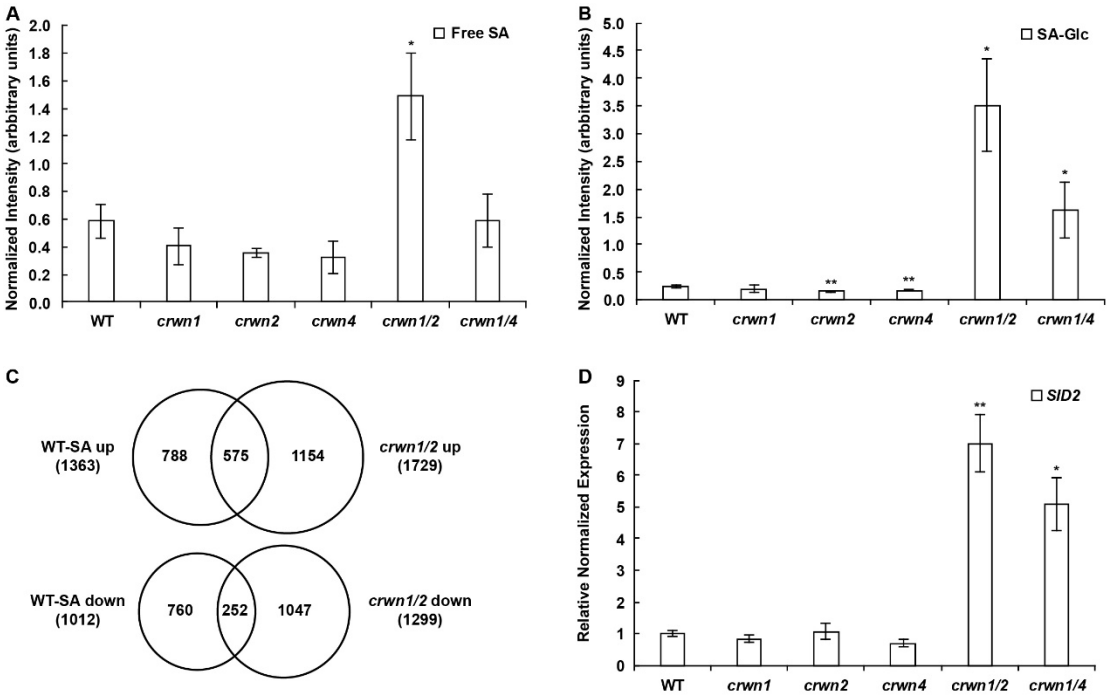

Figure 2.4. SA levels in *crwn1 crwn2* and *crwn1 crwn4* mutants are significantly higher than in wild-type (WT) plants or *crwn* single mutants. A, HPLC/MS detection of free SA levels from 27-d-old plants. Peak intensities of free SA per fresh sample weight were normalized to the spiked internal control d4-SA. Each mutant was compared with the WT using Student's *t* test, and error bars indicate *SD* (*, $P < 0.05$; $n = 3$). B, HPLC/MS detection of glucosylated SA (SA-Glc, indicating either SA glucoside or salicylate Glc ester) levels from each mutant. The detection method, units, and statistical analysis were identical to those described for A (*, $P < 0.05$ and **, $P < 0.01$). C, Overlap of misregulated genes in our RNA-seq data from *crwn1 crwn2* mutants and those in microarray data from 1 mM SA-treated WT plants (Zhou et al., 2015). For SA-treated WT microarray data, genes at least 2-fold increased or decreased with adjusted $P < 0.05$ were used. For the RNA-seq of *crwn1 crwn2* mutants, the criteria described in Figure 2.1. were used. The significance of the overlap of both up-regulated and down-regulated gene comparisons was assessed by the hypergeometric test; the resulting *P* values in both cases were far less than 0.001. D, RT-qPCR data showing expression of the *SID2* gene in 27-d-old plants. Error bars indicate *SE* ($n = 3$). Student's *t* tests were performed based on delta-C_t values (*, $P < 0.05$ and **, $P < 0.01$).

SA is responsible for a significant portion of misregulated genes in *crwn1 crwn2* mutants

To test the prediction that SA overaccumulation is responsible for the altered transcriptome in *crwn* mutants, we compared our RNA-seq data of *crwn1 crwn2* mutants with a microarray data set from SA-treated wild-type plants (Zhou et al., 2015). About 40% of the up-regulated genes in the SA-treated wild-type sample overlapped with the up-regulation profile of *crwn1 crwn2* mutants (Fig. 4C). GO term analysis revealed that genes in the overlap of these sets are closely related to bacterial resistance and SA response (Supplemental Table S4).

Moreover, 25% of the down-regulated genes in the SA-treated wild-type sample overlapped with those down-regulated in *crwn1 crwn2* samples (Fig. 4C). Among the genes down-regulated in both data sets are those featuring the response to jasmonic acid GO term (Supplemental Table S4), reflecting the well-known antagonism between SA and jasmonic acid signaling (Robert-Seilaniantz et al., 2011).

The number of loci misregulated in both SA-treated plants and *crwn* single mutants was reduced relative to the overlap between SA-treated and *crwn1 crwn2* double mutant samples (Supplemental Fig. S5). This pattern is consistent with the fact that the *crwn* single mutants do not accumulate high levels of SA. However, this explanation is incomplete, as the overlap is relatively modest between the SA-treatment data set and the misregulated loci in *crwn1 crwn4* mutants with elevated SA levels. Taken together, our findings indicate that SA signaling accounts for a significant portion of the transcriptomic changes in the *crwn1 crwn2* mutants but that *crwn* mutations cause gene misregulation through additional mechanisms.

SID2 transcripts are abundant in two *crwn* double mutants

To understand the mechanism responsible for SA accumulation in *crwn1 crwn2* and *crwn1 crwn4* mutants, we checked for changes in the transcript levels of genes involved in SA biosynthesis. There are two different SA biosynthetic pathways in plants (Vicente and Plasencia, 2011). First, the phenylpropanoid pathway utilizes Phe in the cytoplasm to produce SA. Phenylalanine ammonia lyases (PALs) are important enzymes in this pathway. The second pathway begins with isochorismate in the chloroplast. In the latter pathway, ICS, where *ICS1* is a synonym of *SID2*, are key enzymes responsible for SA biosynthesis (Seyfferth and Tsuda, 2014). *SID2* is highly expressed when plants are infected with *P. syringae* pv *maculicola* (Wildermuth et al., 2001). We found that *crwn1 crwn2* mutants express very high levels of *SID2* transcripts, while transcription of *PAL1* and *PAL4* is reduced by more than half in our RNA-seq

data (Supplemental Fig. S6). Using RT-qPCR, we validated that the *SID2* transcript level was significantly increased in *crwn1 crwn2* mutants, while *crwn1 crwn4* mutants exhibited an intermediate level of expression (Fig. 4D). These results are consistent with the total SA levels and the magnitude of defense responses in the *crwn* mutants. In addition, we found that the genes encoding several positive regulators of *SID2* (Seyfferth and Tsuda, 2014), including *SARD1* and *CBP60g*, are highly up-regulated in the transcriptomic profiles of *crwn1 crwn2* mutants (Supplemental Fig. S6). These results indicate that loss of *CRWN* genes leads to ectopic pathogen signaling by ramping up the production of SA via overexpression of *SID2*.

Blocking induced SA biosynthesis diminishes but does not abolish lesion formation

After we observed that abnormally high SA levels were synthesized in *crwn* double mutants, we introduced a *sid2-1* mutation to block SA biosynthesis to determine which *crwn* phenotypes are dependent on SA. As shown in Supplemental Figure S7, the *sid2-1* mutation effectively suppressed SA accumulation in the *crwn1 crwn2* background. The lack of SA is consistent with the fact that DC3000 growth in *sid2 crwn1 crwn2* mutants was comparable to that in *sid2* mutants (Supplemental Fig. S8). Therefore, the *sid2-1* allele was epistatic to the *crwn* mutations for both SA accumulation and bacterial growth phenotypes, indicating that the primary reason for ectopic defense responses in *crwn* mutants is a high level of SA.

We observed that the *sid2-1* mutation also suppressed lesion formation in *crwn1 crwn2* mutants, but, in this case, the suppression was incomplete. While no cell death was observed in 22-d-old *sid2 crwn1 crwn2* leaves (Fig. 3C), scattered lesions were still evident in 30-d-old leaf tissue. This result demonstrates that some cell death occurs in *crwn1 crwn2* mutants in an SA-independent manner.

crwn1 crwn2 mutants exhibit SA-independent developmental defects

A number of additional phenotypes exhibited by *crwn1 crwn2* mutants are independent of SA accumulation to varying degrees. For example, the wrinkled leaves and dwarf stature of *crwn* double mutants were only partially suppressed by disruption of *SID2* (Supplemental Fig. S9). In particular, *sid2 crwn1 crwn2* plants still exhibited some dwarfism, most noticeably in bolt stature (Supplemental Fig. S9C). These results indicate that a large component of the dwarfing syndrome displayed by *crwn1 crwn2* mutants is caused by SA overaccumulation, although there is still an SA-independent pathway affecting bolt stature.

Seed shape was also altered in certain *crwn* mutants, especially *crwn1 crwn2*. As shown in Supplemental Figure S10, *crwn1 crwn2* seeds often had deeply creviced surfaces, and we observed a range of seed morphologies, from normal to smaller and darker seeds. Addition of the *sid2-1* allele did not have an appreciable effect on these phenotypes, as seeds harvested from *sid2 crwn1 crwn2* mutants were also misshapened.

We also examined nuclei in the *sid2 crwn1 crwn2* mutant to determine if the reduced organellar size and abnormal spherical shape characteristic of this genotype might be partially attributable to ectopic SA signaling. As shown in Supplemental Figure S11, elongated anther filament cells of *sid2 crwn1 crwn2* mutants retained the small, round nuclear morphology observed in *crwn1 crwn2* mutants. Therefore, the *sid2-1* mutation had no effect on nuclear size or shape. This finding demonstrates that the nuclear phenotypes caused by loss of *CRWN1* and *CRWN2* are primary effects, not downstream consequences of elevated SA production in these mutants.

DISCUSSION

To investigate the importance of three-dimensional genome organization within the nucleus, we asked if perturbation of the plant nuclear periphery leads to aberrant gene

expression patterns. We found that deficiencies of individual NMCP proteins in Arabidopsis, particularly CRWN1 or CRWN4, led to changes in the steady-state levels of a large number of transcripts, and even more transcripts were altered in *crwn1 crwn2* double mutants. A large portion of the overexpressed genes were involved in pathogen defense. The proximate cause of much of this misregulation is the overproduction of the defense signaling molecule SA as a consequence of the up-regulation of the SA biosynthetic gene, *SID2*. A constellation of phenotypes, including elevated bacterial resistance, dwarfism, cell death lesions, and wrinkled leaves, could be either fully or partially suppressed by the null *sid2-1* mutation. Using this approach, we also identified consequences of nuclear defects that are independent of SA signaling, such as reduced plant stature, abnormal seed shape, and a baseline level of cell death.

Synthesizing our findings, we propose two models (Fig. 5) to explain this complex response to altering nuclear structure in plants. The initiating event in both scenarios is the nuclear defect caused by genetic ablation of a subset of CRWN nuclear periphery proteins. In the first model (Fig. 5A), these defects lead to expression changes in vanguard genes, including *SID2*, which leads to SA production and secondary changes to the transcriptome as well as downstream effects on pathogen defense and plant morphology. Several mechanisms might be operating to disrupt gene expression, such as the direct involvement of CRWN proteins in transcriptional regulation (either as part of an NL or as free proteins; see below) or changes in three-dimensional positioning of genes. Support for the latter mechanism was recently reported for mouse embryonic stem cells, where changes in three-dimensional genome structure due to lamin deficiency led to altered gene expression patterns within LADs (Zheng et al., 2018).

Furthermore, an increase in trans- versus cis-chromosomal contacts was detected via Hi-C analysis of *crwn1* and *crwn4* mutants, suggesting that NL changes could reduce local looping interactions or alter other three-dimensional configurations important for transcriptional regulation in interphase plant nuclei (Grob et al., 2014).

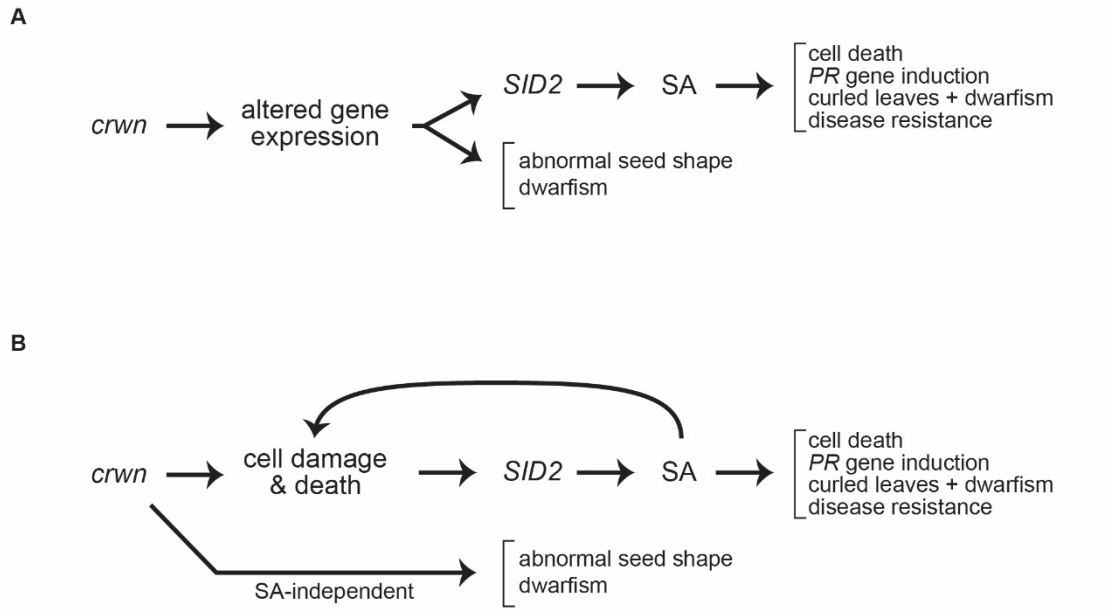

Figure 2.5. Two models to explain how *crwn* mutations affect disease signaling and other phenotypes. A, The first model posits that *crwn* mutations lead to transcriptional changes via the disruption in the direct action of CRWN proteins or epigenetic mechanisms (e.g. through changes in chromatin modification or three-dimensional genomic configuration). In this first model, overexpression of *SID2* and subsequent SA accumulation lead to pathogen defense phenotypes and an LMM syndrome. B, In the alternative model, cell damage and/or death due to nuclear dysfunction is the primary effect of *crwn* mutations. Downstream effects of age-dependent cell damage/death are amplified via an SA-mediated pathway, but an SA-independent pathway also mediates developmental defects.

More localized changes in chromatin could also play a role, mirroring the direct effects that the nuclear periphery exerts on histone modification or chromatin-mediated silencing in animals and fungi (Harr et al., 2015; Harr et al., 2016). Recent work from Schubert and colleagues in Arabidopsis demonstrated a physical and functional connection between CRWN1 and PWWP INTERACTORS OF POLYCOMBS1 (PWO1), a protein associated with the Polycomb Repressive Complex 2 responsible for H3K27 methylation (Mikulski et al., 2019). This mechanism is consistent with our observation that loci packaged in chromatin state 2, featuring both active and repressive (e.g. histone H3K27me3) epigenetic marks, are overrepresented among up-regulated genes in *crwn* mutants (Supplemental Fig. S4). This result, however, could also reflect the fact that SA-modulated genes tend to be packaged in chromatin state 2; approximately 40% of genes overexpressed in response to SA contained at least one domain of state 2 chromatin (relative to the expected occurrence of approximately 25%;

Supplemental Fig. S12). We investigated the possible role of H3K27me3 regulation via chromatin immunoprecipitation (ChIP)/qPCR experiments in different *crwn* genotypes, using the SA-regulated locus *PR1*, as well as *AGAMOUS* (*AG*) as a control locus. *AG* is a well-known target of H3K27me3 repression that is not known to be regulated by SA (Zhang et al., 2007). As shown in Supplemental Figure S13, we observed a trend toward reduced H3K27me3 modification at the *PR1* locus in *crwn1 crwn2* mutants (below the cutoff for significance) but no change in *crwn1* mutants. These results are consistent with the increase in *PR1* expression in the double but not the single mutant. These findings could be interpreted as evidence that histone H3K27me3 changes, mediated by the loss of CRWN proteins, play a role in *PR1* gene induction, but it is possible that chromatin modification changes lie downstream of SA-modulated transcription. It is important to note that the ultimate targets of misregulation in *crwn* mutants are genes in the chromosome arms, rather than the heterochromatic regions surrounding the centromere or TEs (Fransz et al., 2002). Our results are supported by previous findings from Poulet et al. showing that *crwn1 crwn2* mutants do not induce transcription of transposons, such as TSI, or centromeric repeats (Poulet et al., 2017).

The second model (Fig. 5B) does not invoke a role for CRWN proteins or nuclear organization in transcriptional control; rather, it posits that the cascade of transcriptional changes lies downstream of cell death or cell damage perception caused by nuclear defects (e.g. leakage (Denais et al., 2016) or abnormal connection to the cytoskeleton). This model explains the age-dependent effects seen in *crwn* mutants, in which gene expression changes and the incidence of cell death lesions progress in their intensity over time, as a consequence of accumulated cell damage and death. In the second model, SA production lies downstream of this damage and cell death and leads to an amplification and proliferation of cell death in a feed-forward manner. Key support for this model is the low incidence of cell death in the absence of induced SA production in the *sid2 crwn1 crwn2* mutant (Fig. 3C). This result suggests that age-

dependent cell death/damage precipitated by nuclear changes initiates the subsequent SA-dependent lesion-mimic syndrome, with its characteristic dwarfing, wrinkled leaves, and *PR* gene induction. The age-dependent effects seen in *crwn* mutants are consistent with the types of progressive changes in nuclear structure that are associated with both natural aging as well as progeria syndromes caused by human laminopathies (Scaffidi and Misteli, 2006).

Several recent publications shed light on these models and highlight the importance of the plant nucleus in defense signaling. Most relevant is a recently published study claiming that CRWN1 acts as a corepressor, with NAC WITH TRANSMEMBRANE MOTIF1-LIKE9 (NTL9), of *PR* genes (Guo et al., 2017). These data support aspects of the transcriptional control model (Fig. 5A) in which CRWN proteins can play a direct role in transcriptional regulation. However, this specific corepressor activity for CRWN1 with NTL9 fails to explain the up-regulation of *SID2*, as NTL9 is an activator of this SA biosynthetic locus (Zheng et al., 2015). An alternative possibility is that CRWN1 interacts with NTL9 to block its activation of *SID2* by sequestering the transcription factor at the nuclear periphery. We note that Guo et al. did not observe a spike in SA production in *crwn1 crwn2* mutants (Guo et al., 2017), which we demonstrate here (Fig. 4), an observation that can account for *PR* gene induction as well as the broader changes in gene expression and the elevated bacterial pathogen resistance exhibited by these mutants. The increase in SA levels in *crwn* double mutants can also explain the observed induction of reactive oxygen species recently noted by Wang et al., which they associated with their independent observation of the elevated level of cell death (Wang et al., 2019).

The role of the nuclear structure in defense signaling has also been brought into focus by studies showing that plant nucleoporins play important roles. For example, Gu et al. demonstrated that *CONSTITUTIVE EXPRESSION OF PR GENES5* (*CPR5*; Bowling et al., 1997), long known for its roles in systemic acquired resistance, is a nucleoporin that regulates the release of cyclin-dependent kinase inhibitors and the transport of signaling complexes (Gu

et al., 2016). Furthermore, they showed that *cpr5* mutants, which are LMMs exhibiting spontaneous defense response, have round nuclei similar to those of *crwn* mutants. These findings suggest that the nuclear structural changes that occur in *cpr5* and *crwn* mutants might be mechanistically related. For instance, defects at the nuclear periphery could alter the organization or activity of nuclear pore complexes (Al-Haboubi et al., 2011; Guo et al., 2014). Other recent work points to nuclear pores as a site of defense signaling in plants. Tamura et al. (2017) reported that the nucleoporin mutant *nup136* shows compromised resistance against DC3000, while Gu et al. (2016) suggested that the same mutants have enhanced effector-triggered immunity resistance against another bacterial pathogen (*Psm/AvrRpt2*). Although these two studies suggest different roles of this particular nucleoporin, it is now indisputable that components at the nuclear periphery participate in regulation of plant defense responses.

MATERIALS AND METHODS

Plant materials and growth conditions

Arabidopsis (*Arabidopsis thaliana*) plants were grown on MetroMix 360 soil (Sun Gro Horticulture) under long-day conditions (16 h of light/8 h of dark) at approximately 22°C in environmental growth chambers after 2 d of stratification in a 4°C cold room. All genotypes are in the Columbia background. The *crwn* mutant material used was described by Wang et al. (2013); the original allele sources are *crwn1* (SALK_025347), *crwn2* (SALK_076653), and *crwn4* (SALK_079296RP), which were acquired from the Arabidopsis Biological Resource Center at Ohio State University. The *sid2-1* mutant material originated from the Metraux group (Nawrath and Metraux, 1999). The *sid2-1 crwn1 crwn2* triple mutants were generated by crossing *sid2-1* (♀) mutants to *crwn1 crwn2* (♂) mutants and subsequent segregation. The genotypes of all the mutants used in this study were identified by PCR amplification with primers listed below and reference to marker polymorphisms (Supplemental Table S5).

RNA-seq and bioinformatic analysis

Three biological replicates from each genotype were used for RNA-seq (National Center for Biotechnology Information [NCBI] SRA BioProject ID PRJNA485018). Rosette leaves from 4-week-old adult plants were used to extract total RNA using TRIzol reagent (Thermo Fisher Scientific) and further purified with the Qiagen RNeasy kit. RNA samples were processed by the Genomic Core Facility at Cornell's Weill Medical School using a standard Illumina protocol to construct single-stranded mRNA libraries. The Illumina Hi-Seq 2000 platform was used for the sequencing. The resulting 51 nucleotide reads were analyzed using the Tuxedo Suite software (Trapnell et al., 2012). Briefly, Bowtie2 (v. 2.2.2) and Tophat2 (v. 2.1.1) were used to build an index for the TAIR10 Arabidopsis genome to map RNA-seq reads and to identify splice junctions between exons (Arabidopsis_Genome_Initiative, 2000; Langmead et al., 2009; Kim et al., 2013). Finally, Cufflinks (v. 2.2.1) was used to calculate differential gene expression (Trapnell et al., 2010). GO term analysis was conducted using PANTHER (Mi et al., 2017). The overrepresentation test (released July 15, 2016) was performed with misregulated gene sets against the annotation data set GO biological process complete (GO ontology database released November 30, 2016). Note that the numbers of genes listed for the different GO terms in Table 1 do not match the values in the Venn diagrams in Figure 1 and Supplemental Figure S1 because not all genes in our data set are assigned GO terms in the PANTHER database.

Venn diagrams for all five genotypes in Supplemental Figure S1 were generated using InteractiVenn (Heberle et al., 2015).

For TE analysis, STAR (v. 2.5.3a_modified) was used for index building and read mapping (Dobin et al., 2013). Mapping employed -winAnchorMultimapNmax 100 and -outFilterMultimapNmax 100 options. Next, TEtranscripts (v. 1.5.1) was used to analyze TE expression in alignment files from the STAR output (Jin et al., 2015). The annotation GFF3 file

for genes was obtained from TAIR10 and converted to GTF by gffread (Trapnell et al., 2010) with -FTo option. The TE annotation file was provided by the Hammell lab (http://labshare.cshl.edu/shares/mhammelllab/www-data/TEToolkit/TE_GTF/). The GTF file from the Hammell lab grouped TEs by family name. We also modified this file so that reads could be mapped to individual TEs. Read count tables produced by TEtranscripts were analyzed by DESeq2 (Love et al., 2014).

For the comparison between SA-treated wild type and *crwn* mutants, microarray data from 23-d-old wild-type plants sampled 3 h after 1 mm SA treatment (GSM1496067, 1496075, and 1496083) and water-treated controls (GSM1496065, 1496073, and 1496081) were obtained from the NCBI Gene Expression Omnibus database (series no. GSE61059; (Zhou et al., 2015)). Genes misregulated more than 2-fold with adjusted $P < 0.05$ were screened with GEO2R using default options (Edgar et al., 2002; Barrett et al., 2013). The resulting list of misregulated microarray elements were converted to locus identifiers by TAIR Microarray Elements Search and Download tool. These genes were compared with our RNA-seq data from the *crwn* mutants.

Our chromatin state analysis was based on the study by Sequeira-Mendes et al. (2014) of the epigenetic landscape of the wild-type Arabidopsis genome. We overlapped chromatin states of Arabidopsis genomes onto misregulated genes in *crwn* mutants by using Intersect the intervals of two data sets under the Operate on Genomic Intervals tool in Galaxy (Afgan et al., 2016). Minimum overlapping was set as 200 bp, which is the length of a nucleosome. Because of this overlapping definition, one gene can exist as more than two states.

To examine the distribution of misregulated genes across the genome, chromosomal maps were drawn based on the Columbia reference genome sequence (TAIR10) with the genoPlotR package (Guy et al., 2010). Pericentromeric regions were marked based on Stroud et al. (2013). Genes depicted on the map are the same as the ones used to draw the Venn diagrams in Figure 1 and Supplemental Figure S1.

Pseudomonas syringae DC3000 bacterial growth assays

DC3000 was grown on King's B medium (20 g L^{-1} Proteose Peptone no. 3, 10 mL L^{-1} glycerol, 0.4 g L^{-1} $MgSO_4$, 1.5 g L^{-1} K_2HPO_4, and 18 g L^{-1} agar) containing 50 μg mL^{-1} rifampicin and 50 μg mL^{-1} kanamycin. Bacterial cells were collected and suspended in 10 mm $MgCl_2$ solution to a final concentration of 105 cells mL^{-1}. The abaxial sides of three fully expanded rosette leaves of 22-d-old plants were infiltrated with the bacterial suspension using a syringe without a needle. Four plants per genotype were used for biological replicates. Infected leaves were harvested 2 and 4 d after inoculation. For the set of infections investigating the effect of *sid2* mutations, only 0 and 2 d after inoculation were checked. Bacterial growth experiments were repeated multiple times, with each replicate showing a significant reduction of DC3000 growth in the *crwn* double mutants.

RNA extraction and RT-qPCR

Aboveground shoot material, excluding bolts and flowers, was harvested and frozen in liquid nitrogen. Frozen samples were ground using three metal beads or mortars and pestles. The E.Z.N.A. Plant RNA Kit (Omega Bio-tek) was used to extract total RNA, followed by DNase I (New England Biolabs) treatment. cDNA synthesis was performed with either the SuperScript III or SuperScript IV First-Strand Synthesis System (Thermo Fisher Scientific) using oligo(dT) primers. For the RT-qPCR, iTaq Universal SYBR Green Supermix (Bio-Rad) was used. Three biological replicates were tested (plant cohorts grown independently at separate times; one plant per sample), and each replicate consisted of at least three reactions per target gene. The size of amplicons was designed to be approximately 100 bp. A CFX 96 Real-Time System (Bio-Rad) mounted on a C1000 Thermal Cycler (Bio-Rad) was used to detect products. The results were analyzed using the Bio-Rad CFX Manager 3.1. software package.

Cell death lesion detection and imaging

Fully expanded rosette leaves were used for cell death lesion analysis. Whenever possible, the fifth leaf that emerged from the meristem was used. However, similar patterns were found in all fully expanded leaves of similar size. Leaves were harvested and stained as described (van Wees, 2008). Briefly, leaves were immersed in 2.5 mg mL^{-1} Trypan Blue-lactophenol solution with 2 volumes of ethanol added. Samples were then boiled for 1 min and left on a shaker at room temperature for 2 to 3 h. Destaining was performed twice with 2.5 g mL^{-1} chloral hydrate solution. Final samples were stored with 70% (v/v) glycerol and observed with a Leica DM5500B microscope with 10× magnification to check stained foci.

SA extraction and HPLC/MS analysis

Extraction of SA was performed as indicated in the protocol from Stingl et al. (2013) with slight modifications. Briefly, leaves were frozen in liquid nitrogen and ground using metal beads. Samples were suspended with 950 µL of ethylacetate:formic acid solution (99:1, v/v). To make the d4-SA internal control solution, d6-SA (#616796; Sigma-Aldrich) was dissolved in methanol. Fifty microliters of 7.5 ng μL^{-1} d4-SA solution was added to the sample as an internal control. Nine hundred microliters of the supernatants was isolated, and solvents were evaporated with a SpeedVac concentrator (Savant ISS110; Thermo Scientific). The final residues were dissolved in 100 µL of acetonitrile:water (1:1, v/v) solution and filtered with a 0.45-µm MultiScreen HTS HV Filter Plate (MSHVN4510; Millipore).

The analytical reverse-phase separation was performed with a Dionex Ultimate 3000 Series LC system with a Titan C18 UHPLC Column (7.5 cm × 2.1 mm, 1.9 µm; Sigma-Aldrich) at 40°C. The flow rate was set at 0.5 mL min−1. The starting condition was 95% solvent A (0.1% [v/v] formic acid in water) and 5% solvent B (acetonitrile) for 0.5 min, rising to 95% B at 19

min, held for 1 min, followed by 2 min of reequilibration at the starting condition. The separation was sent to an Orbitrap Q-Exactive mass spectrometer (Thermo Fisher Scientific) equipped with a HESI-II heated electrospray ionization source. Samples were analyzed in triplicate under a negative spray mode: voltage, 3,500 V; capillary and auxiliary gas heater temperatures, 300°C; sheath, auxiliary, and sweep gas flow rates of 70, 10, and 5, respectively (arbitrary units). The data were acquired under full-scan mass spectra in mass-to-charge ratio range of 100 to 600, 140,000 full width at half maximum resolution (at mass-to-charge ratio = 200), AGC target 1e6, and maximum injection time of 200 ms.

Nuclear morphology phenotyping

We observed nuclear morphology in anther filament cells, which are nonpigmented and contain elongated, endopolyploid nuclei in wild-type plants (Dittmer et al., 2007). Anther filaments were fixed with ethanol:acetic acid solution (3:1, v/v) for 10 min, followed by exposure to 10 μg mL^{-1} 4′,6-diamidino-2-phenylindole staining solution for 15 to 30 s. Samples were immersed in distilled water for 1 min and then observed with an epifluorescence microscope (DM5500; Leica).

ChIP

ChIP was performed based on the protocol from Yamaguchi et al. (2014) with the following modifications. Anti-H3K27me3 antibodies were purchased from Abcam (catalog no. ab6002). Vacuum infiltration of formaldehyde solution was adjusted to 6 min followed by 4 min of incubation on ice. This procedure was repeated three times. Vacuum infiltration of Gly solution was modified to 5 min. Sonication was applied with a Bioruptor UCD-200 (Diagenode) for 30 s with the high-intensity option followed by 30 s of pause; this 1-min cycle was repeated 15 times. For preclearing and immunoprecipitation capture, 45 μL of Dynabeads Protein A

(ThermoFisher) was used. To purify the resulting ChIP DNA, the ChIP DNA Clean & Concentrator Kit (Zymo) was used. qPCR was performed as described for our RT-qPCR analysis. Primers are listed in Supplemental Table S5.

Accession numbers

Locus identifiers of genes investigated in this study include AT1G67230 (*CRWN1*), AT1G13220 (*CRWN2*), AT1G68790 (*CRWN3*), AT5G65770 (*CRWN4*), AT1G74710 (*ICS1/SID2*), AT2G14610 (*PR1*), AT3G57260 (*PR2*), AT1G75040 (*PR5*), AT4G38740 (*ROC1*), AT5G09810 (*ACT7*), and AT4G18960 (*AG*). The RNA-seq data described here are available through NCBI (SRA BioProject ID PRJNA485018).

SUPPLEMENTAL DATA

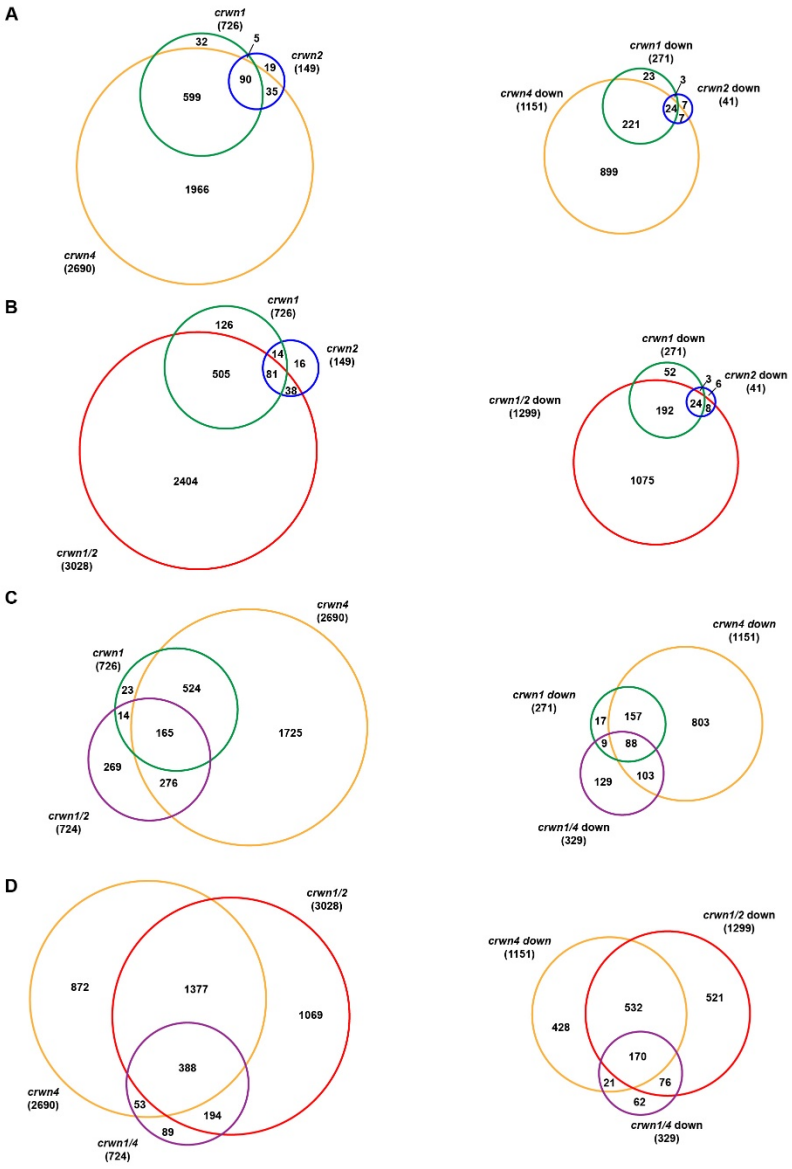
A
crwn1
(726)
32
5
19
90
35
599
crwn2
(149)
1966
crwn4
(2690)
crwn1 down
(271)
23
3
crwn4 down
(1151)
crwn2 down
(41)
24
7
7
221
899
B
crwn1
(726)
126
14
16
crwn2
(149)
81
38
505
2404
crwn1/2
(3028)
crwn1 down
(271)
52
3
6
crwn2 down
(41)
crwn1/2 down
(1299)
24
8
192
1075
C
crwn4
(2690)
crwn1
(726)
23
524
14
165
1725
269
276
crwn1/2
(724)
crwn4 down
(1151)
crwn1 down
(271)
17
157
803
9
88
129
103
crwn1/4 down
(329)
D
crwn1/2
(3028)
872
1377
1069
388
crwn4
(2690)
53
194
89
crwn1/4
(724)
crwn1/2 down
(1299)
crwn4 down
(1151)
532
521
428
170
21
76
62
crwn1/4 down
(329)

E

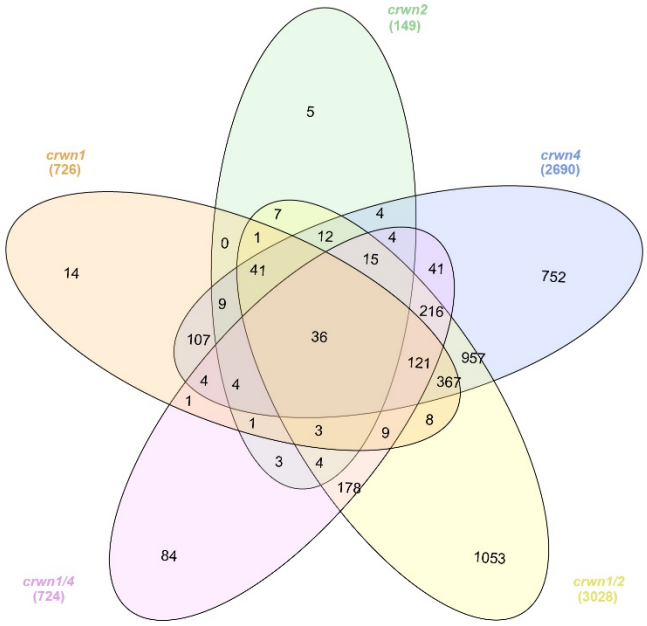
crwn2
(149)
crwn1
(726)
crwn4
(2690)
crwn1/4
(724)
crwn1/2
(3028)
5
14
752
84
1053
7
4
0
1
12
4
15
41
41
9
216
107
36
121
957
4
4
367
1
1
3
9
8
3
4
178

F

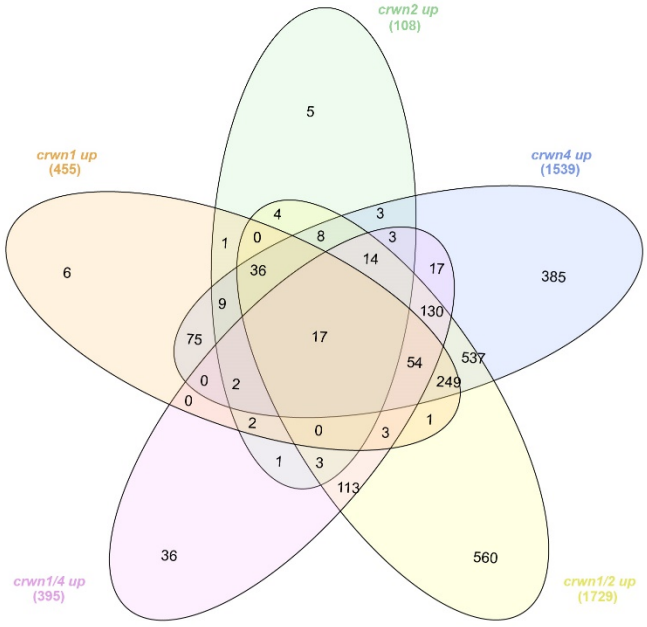
crwn2 up
(108)
crwn1 up
(455)
crwn4 up
(1539)
crwn1/4 up
(395)
crwn1/2 up
(1729)
5
6
385
36
560
4
3
1
0
8
3
14
17
36
9
130
75
17
54
537
0
2
249
0
2
0
3
1
1
3
113

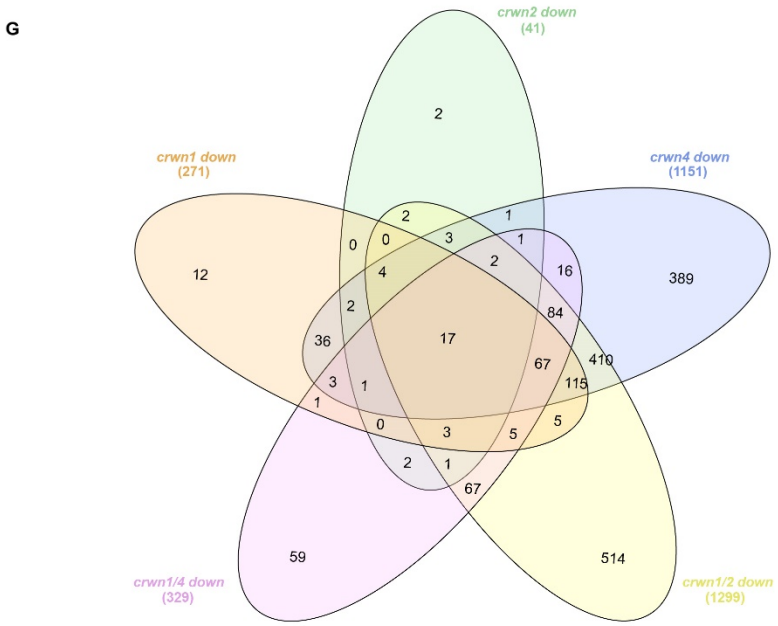

Supplemental Figure S1. Mutations in *Arabidopsis thaliana CRWN* genes result in widespread changes in transcript levels. The size of each circle in the Venn diagrams shown in panels A - D is proportional to the number of genes that are mis-regulated (either up- or down-regulated at least two-fold) (as in Fig. 1, $q < 0.01$). In A - D, the left column includes the entire set of mis-regulated genes, while down-regulated genes are shown in the right column (see Fig. 1 for up-regulated genes). A, Venn diagrams show the relationship of mis-regulated genes in three *crwn* single mutants, *crwn1*, *crwn2* and *crwn4*. B, Venn diagrams of mis-regulated genes in the double mutant *crwn1 crwn2* and the corresponding single mutants, *crwn1* and *crwn2*, showing a synergistic effect. C, Venn diagrams of mis-regulated genes in the double mutant *crwn1 crwn4* and corresponding single mutants, *crwn1* and *crwn4*, showing an antagonistic relationship between *crwn1* and *crwn4*. D, Venn diagrams of mis-regulated genes in two double mutants, *crwn1 crwn2* and *crwn1 crwn4*, as well as the *crwn4* single mutant, illustrating the overlap in transcriptomic profiles between *crwn4* mutants and the two double mutants. In E - G, all five mutants are incorporated in each Venn diagram. E, mis-regulated genes; F, up-regulated genes; and G, down-regulated genes.

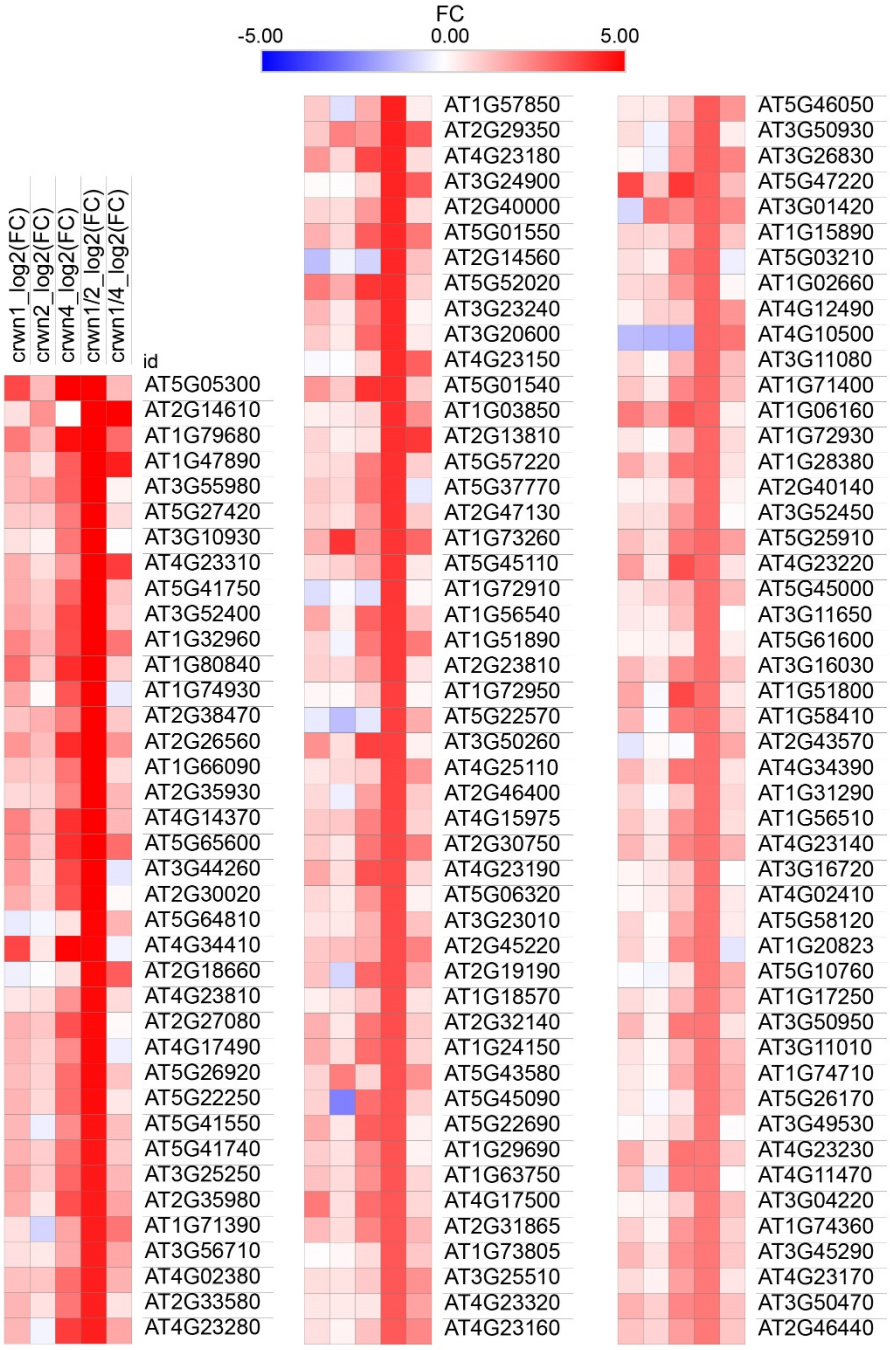
FC
-5.00
0.00
5.00
crwn1_log2(FC)
crwn2_log2(FC)
crwn4_log2(FC)
crwn1/2_log2(FC)
crwn1/4_log2(FC)
id
AT5G05300
AT2G14610
AT1G79680
AT1G47890
AT3G55980
AT5G27420
AT3G10930
AT4G23310
AT5G41750
AT3G52400
AT1G32960
AT1G80840
AT1G74930
AT2G38470
AT2G26560
AT1G66090
AT2G35930
AT4G14370
AT5G65600
AT3G44260
AT2G30020
AT5G64810
AT4G34410
AT2G18660
AT4G23810
AT2G27080
AT4G17490
AT5G26920
AT5G22250
AT5G41550
AT5G41740
AT3G25250
AT2G35980
AT1G71390
AT3G56710
AT4G02380
AT2G33580
AT4G23280
AT1G57850
AT2G29350
AT4G23180
AT3G24900
AT2G40000
AT5G01550
AT2G14560
AT5G52020
AT3G23240
AT3G20600
AT4G23150
AT5G01540
AT1G03850
AT2G13810
AT5G57220
AT5G37770
AT2G47130
AT1G73260
AT5G45110
AT1G72910
AT1G56540
AT1G51890
AT2G23810
AT1G72950
AT5G22570
AT3G50260
AT4G25110
AT2G46400
AT4G15975
AT2G30750
AT4G23190
AT5G06320
AT3G23010
AT2G45220
AT2G19190
AT1G18570
AT2G32140
AT1G24150
AT5G43580
AT5G45090
AT5G22690
AT1G29690
AT1G63750
AT4G17500
AT2G31865
AT1G73805
AT3G25510
AT4G23320
AT4G23160
AT5G46050
AT3G50930
AT3G26830
AT5G47220
AT3G01420
AT1G15890
AT5G03210
AT1G02660
AT4G12490
AT4G10500
AT3G11080
AT1G71400
AT1G06160
AT1G72930
AT1G28380
AT2G40140
AT3G52450
AT5G25910
AT4G23220
AT5G45000
AT3G11650
AT5G61600
AT3G16030
AT1G51800
AT1G58410
AT2G43570
AT4G34390
AT1G31290
AT1G56510
AT4G23140
AT3G16720
AT4G02410
AT5G58120
AT1G20823
AT5G10760
AT1G17250
AT3G50950
AT3G11010
AT1G74710
AT5G26170
AT3G49530
AT4G23230
AT4G11470
AT3G04220
AT1G74360
AT3G45290
AT4G23170
AT3G50470
AT2G46440

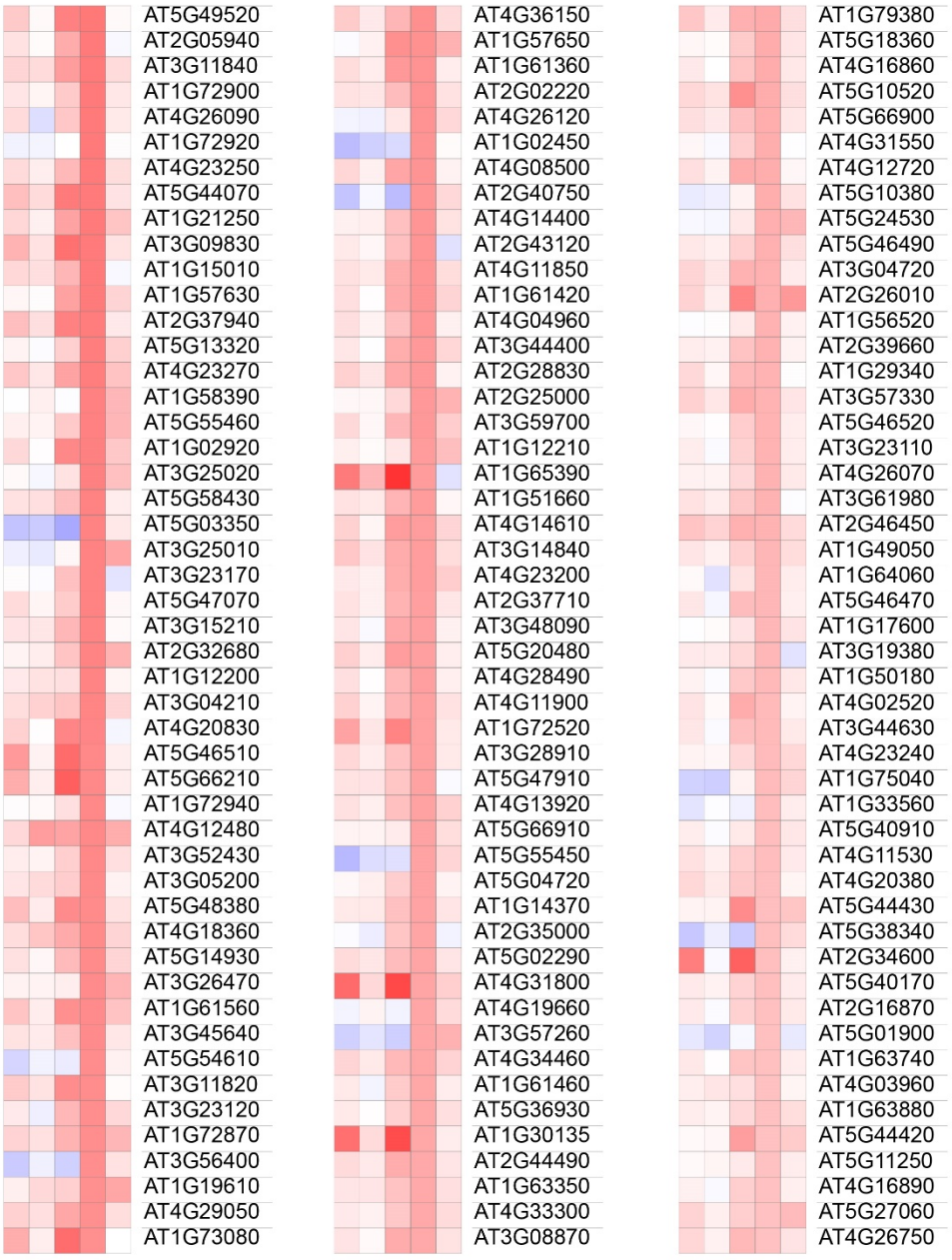
AT5G49520
AT2G05940
AT3G11840
AT1G72900
AT4G26090
AT1G72920
AT4G23250
AT5G44070
AT1G21250
AT3G09830
AT1G15010
AT1G57630
AT2G37940
AT5G13320
AT4G23270
AT1G58390
AT5G55460
AT1G02920
AT3G25020
AT5G58430
AT5G03350
AT3G25010
AT3G23170
AT5G47070
AT3G15210
AT2G32680
AT1G12200
AT3G04210
AT4G20830
AT5G46510
AT5G66210
AT1G72940
AT4G12480
AT3G52430
AT3G05200
AT5G48380
AT4G18360
AT5G14930
AT3G26470
AT1G61560
AT3G45640
AT5G54610
AT3G11820
AT3G23120
AT1G72870
AT3G56400
AT1G19610
AT4G29050
AT1G73080
AT4G36150
AT1G57650
AT1G61360
AT2G02220
AT4G26120
AT1G02450
AT4G08500
AT2G40750
AT4G14400
AT2G43120
AT4G11850
AT1G61420
AT4G04960
AT3G44400
AT2G28830
AT2G25000
AT3G59700
AT1G12210
AT1G65390
AT1G51660
AT4G14610
AT3G14840
AT4G23200
AT2G37710
AT3G48090
AT5G20480
AT4G28490
AT4G11900
AT1G72520
AT3G28910
AT5G47910
AT4G13920
AT5G66910
AT5G55450
AT5G04720
AT1G14370
AT2G35000
AT5G02290
AT4G31800
AT4G19660
AT3G57260
AT4G34460
AT1G61460
AT5G36930
AT1G30135
AT2G44490
AT1G63350
AT4G33300
AT3G08870
AT1G79380
AT5G18360
AT4G16860
AT5G10520
AT5G66900
AT4G31550
AT4G12720
AT5G10380
AT5G24530
AT5G46490
AT3G04720
AT2G26010
AT1G56520
AT2G39660
AT1G29340
AT3G57330
AT5G46520
AT3G23110
AT4G26070
AT3G61980
AT2G46450
AT1G49050
AT1G64060
AT5G46470
AT1G17600
AT3G19380
AT1G50180
AT4G02520
AT3G44630
AT4G23240
AT1G75040
AT1G33560
AT5G40910
AT4G11530
AT4G20380
AT5G44430
AT5G38340
AT2G34600
AT5G40170
AT2G16870
AT5G01900
AT1G63740
AT4G03960
AT1G63880
AT5G44420
AT5G11250
AT4G16890
AT5G27060
AT4G26750

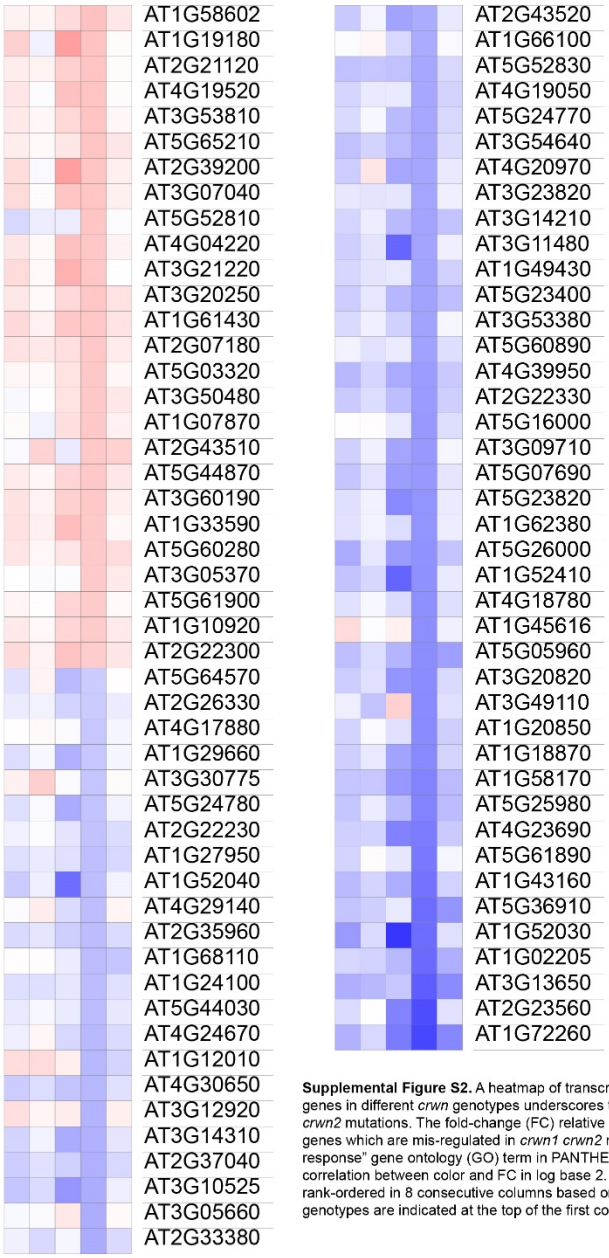

Supplemental Figure S2. A heatmap of transcript level differences of a subset of mis-regulated genes in different *crwn* genotypes underscores the synergy among the effects of the *crwn1* and *crwn2* mutations. The fold-change (FC) relative to the wild-type sample is depicted for 373 genes which are mis-regulated in *crwn1 crwn2* mutants and grouped under the "defense response" gene ontology (GO) term in PANTHER. The legend at the top indicates the correlation between color and FC in log base 2. Gene loci identifiers are indicated and rank-ordered in 8 consecutive columns based on FC in the *crwn1 crwn2* samples. The genotypes are indicated at the top of the first column on the left.

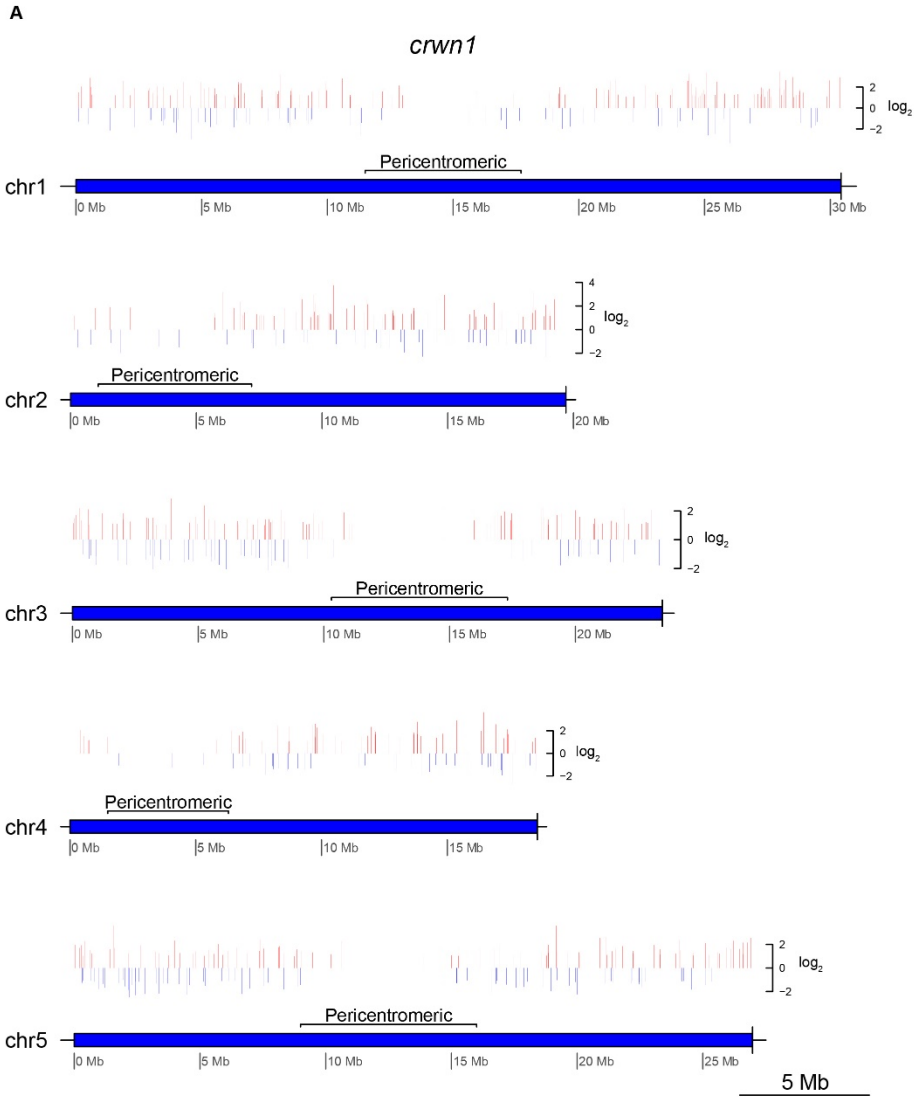
A
crwn1
log2
Pericentromeric
chr1
0 Mb
5 Mb
10 Mb
15 Mb
20 Mb
25 Mb
30 Mb
chr2
chr3
chr4
chr5
5 Mb

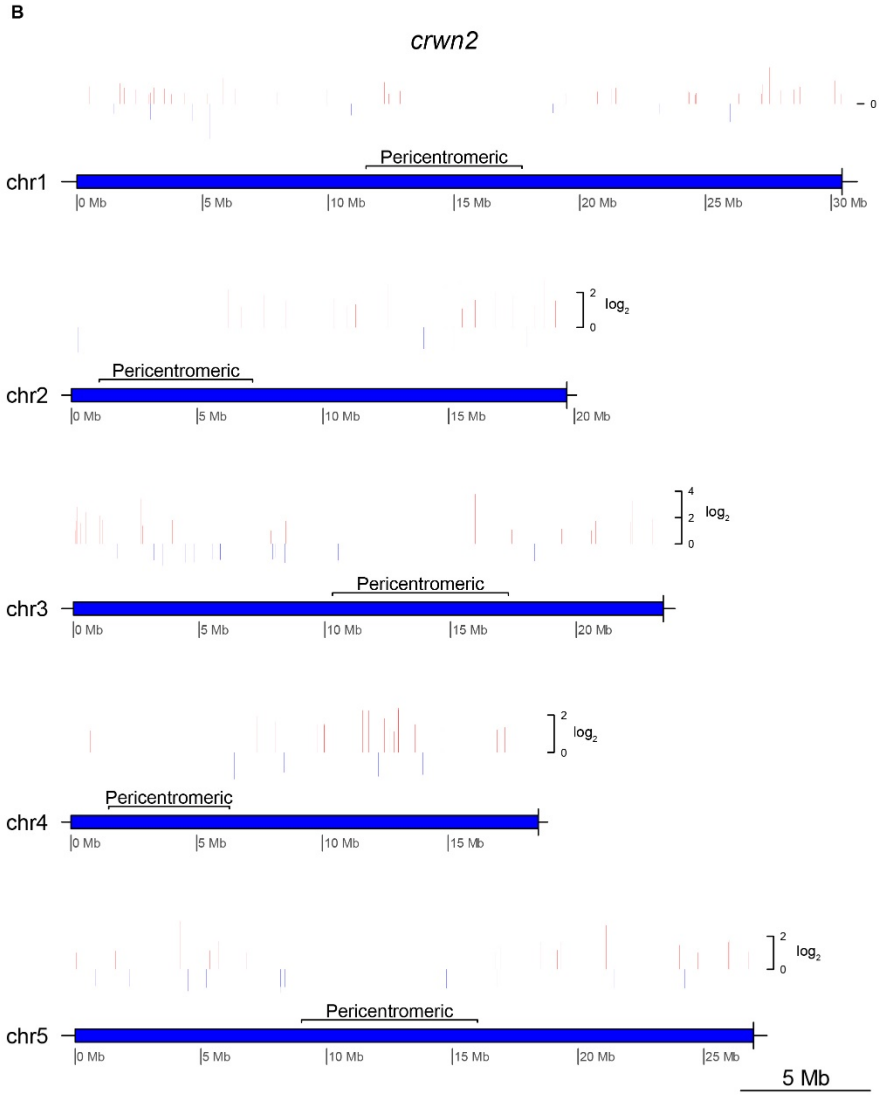
B
crwn2
log2
Pericentromeric
chr1
0 Mb
5 Mb
10 Mb
15 Mb
20 Mb
25 Mb
30 Mb
chr2
chr3
chr4
chr5
5 Mb

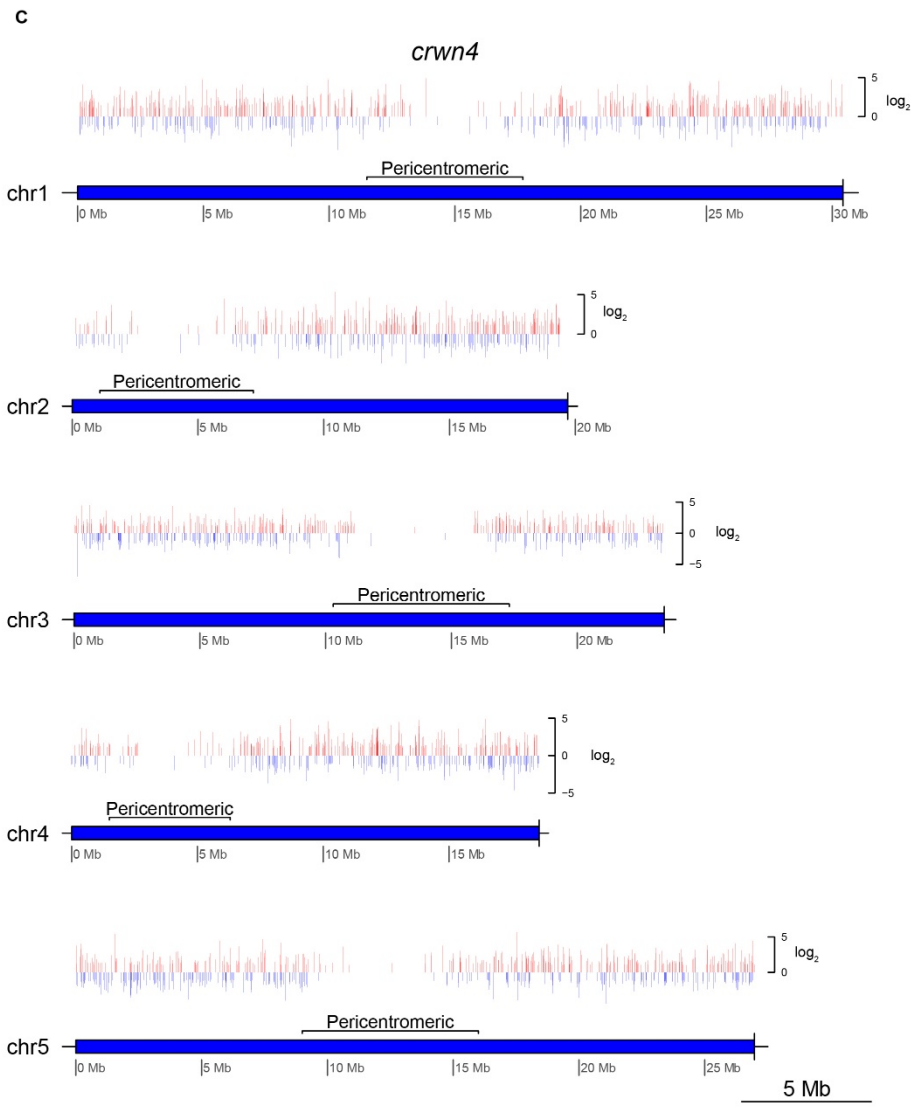
c
crwn4
log2
5
0
Pericentromeric
chr1
0 Mb
5 Mb
10 Mb
15 Mb
20 Mb
25 Mb
30 Mb
chr2
chr3
−5
chr4
chr5
5 Mb

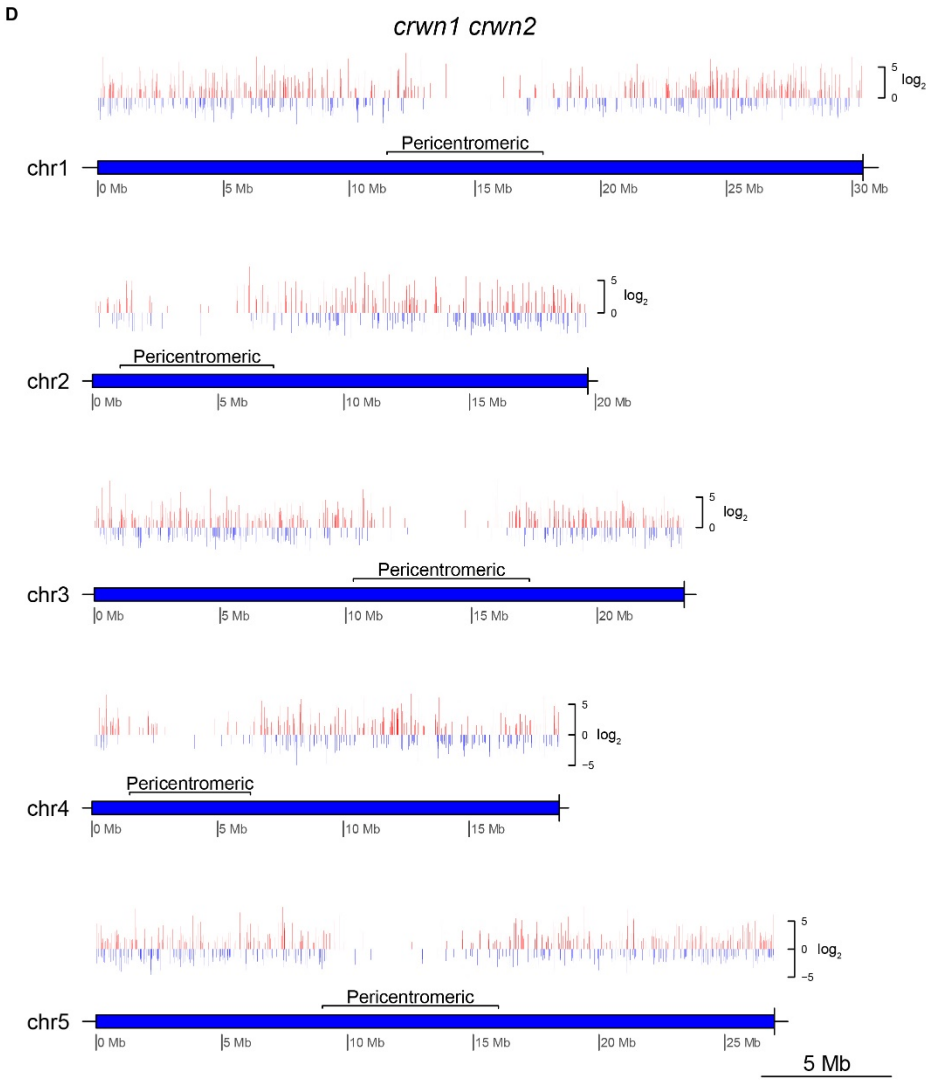
D
crwn1 crwn2
5
0
log2
Pericentromeric
chr1
0 Mb
5 Mb
10 Mb
15 Mb
20 Mb
25 Mb
30 Mb
chr2
chr3
chr4
chr5
−5
5 Mb

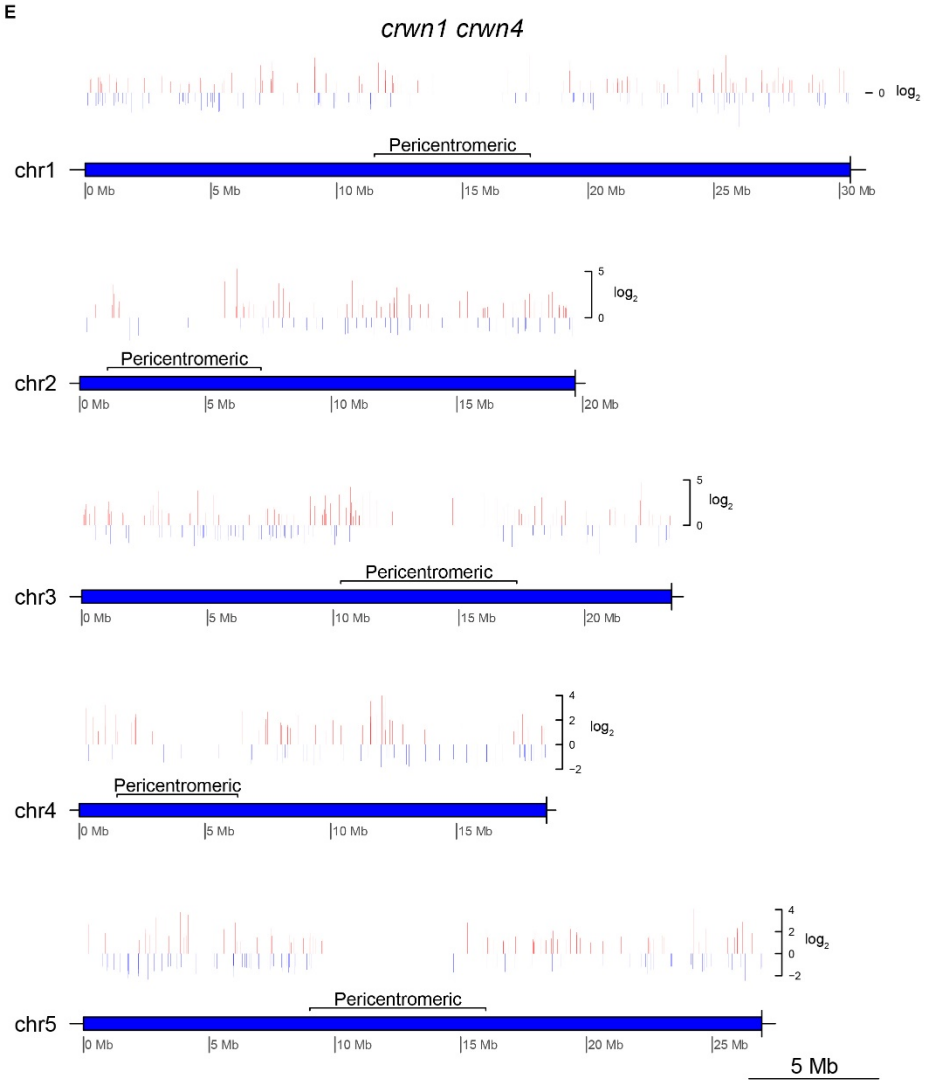

Supplemental Figure S3. Mis-regulated genes are distributed evenly across the chromosome arms. Each vertical bar above the chromosomes represents one gene at its genomic position; the height of the bar indicates the direction and magnitude of mis-regulation relative to wild type. The loci shown here correspond to list of mis-regulated genes represented in Fig.1 and Supplemental Fig. S1. Maps for *crwn1* (A), *crwn2* (B), *crwn4* (C), *crwn1 crwn2* (D) and *crwn1 crwn4* (E) mutants are shown. The position of the pericentromeric domains encompassing the centromere are indicated.

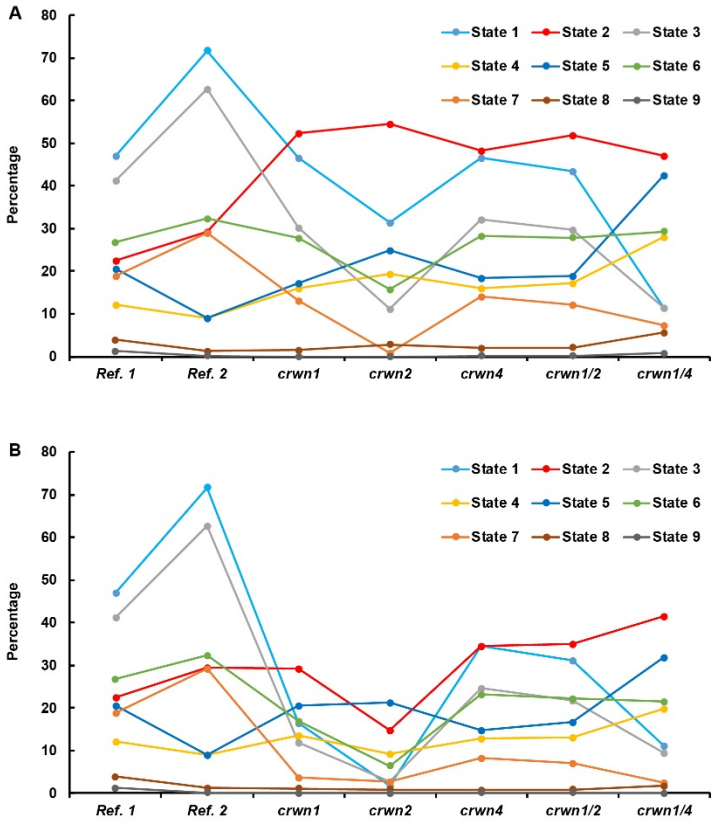

Supplemental Figure S4. Chromatin states of genes mis-regulated in each *crwn* mutant are shown. Note that sum of percentage of each chromatin state in one genotype can add up to more than 100 percent because one gene can have multiple domains with different chromatin states. Reference 1 (Ref. 1) indicates the ratio of genes, relative to all genes in *Arabidopsis thaliana* based on TAIR10 annotation, having at least one domain of each of the nine chromatin states defined by Sequeira-Mendes et al. (2014). Reference 2 (Ref. 2) indicates the ratio of genes with each chromatin state relative to all tested genes in our RNA-seq data. A, The representation of chromatin states among up-regulated genes in the indicated mutants. Note the over-representation of chromatin state 2, and the under-representation of states 1 and 3. B, The representation of chromatin states among down-regulated genes in the indicated mutants.

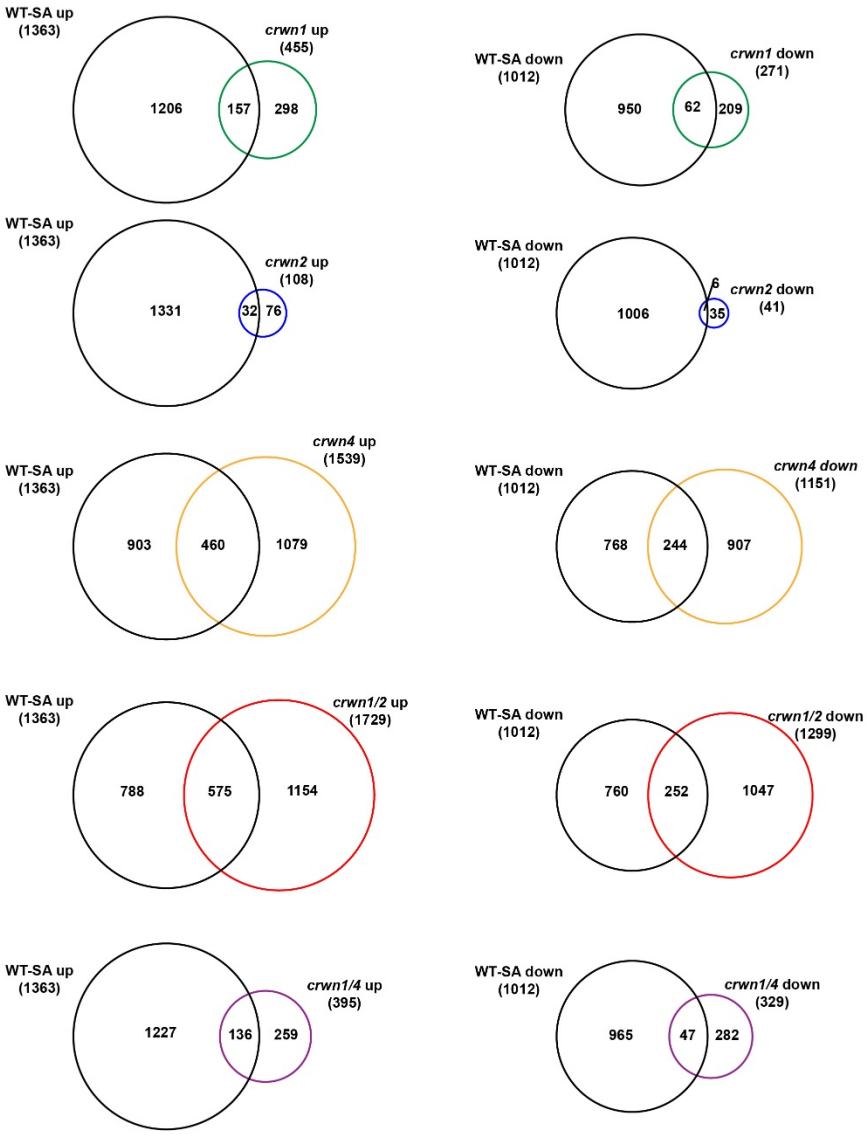

Supplemental Figure S5. Salicylic acid (SA)-regulated genes overlap with mis-regulated genes in *crwn* mutants. Microarray data (black circles on the left of each Venn diagram) show SA-regulated genes in 23-d-old wild-type (WT) plants sampled 3 h after 1mM SA treatment (Zhou *et al.*, 2015). Both up-regulated and down-regulated genes were compared to mis-regulated genes in each *crwn* mutant shown (colored circles on the right of each diagram). The mis-regulated genes in *crwn* mutants are identical to those in Fig. 1 and Supplemental Fig. S1.

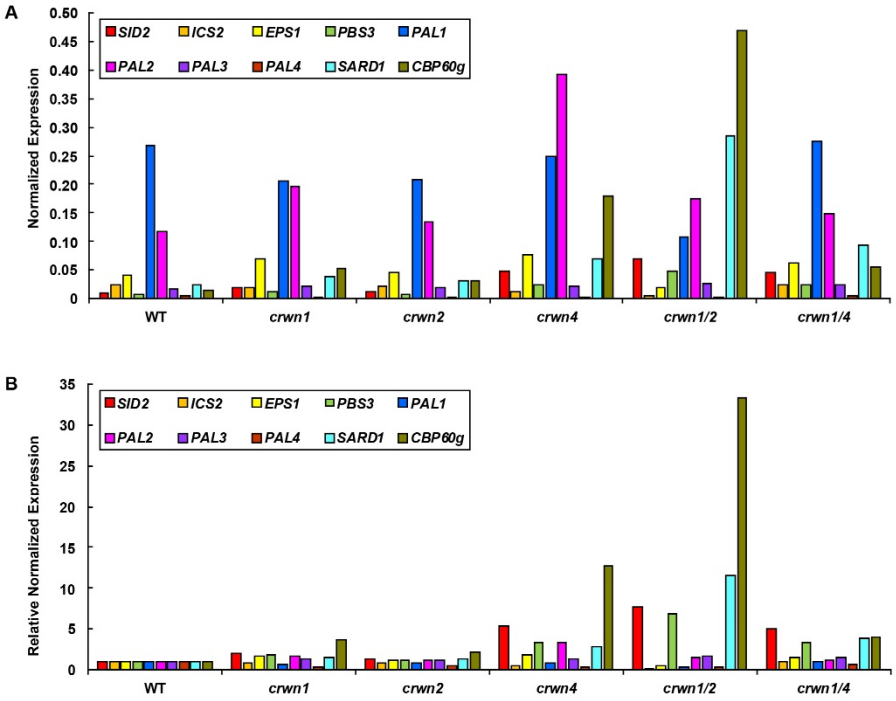

Supplemental Figure S6. RNA-seq data showing expression levels of salicylic acid (SA) biosynthesis genes and genes regulating SA biosynthesis genes. WT indicates wild type. A, Normalized expression levels of indicated genes in *crwn* mutants. RNA-seq profile in 'fragments per kilobase of transcript per million mapped reads' (FPKM) was normalized to cytosolic cyclophilin *ROC1* transcripts. B, Expression of the same genes were shown as relative normalized expression, where WT expression level is considered as 1-fold. Note that the over-expression of *SID2* observed in the *crwn4* RNA-seq data was not verified by RT-qPCR (see Fig. 4D); however, *SID2* over-expression was validated for the *crwn1 crwn2* and *crwn1 crwn4* mutants.

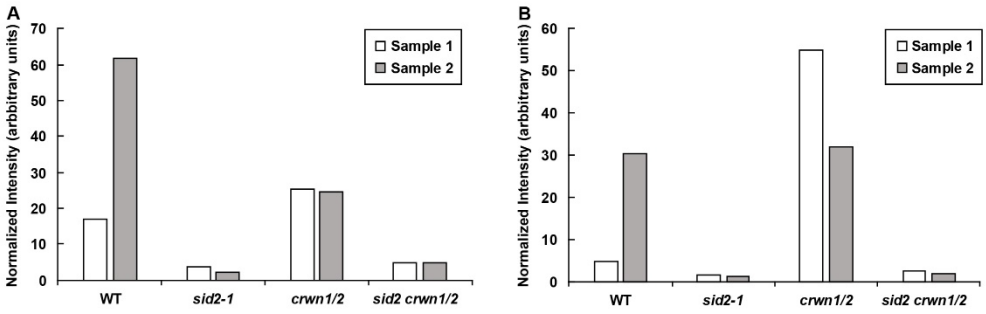

Supplemental Figure S7. HPLC/mass spectrometry data demonstrating that the *sid2-1* mutation diminishes both salicylic acid (SA) and glucosylated SA (SA-Glc) levels. Integrated peak intensity of free SA (A) and SA-Glc (B) was normalized to the recovery of the spiked internal control d4-SA. Note, that wild type (WT) SA levels in sample 2 should be considered an anomaly because of the low recovery level of the internal control, hence a higher level of SA was inferred after normalization.

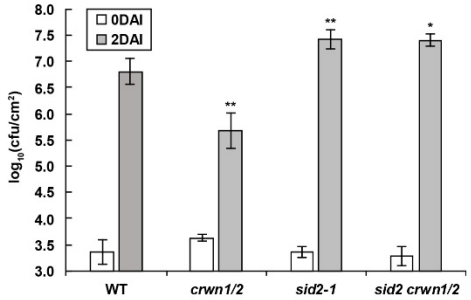

Supplemental Figure S8. The *sid2-1* mutation suppresses *Pseudomonas syringae* pathovar *tomato* strain DC3000 (DC3000) resistance in *crwn1 crwn2* mutants. Fully expanded rosette leaves of 22-d-old plants were inoculated with DC3000 and processed as explained for Fig. 2A. Error bars indicate SD (n = 3 for 0 DAI and n = 4 for 2 DAI). Student's t-tests (*P < 0.05 and **P < 0.01) were performed between each mutant and wild type (WT).

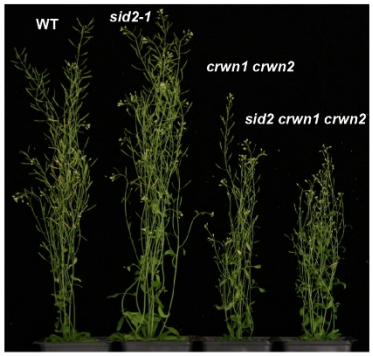

Supplemental Figure S9. The *sid2-1* mutation partially suppresses the rosette dwarfism of the *crwn1 crwn2* mutant while the length of the bolts are not affected. WT indicates wild type. A, The rosette size of *sid2 crwn1 crwn2* mutants is larger than *crwn1 crwn2* mutants at 23 d. B, The same plants shown at 30 d. Note that at 30 d, the *sid2 crwn1 crwn2* rosette is larger than *crwn1 crwn2* mutants, but smaller than WT or *crwn* single mutants. C, *sid2 crwn1 crwn2* mutants still retain dwarfism in bolt stature. Despite their slightly bigger size in rosette leaves, the length of bolts in *sid2 crwn1 crwn2* mutants are comparable to *crwn1 crwn2* mutants at 44 d.

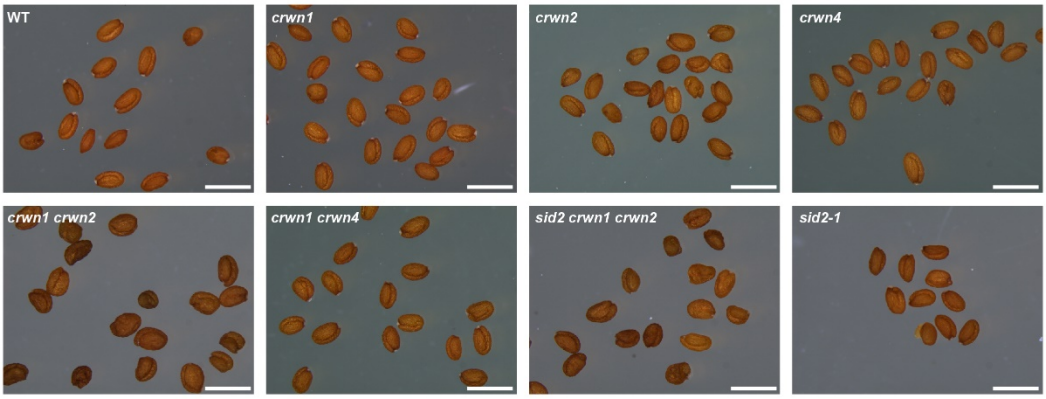

Supplemental Figure S10. *crwn1 crwn2* mutants exhibit abnormal seed shape, which is not suppressed by *sid2* mutations. WT indicates wild type. Note the elevated irregularity and variability of seed shape both *crwn1 crwn2* and *sid2 crwn1 crwn2* mutants. Images were taken with a Leica M205 stereomicroscope. Bar = 1 mm.

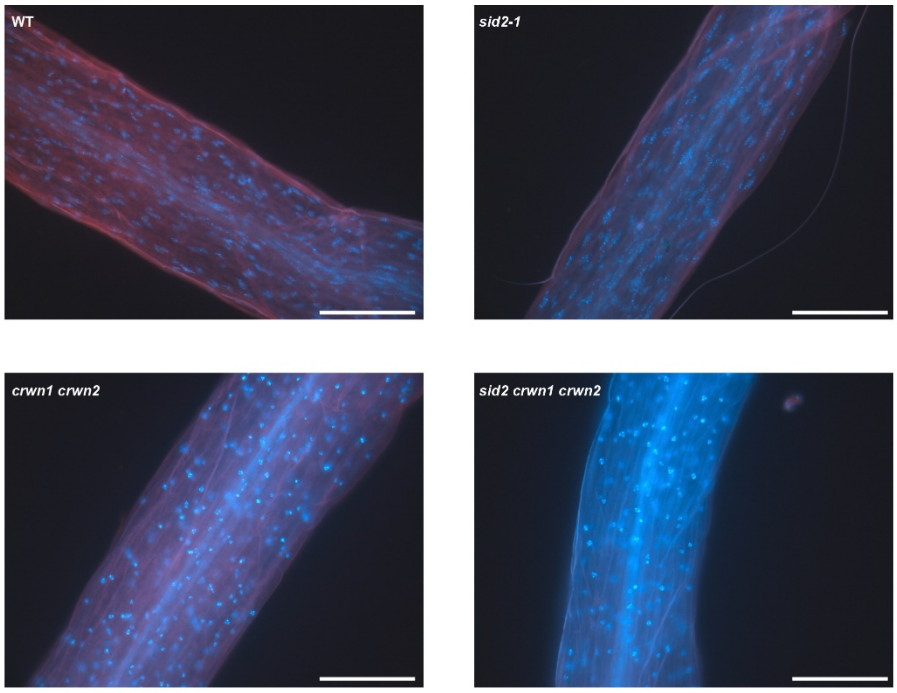

Supplemental Figure S11. Salicylic acid (SA) over-production does not explain the nuclear morphology phenotypes of *crwn1 crwn2* mutants. Anther filaments from 44-day-old plants were fixed, stained with DAPI (4',6'-diamidino-2-phenylindole), and observed under a Leica DM 5500B epifluorescence microscope. Wild-type (WT) nuclei are elongated, as are the nuclei in the *sid2-1* mutant. Small, round nuclei characteristic of *crwn1 crwn2* mutants are retained in *sid2 crwn1 crwn2* mutants. Bar = 100 μm.

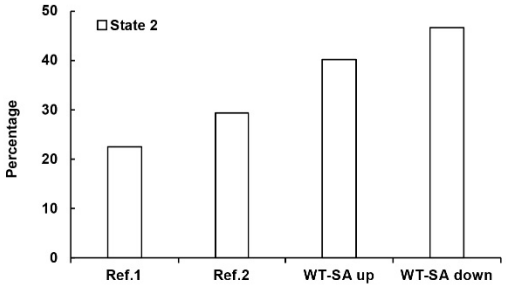

Supplemental Figure S12. Over-representation of chromatin state 2 within genes regulated in response to SA treatment. WT indicates wild type and SA indicates salicylic acid. Reference 1 (Ref. 1) indicates the ratio of genes having at least one domain of chromatin state 2 (Sequeira-Mendes *et al.*, 2014) to all the genes in Arabidopsis based on TAIR10 annotation. Reference 2 (Ref. 2) indicates the ratio of genes with chromatin state 2 relative to all tested genes in our RNA-seq data. The percentages of genes with chromatin state 2 domains that are either up-regulated or down regulated in response to SA treatment (Zhou *et al.*, 2015) are indicated relative to the total number of mis-regulated genes by SA.

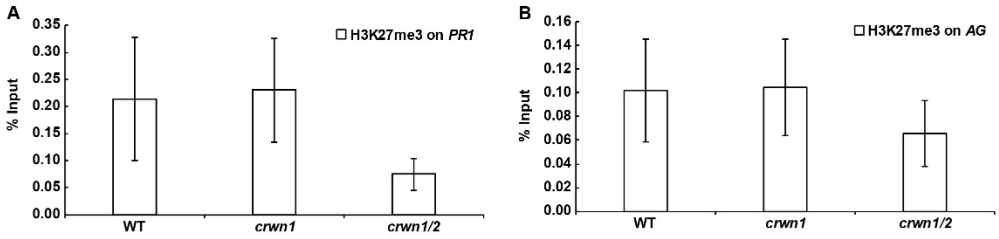

Supplemental Figure S13. Histone H3 lysine 27 trimethylation (H3K27me3) levels at *PR1* are decreased in *crwn1 crwn2* mutants. Chromatin immunoprecipitation followed by quantitative PCR (ChIP/qPCR) results are expressed as a percentage of the signal derived from the input chromatin sample before immunoprecipitation with an anti-H3K27me3 antibody. The data shown are means +/- SD (error bars) from five independent biological replicates. A, The ChIP/qPCR results for the *PR1* locus detected a decrease in H3K27me3 levels in the *crwn1 crwn2* mutants, but the *P* value calculated by the Tukey HSD test comparing wild type (WT) and *crwn1 crwn2* is just outside the cut off for significance (P = 0.065; *n* = 5 biological replicates). B, H3K27me3 levels at the control locus *AG* were not significantly different among the three genotypes tested.

Supplemental Table S1. *Differential expression of transposable elements (TEs) (sorted as family) in crwn mutants (adj. P < 0.01)*

Mutants	Up-regulated TEs (log2 ≥ 1)	log2	adj. *P*	Down-regulated TEs (log2 ≤ 1)	log2	adj. *P*
crwn1	none	N/A	N/A	none	N/A	N/A
crwn2	none	N/A	N/A	none	N/A	N/A
crwn4	ATCOPIA78:Copia:LTR	1.36	0.0000	ATGP1:Gypsy:LTR	-1.03	0.0001
	ATDNA12T3A:ATDNA12T3A:DNA	2.97	0.0000	ATGP2:Gypsy:LTR	-2.05	0.0000
	ATENSPM11:En-Spm:DNA	1.57	0.0047	ATREP10C:Helitron:RC	-1.29	0.0093
	ATENSPM3:En-Spm:DNA	1.73	0.0000	ATREP13:Helitron:RC	-1.63	0.0000
	ATHILA7:Gypsy:LTR	1.52	0.0000			
	HELITRONY1B:Helitron:RC	1.23	0.0000			
	VANDAL5A:MuDR:DNA	2.67	0.0000			
crwn1 crwn2	ATCOPIA22:Copia:LTR	2.01	0.0011	ATCOPIA8A:Copia:LTR	-1.63	0.0001
	ATCOPIA28:Copia:LTR	2.48	0.0071	ATENSPM9:En-Spm:DNA	-1.05	0.0017
	ATCOPIA87:Copia:LTR	1.36	0.0002	ATGP2:Gypsy:LTR	-2.98	0.0000
	ATCOPIA8B:Copia:LTR	2.17	0.0001	ATHILA6A:Gypsy:LTR	-1.33	0.0092
	ATCOPIA95:Copia:LTR	3.22	0.0004	ATREP10C:Helitron:RC	-1.72	0.0008
	ATDNA12T3A:ATDNA12T3A:DNA	2.95	0.0000	ATREP13:Helitron:RC	-1.74	0.0000
	ATDNAI27T9C:MuDR:DNA	1.57	0.0000	VANDAL6:MuDR:DNA	-1.41	0.0000
	ATENSPM10:En-Spm:DNA	1.66	0.0051			
	ATENSPM11:En-Spm:DNA	2.31	0.0002			
	ATENSPM3:En-Spm:DNA	1.86	0.0005			
	ATGP2N:Gypsy:LTR	2.23	0.0000			
	ATHATN3:HAT:DNA	1.78	0.0008			
	ATHILA2:Gypsy:LTR	4.06	0.0000			
	ATHILA7:Gypsy:LTR	1.57	0.0000			
	ATREP11:Helitron:RC	1.40	0.0008			
	ATTIRX1C:ATTIRX1C:DNA	2.37	0.0059			
	HELITRONY1B:Helitron:RC	1.88	0.0000			
	HELITRONY2:Helitron:RC	1.43	0.0000			
	VANDAL1N1:MuDR:DNA	1.74	0.0001			
	VANDAL5A:MuDR:DNA	4.43	0.0000			
crwn1 crwn4	ATCOPIA8B:Copia:LTR	1.23	0.0000	none	N/A	N/A
	ATHILA2:Gypsy:LTR	1.11	0.0004		N/A	N/A

Supplemental Table S2. *Differential expression of transposable elements (TEs) (sorted as individual) in crwn mutants (adj. P < 0.01)*

Mutants	Up-regulated TEs (log2 ≥ 1)	log2	adj. *P*	Down-regulated TEs (log2 ≤ 1)	log2	adj. *P*
crwn1	AT1TE34290:Helitron:RC	1.57	0.0082	AT2TE18115:Gypsy:LTR	-1.33	0.0034
	AT1TE70175:En-Spm:DNA	1.77	0.0003	AT5TE68230:MuDR:DNA	-1.76	0.0000
crwn2	none	N/A	N/A	none	N/A	N/A
crwn4	AT1TE03050:MuDR:DNA	1.59	0.0000	AT1TE56700:Helitron:RC	-1.48	0.0000
	AT1TE06650:Harbinger:DNA	1.35	0.0039	AT1TE78550:En-Spm:DNA	-1.55	0.0000
	AT1TE34290:Helitron:RC	4.05	0.0000	AT1TE85165:Helitron:RC	-2.62	0.0004
	AT1TE39775:MuDR:DNA	2.10	0.0000	AT2TE12510:Copia:LTR	-1.51	0.0019
	AT1TE69990:Helitron:RC	1.63	0.0045	AT2TE26660:L1:LINE	-1.86	0.0000
	AT1TE69995:Helitron:RC	2.01	0.0001	AT2TE41380:En-Spm:DNA	-1.44	0.0000
	AT1TE70175:En-Spm:DNA	2.88	0.0000	AT2TE41390:MuDR:DNA	-1.67	0.0000
	AT1TE80025:L1:LINE	2.53	0.0008	AT2TE61100:Gypsy:LTR	-1.64	0.0000
	AT1TE86120:MuDR:DNA	1.67	0.0001	AT3TE15195:Helitron:RC	-2.12	0.0015
	AT1TE91440:MuDR:DNA	1.25	0.0000	AT3TE16310:Helitron:RC	-1.69	0.0079
	AT1TE99345:MuDR:DNA	3.96	0.0000	AT3TE32730:Gypsy:LTR	-1.42	0.0001
	AT2TE07190:Gypsy:LTR	2.27	0.0044	AT3TE40370:MuDR:DNA	-1.15	0.0007
	AT2TE08275:MuDR:DNA	3.05	0.0000	AT3TE43770:Helitron:RC	-2.06	0.0021
	AT2TE10885:Helitron:RC	3.04	0.0000	AT3TE43830:MuDR:DNA	-1.23	0.0001
	AT2TE22075:En-Spm:DNA	2.51	0.0001	AT3TE43945:MuDR:DNA	-1.23	0.0001
	AT2TE34500:Helitron:RC	1.52	0.0082	AT4TE06880:Helitron:RC	-2.69	0.0000
	AT2TE46220:Helitron:RC	2.47	0.0019	AT4TE34435:Helitron:RC	-1.70	0.0030
	AT2TE56040:MuDR:DNA	2.56	0.0000	AT4TE35205:Helitron:RC	-1.00	0.0037
	AT2TE72160:MuDR:DNA	2.45	0.0000	AT4TE39495:Helitron:RC	-1.84	0.0000
	AT3TE02890:Gypsy:LTR	1.92	0.0000	AT4TE61260:MuDR:DNA	-1.49	0.0099
	AT3TE06390:Copia:LTR	1.71	0.0035	AT5TE07900:Helitron:RC	-2.77	0.0000
	AT3TE11175:Helitron:RC	1.59	0.0000	AT5TE56255:MuDR:DNA	-1.39	0.0018
	AT3TE25420:Helitron:RC	2.00	0.0003	AT5TE68230:MuDR:DNA	-2.89	0.0000
	AT3TE41160:Helitron:RC	1.95	0.0078	AT5TE91490:MuDR:DNA	-1.28	0.0000
	AT3TE66330:MuDR:DNA	1.46	0.0039			
	AT4TE11410:L1:LINE	2.38	0.0000			
	AT4TE11855:Copia:LTR	1.16	0.0093			
	AT4TE37565:MuDR:DNA	1.28	0.0001			
	AT4TE55430:En-Spm:DNA	3.28	0.0000			
	AT4TE56380:ATDNA12T3A:DNA	3.09	0.0000			
	AT4TE64410:Copia:LTR	2.99	0.0000			
	AT5TE15240:Copia:LTR	1.41	0.0000			
	AT5TE37200:HAT:DNA	1.95	0.0011			
	AT5TE37215:Helitron:RC	2.54	0.0000			
	AT5TE37230:MuDR:DNA	2.88	0.0002			
	AT5TE38735:En-Spm:DNA	3.55	0.0000			
	AT5TE49540:Helitron:RC	2.69	0.0000			
	AT5TE55210:Helitron:RC	3.08	0.0000			
	AT5TE55270:En-Spm:DNA	1.79	0.0023			
	AT5TE58300:En-Spm:DNA	1.55	0.0083			
	AT5TE58305:MuDR:DNA	1.26	0.0000			
	AT5TE58315:MuDR:DNA	1.65	0.0021			
	AT5TE58950:Helitron:RC	1.43	0.0000			
	AT5TE64430:MuDR:DNA	1.26	0.0000			
	AT5TE74135:En-Spm:DNA	1.84	0.0000			
	AT5TE74255:En-Spm:DNA	1.84	0.0000			
	AT5TE80010:MuDR:DNA	2.31	0.0000			
	AT5TE80015:Helitron:RC	2.14	0.0023			
crwn1 crwn4	AT1TE70175:En-Spm:DNA	1.06	0.0012	AT4TE61260:MuDR:DNA	-1.28	0.0007
	AT1TE71775:Copia:LTR	1.25	0.0000	AT5TE68230:MuDR:DNA	-1.05	0.0012
	AT2TE25295:Gypsy:LTR	1.38	0.0001			
	AT2TE26610:Gypsy:LTR	1.06	0.0001			
	AT3TE41160:Helitron:RC	1.16	0.0031			
	AT3TE44395:MuDR:DNA	1.67	0.0000			
	AT3TE44530:En-Spm:DNA	1.12	0.0049			

	AT1TE03050:MuDR:DNA	1.86	0.0003	AT1TE30235:Helitron:RC	-2.46	0.0001
	AT1TE17410:Helitron:RC	1.64	0.0031	AT1TE56700:Helitron:RC	-2.13	0.0000
	AT1TE32095:Helitron:RC	2.96	0.0059	AT1TE78550:En-Spm:DNA	-1.64	0.0000
	AT1TE34290:Helitron:RC	2.32	0.0030	AT1TE85165:Helitron:RC	-3.77	0.0001
	AT1TE36570:En-Spm:DNA	3.79	0.0000	AT2TE12510:Copia:LTR	-2.57	0.0000
	AT1TE69970:Helitron:RC	2.67	0.0095	AT2TE18115:Gypsy:LTR	-3.69	0.0000
	AT1TE69990:Helitron:RC	3.23	0.0000	AT2TE26660:L1:LINE	-1.89	0.0010
	AT1TE69995:Helitron:RC	2.86	0.0000	AT2TE41380:En-Spm:DNA	-2.81	0.0000
	AT1TE70175:En-Spm:DNA	3.12	0.0000	AT2TE41385:En-Spm:DNA	-2.06	0.0094
	AT1TE70490:Copia:LTR	2.17	0.0036	AT2TE41390:MuDR:DNA	-2.85	0.0000
	AT1TE70735:Helitron:RC	4.14	0.0000	AT2TE61100:Gypsy:LTR	-1.66	0.0026
	AT1TE71770:HAT:DNA	1.95	0.0014	AT2TE64130:MuDR:DNA	-2.54	0.0000
	AT1TE71775:Copia:LTR	2.19	0.0001	AT3TE32775:MuDR:DNA	-2.93	0.0018
	AT1TE71790:MuDR:DNA	1.90	0.0000	AT3TE35255:Gypsy:LTR	-2.60	0.0000
	AT1TE71905:Copia:LTR	1.35	0.0006	AT3TE35260:MuDR:DNA	-2.48	0.0032
	AT1TE72010:Copia:LTR	1.39	0.0005	AT3TE43830:MuDR:DNA	-1.93	0.0000
	AT1TE77880:ATTIRX1C:DNA	3.17	0.0023	AT3TE43945:MuDR:DNA	-1.93	0.0000
	AT1TE80025:L1:LINE	3.38	0.0001	AT4TE10335:Copia:LTR	-3.26	0.0017
	AT1TE80800:Helitron:RC	3.91	0.0000	AT4TE34440:Helitron:RC	-2.47	0.0002
	AT1TE80810:Helitron:RC	4.75	0.0000	AT4TE39495:Helitron:RC	-2.32	0.0000
	AT1TE89775:L1:LINE	2.77	0.0000	AT4TE39505:Copia:LTR	-2.11	0.0000
	AT1TE99345:MuDR:DNA	4.52	0.0000	AT4TE42160:Helitron:RC	-3.50	0.0002
	AT2TE07190:Gypsy:LTR	4.04	0.0000	AT4TE61260:MuDR:DNA	-1.78	0.0063
	AT2TE08275:MuDR:DNA	4.84	0.0000	AT4TE74475:Harbinger:DNA	-1.22	0.0065
	AT2TE10885:Helitron:RC	1.53	0.0087	AT4TE85940:MuDR:DNA	-1.27	0.0028
	AT2TE18410:Gypsy:LTR	3.13	0.0011	AT5TE37605:MuDR:DNA	-2.84	0.0000
	AT2TE25290:Helitron:RC	2.28	0.0072	AT5TE46165:MuDR:DNA	-1.53	0.0076
	AT2TE25295:Gypsy:LTR	5.07	0.0000	AT5TE56255:MuDR:DNA	-1.62	0.0014
	AT2TE25300:MuDR:DNA	4.32	0.0000	AT5TE68230:MuDR:DNA	-2.04	0.0015
	AT2TE25320:MuDR:DNA	3.35	0.0001			
	AT2TE26610:Gypsy:LTR	2.37	0.0000			
	AT2TE26680:En-Spm:DNA	2.16	0.0015			
	AT2TE28430:Helitron:RC	3.44	0.0001			
	AT2TE34500:Helitron:RC	2.57	0.0000			
	AT2TE36460:MuDR:DNA	3.16	0.0010			
	AT2TE56040:MuDR:DNA	4.37	0.0000			
	AT2TE57405:MuDR:DNA	3.01	0.0046			
	AT2TE57465:Helitron:RC	1.34	0.0011			
	AT2TE59980:Helitron:RC	2.98	0.0026			
	AT2TE59985:MuDR:DNA	4.41	0.0000			
	AT2TE72160:MuDR:DNA	4.80	0.0000			
crwn1 crwn2	AT3TE02890:Gypsy:LTR	1.91	0.0000			
	AT3TE06390:Copia:LTR	2.28	0.0003			
	AT3TE11175:Helitron:RC	2.00	0.0004			
	AT3TE25420:Helitron:RC	2.54	0.0000			
	AT3TE41160:Helitron:RC	3.85	0.0000			
	AT3TE44395:MuDR:DNA	5.01	0.0000			
	AT3TE44400:Helitron:RC	4.02	0.0000			
	AT3TE44530:En-Spm:DNA	4.60	0.0000			
	AT3TE65130:Harbinger:DNA	1.80	0.0005			
	AT3TE65700:Harbinger:DNA	1.83	0.0005			
	AT3TE73025:Helitron:RC	4.55	0.0000			
	AT3TE73035:Helitron:RC	3.70	0.0002			
	AT3TE73040:Helitron:RC	3.52	0.0001			
	AT3TE91745:Gypsy:LTR	1.49	0.0022			
	AT3TE92470:Helitron:RC	2.32	0.0000			
	AT4TE05245:Helitron:RC	3.23	0.0001			
	AT4TE10520:Helitron:RC	3.05	0.0038			
	AT4TE10620:RathE1_cons	1.31	0.0028			
	AT4TE11855:Copia:LTR	1.92	0.0000			
	AT4TE11860:Helitron:RC	1.70	0.0045			
	AT4TE21670:MuDR:DNA	2.90	0.0002			
	AT4TE43140:Copia:LTR	1.76	0.0023			
	AT4TE55210:Helitron:RC	1.97	0.0006			
	AT4TE55430:En-Spm:DNA	3.34	0.0000			
	AT4TE56380:ATDNA12T3A:DNA	3.05	0.0000			
	AT4TE64410:Copia:LTR	2.75	0.0033			
	AT5TE27115:MuDR:DNA	2.70	0.0011			
	AT5TE32420:Gypsy:LTR	1.21	0.0073			
	AT5TE36475:Copia:LTR	3.02	0.0043			
	AT5TE38735:En-Spm:DNA	2.85	0.0000			
	AT5TE49540:Helitron:RC	3.66	0.0000			
	AT5TE55210:Helitron:RC	3.71	0.0000			
	AT5TE55270:En-Spm:DNA	2.53	0.0001			
	AT5TE58950:Helitron:RC	2.20	0.0000			
	AT5TE61365:Helitron:RC	2.65	0.0061			
	AT5TE64785:Helitron:RC	2.83	0.0000			
	AT5TE71005:TNAT1A:DNA	3.00	0.0013			
	AT5TE74135:En-Spm:DNA	1.81	0.0060			
	AT5TE74255:En-Spm:DNA	1.81	0.0060			
	AT5TE77555:Helitron:RC	2.94	0.0060			
	AT5TE80010:MuDR:DNA	2.51	0.0000			
	AT5TE80015:Helitron:RC	2.98	0.0001			

Supplemental Table S3. *Statistical overrepresentation test for down-regulated genes in crwn mutants*

Input	GO Terms (Biological Process Complete)	Total no. of Arabidopsis genes in the term	Input gene #	Expected no. of genes	Fold enrichment	*P* value
Down-regulated genes in *crwn1* mutants (266 genes mapped)	Syncytium formation	15	5	0.15	33.77	1.10E-03
	Glucosinolate biosynthetic process	31	6	0.31	19.61	1.82E-03
	Plant-type cell wall loosening	36	6	0.36	16.88	4.28E-03
	Response to acid chemical	896	24	8.84	2.71	2.64E-02
Down-regulated genes in *crwn2* mutants (37 genes mapped)	Unclassified					
Down-regulated genes in *crwn4* mutants (1311 genes mapped)	Response to insect	24	12	1	12.02	1.70E-06
	Wax biosynthetic process	19	7	0.79	8.86	4.13E-02
	Glucosinolate biosynthetic process	31	11	1.29	8.53	2.66E-04
	Transmembrane receptor protein tyrosine kinase signaling pathway	100	20	4.16	4.81	3.77E-05
	Response to gibberellin	122	19	5.08	3.74	3.49E-03
	Phenylpropanoid metabolic process	130	18	5.41	3.33	3.10E-02
	Response to jasmonic acid	174	23	7.24	3.18	4.58E-03
	Regulation of growth	201	23	8.36	2.75	4.46E-02
	Carboxylic acid biosynthetic process	429	41	17.85	2.3	3.23E-03
	Cell wall organization	412	39	17.14	2.28	7.20E-03
Down-regulated genes in *crwn1 crwn2* mutants (1273 genes mapped)	Regulation of organ growth	17	8	0.8	10.01	4.35E-03
	Syncytium formation	15	7	0.71	9.93	2.00E-02
	Plant-type secondary cell wall biogenesis	35	13	1.65	7.9	4.73E-05
	Regulation of secondary metabolic process	30	9	1.41	6.38	3.68E-02
	Transmembrane receptor protein tyrosine kinase signaling pathway	100	19	4.7	4.04	1.16E-03
	Phenylpropanoid biosynthetic process	104	18	4.89	3.68	8.20E-03
	Auxin-activated signaling pathway	163	27	7.66	3.52	8.46E-05
	Cell wall modification	134	22	6.3	3.49	1.71E-03
	Response to water deprivation	235	36	11.05	3.26	3.77E-06
	Response to jasmonic acid	174	26	8.18	3.18	1.03E-03
Down-regulated genes in *crwn1 crwn4* mutants (322 genes mapped)	Phenylpropanoid biosynthetic process	104	13	1.23	10.55	1.38E-06
	Anion transport	189	11	2.24	4.91	4.52E-02

Supplemental Table S4. *Statistical overrepresentation test for genes mis-regulated in both crwn1 crwn2 mutants and salicylic acid (SA)-treated wild-type plants*

Input	GO Terms (Biological Process Complete)	Total no. of Arabidopsis genes in the term	Input gene #	Expected no. of genes	Fold enrichment	*P* value
Genes up-regulated in both *crwn1 crwn2* and SA-treated wild-type plants	Response to molecule of bacterial origin	20	7	0.42	16.77	6.24E-04
	Regulation of salicylic acid mediated signaling pathway	20	6	0.42	14.37	1.06E-02
	Defense response to bacterium, incompatible interaction	40	11	0.84	13.17	3.13E-06
	Negative regulation of cell death	23	6	0.48	12.5	2.34E-02
	Response to chitin	109	26	2.28	11.43	6.98E-16
	Plant-type hypersensitive response	66	15	1.38	10.89	4.68E-08
	Salicylic acid mediated signaling pathway	38	8	0.79	10.08	3.92E-03
	Regulation of response to biotic stimulus	51	8	1.06	7.51	3.26E-02
	Positive regulation of defense response	65	10	1.36	7.37	3.41E-03
	Toxin metabolic process	54	8	1.13	7.1	4.88E-02
Genes down-regulated in both *crwn1 crwn2* and SA-treated wild-type plants	Regulation of secondary metabolite biosynthetic process	16	4	0.15	27.46	3.45E-02
	Response to wounding	185	11	1.68	6.53	3.00E-03
	Response to jasmonic acid	177	10	1.61	6.21	1.41E-02
	Lipid catabolic process	191	10	1.74	5.75	2.70E-02
	Cell wall organization	417	15	3.8	3.95	1.82E-02

Supplemental Table S5. *Statistical overrepresentation test for genes mis-regulated in both crwn1 crwn2 mutants and SA-treated wild-type plants*

Experiment	Name	Sequence
RT-qPCR	ROC1 FP	CGG ATC TCA GTT CTT CAT CTG
	ROC1 RP	CCT TCT CGA TGG CCT TTA C
	UBQ5 FP	CCA AGC CGA AGA AGA TCA AG
	UBQ5 RP	GCT GAA CCT TTC CAG ATC CA
	PR1 FP	GGC AAC TGC AGA CTC ATA C
	PR1 RP	CTC GCT AAC CCA CAT GTT C
	PR2 FP	GCA ATG CAG AAC ATC GAG AA
	PR2 RP	CGG AGG AGA CGT ATC AGT GG
	PR5 FP	CTG CAA GAG TGC CTG TGA GA
	PR5 RP	GAG TAG TCC GTG GGA GGA CA
	SID2 FP	GGT GGC GAG GAG AGT GAA TT
	SID2 RP	AGC TAC TAT CCC TGT CCC CG
ChIP-qPCR	ACT7 FP	CGT TTC GCT TTC CTT AGT GTT AGC T
	ACT7 RP	AGC GAA CGG ATC TAG AGA CTC ACC TTG
	PR1 FP	GGC AAC TGC AGA CTC ATA C
	PR1 RP	CTC GCT AAC CCA CAT GTT C
	AGi2 FP	CGT TGT GAT GTT ACT CGG ACA
	AGi2 RP	CAA CAA CCC ATT AAC ACA TTG G
Genotyping	CRWN1-1 RP (SALK_025347 RP)	TGC GTG AAT GGG AAA GAA AGT TG
	CRWN1-1 LP (SALK_025347 LP)	TGC CTT CTC CTC GCT TTT CAA
	CRWN2 RP (SALK_076653)	TGG CTT CAA ATG ATT CTC TCT GCA GT
	CRWN2 LP (SALK_076653)	ACA CTC CAG ATC ACG CTA TTG GCA
	CRWN4-1 RP (SALK_079296RP)	GCT TCA GCC AGC ATT TCA AGC
	CRWN4-1 LP (SALK_079296LP)	CGC AAA GCC TTC GAA GAC AAA
	LBb1.3	ATT TTG CCG ATT TCG GAA C
	SID2-1 FP	GCT CTG CAG CTT CAA TGC
	SID2-1 RP	CGA AGA AAT GAA GAG CTT GG

REFERENCES

Aebi U, Cohn J, Buhle L, Gerace L (1986) The Nuclear Lamina Is a Meshwork of Intermediate-Type Filaments. Nature **323:** 560-564

Afgan E, Baker D, van den Beek M, Blankenberg D, Bouvier D, Cech M, Chilton J, Clements D, Coraor N, Eberhard C, Gruning B, Guerler A, Hillman-Jackson J, Von Kuster G, Rasche E, Soranzo N, Turaga N, Taylor J, Nekrutenko A, Goecks J (2016) The Galaxy platform for accessible, reproducible and collaborative biomedical analyses: 2016 update. Nucleic Acids Research **44:** W3-W10

Al-Haboubi T, Shumaker DK, Koser J, Wehnert M, Fahrenkrog B (2011) Distinct association of the nuclear pore protein Nup153 with A- and B-type lamins. Nucleus-Austin **2:** 500-509

Arabidopsis_Genome_Initiative (2000) Analysis of the genome sequence of the flowering plant Arabidopsis thaliana. Nature **408:** 796-815

Barrett T, Wilhite SE, Ledoux P, Evangelista C, Kim IF, Tomashevsky M, Marshall KA, Phillippy KH, Sherman PM, Holko M, Yefanov A, Lee H, Zhang NG, Robertson CL, Serova N, Davis S, Soboleva A (2013) NCBI GEO: archive for functional genomics data sets-update. Nucleic Acids Research **41:** D991-D995

Bi XL, Cheng YJ, Hu B, Ma XL, Wu R, Wang JW, Liu C (2017) Nonrandom domain organization of the Arabidopsis genome at the nuclear periphery. Genome Research **27:** 1162-1173

Bowling SA, Clarke JD, Liu YD, Klessig DF, Dong XN (1997) The cpr5 mutant of Arabidopsis expresses both NPR1-dependent and NPR1-independent resistance. Plant Cell **9:** 1573-1584

Bruggeman Q, Raynaud C, Benhamed M, Delarue M (2015) To die or not to die? Lessons from lesion mimic mutants. Frontiers in Plant Science **6**

Chytilova E, Macas J, Sliwinska E, Rafelski SM, Lambert GM, Galbraith DW (2000) Nuclear dynamics in Arabidopsis thaliana. Molecular Biology of the Cell **11:** 2733-2741

Csoka AB, English SB, Simkevich CP, Ginzinger DG, Butte AJ, Schatten GP, Rothman FG, Sedivy JM (2004) Genome-scale expression profiling of Hutchinson-Gilford progeria syndrome reveals widespread transcriptional misregulation leading to mesodermal/mesenchymal defects and accelerated atherosclerosis. Aging Cell **3:** 235-243

Davidson PM, Lammerding J (2014) Broken nuclei - lamins, nuclear mechanics, and disease. Trends in Cell Biology **24:** 247-256

Dempsey DA, Vlot AC, Wildermuth MC, Klessig DF (2011) Salicylic Acid biosynthesis and metabolism. Arabidopsis Book **9:** e0156

Denais CM, Gilbert RM, Isermann P, McGregor AL, te Lindert M, Weigelin B, Davidson PM, Friedl P, Wolf K, Lammerding J (2016) Nuclear envelope rupture and repair during cancer cell migration. Science **352:** 353-358

Dittmer TA, Richards EJ (2008) Role of LINC proteins in plant nuclear morphology. Plant Signal Behav **3:** 485-487

Dittmer TA, Stacey NJ, Sugimoto-Shirasu K, Richards EJ (2007) LITTLE NUCLEI genes affecting nuclear morphology in Arabidopsis thaliana. Plant Cell **19:** 2793-2803

Dobin A, Davis CA, Schlesinger F, Drenkow J, Zaleski C, Jha S, Batut P, Chaisson M, Gingeras TR (2013) STAR: ultrafast universal RNA-seq aligner. Bioinformatics **29:** 15-21

Edgar R, Domrachev M, Lash AE (2002) Gene Expression Omnibus: NCBI gene expression and hybridization array data repository. Nucleic Acids Research **30:** 207-210

Egecioglu D, Brickner JH (2011) Gene positioning and expression. Current Opinion in Cell Biology **23:** 338-345

Fransz P, de Jong JH, Lysak M, Castiglione MR, Schubert I (2002) Interphase chromosomes in Arabidopsis are organized as well defined chromocenters from which euchromatin loops emanate. Proceedings of the National Academy of Sciences of the United States of America **99:** 14584-14589

Gilford H (1904) Progeria: A form of senilism. Practitioner **73**

Goldman RD, Shumaker DK, Erdos MR, Eriksson M, Goldman AE, Gordon LB, Gruenbaum Y, Khuon S, Mendez M, Varga R, Collins FS (2004) Accumulation of mutant lamin A causes progressive changes in nuclear architecture in Hutchinson-Gilford progeria syndrome. Proceedings of the National Academy of Sciences of the United States of America **101:** 8963-8968

Grob S, Schmid MW, Grossniklaus U (2014) Hi-C Analysis in Arabidopsis Identifies the KNOT, a Structure with Similarities to the flamenco Locus of Drosophila. Molecular Cell **55:** 678-693

Gruenbaum Y, Foisner R (2015) Lamins: Nuclear Intermediate Filament Proteins with Fundamental Functions in Nuclear Mechanics and Genome Regulation. Annual Review of Biochemistry, Vol 84 **84:** 131-164

Gu YN, Zebell SG, Liang ZZ, Wang S, Kang BH, Dong XN (2016) Nuclear Pore Permeabilization Is a Convergent Signaling Event in Effector-Triggered Immunity. Cell **166:** 1526-+

Guelen L, Pagie L, Brasset E, Meuleman W, Faza MB, Talhout W, Eussen BH, de Klein A, Wessels L, de Laat W, van Steensel B (2008) Domain organization of human chromosomes revealed by mapping of nuclear lamina interactions. Nature **453:** 948-U983

Guo TT, Mao XG, Zhang H, Zhang Y, Fu MD, Sun ZF, Kuai P, Lou YG, Fang YD (2017) Lamin-like Proteins Negatively Regulate Plant Immunity through NAC WITH TRANSMEMBRANE MOTIF1-LIKE9 and NONEXPRESSOR OF PR GENES1 in Arabidopsis thaliana. Molecular Plant **10:** 1334-1348

Guo YX, Kim Y, Shimi T, Goldman RD, Zheng YX (2014) Concentration-dependent lamin assembly and its roles in the localization of other nuclear proteins. Molecular Biology of the Cell **25:** 1287-1297

Guy L, Roat Kultima J, Andersson SGE (2010) genoPlotR: comparative gene and genome visualization in R. Bioinformatics **26:** 2334-2335

Harr JC, Gonzalez-Sandoval A, Gasser SM (2016) Histones and histone modifications in perinuclear chromatin anchoring: from yeast to man. Embo Reports **17:** 139-155

Harr JC, Luperchio TR, Wong XR, Cohen E, Wheelan SJ, Reddy KL (2015) Directed targeting of chromatin to the nuclear lamina is mediated by chromatin state and A-type lamins. Journal of Cell Biology **208:** 33-52

Heberle H, Meirelles GV, da Silva FR, Telles GP, Minghim R (2015) InteractiVenn: a web-based tool for the analysis of sets through Venn diagrams. Bmc Bioinformatics **16**

Hutchinson J (1886) Congenital Absence of Hair and Mammary Glands with Atrophic Condition of the Skin and its Appendages, in a Boy whose Mother had been almost wholly Bald from Alopecia Areata from the age of Six. Med Chir Trans **69:** 473-477

Ikegami K, Egelhofer TA, Strome S, Lieb JD (2010) Caenorhabditis elegans chromosome arms are anchored to the nuclear membrane via discontinuous association with LEM-2. Genome Biology **11**

Jin Y, Tam OH, Paniagua E, Hammell M (2015) TEtranscripts: a package for including transposable elements in differential expression analysis of RNA-seq datasets. Bioinformatics **31:** 3593-3599

Kim D, Pertea G, Trapnell C, Pimentel H, Kelley R, Salzberg SL (2013) TopHat2: accurate alignment of transcriptomes in the presence of insertions, deletions and gene fusions. Genome Biology **14**

Kuhlbrandt W (2015) Structure and function of mitochondrial membrane protein complexes. Bmc Biology **13**

Langmead B, Trapnell C, Pop M, Salzberg SL (2009) Ultrafast and memory-efficient alignment of short DNA sequences to the human genome. Genome Biology **10**

Lombardi ML, Lammerding J (2011) Keeping the LINC: the importance of nucleocytoskeletal coupling in intracellular force transmission and cellular function. Biochemical Society Transactions **39:** 1729-1734

Love MI, Huber W, Anders S (2014) Moderated estimation of fold change and dispersion for RNA-seq data with DESeq2. Genome Biology **15**

Masuda K, Takahashi S, Nomura K, Arimoto M, Inoue M (1993) Residual Structure and Constituent Proteins of the Peripheral Framework of the Cell-Nucleus in Somatic Embryos from Daucus-Carota L. Planta **191:** 532-540

Masuda K, Xu ZJ, Takahashi S, Ito A, Ono M, Nomura K, Inoue M (1997) Peripheral framework of carrot cell nucleus contains a novel protein predicted to exhibit a long alpha-helical domain. Experimental Cell Research **232:** 173-181

Meier I (2016) LINCing the eukaryotic tree of life - towards a broad evolutionary comparison of nucleocytoplasmic bridging complexes. Journal of Cell Science **129:** 3523-3531

Meier I, Griffis AHN, Groves NR, Wagner A (2016) Regulation of nuclear shape and size in plants. Current Opinion in Cell Biology **40:** 114-123

Meier I, Richards EJ, Evans DE (2017) Cell Biology of the Plant Nucleus. Annual Review of Plant Biology, Vol 68 **68:** 139-172

Mi HY, Huang XS, Muruganujan A, Tang HM, Mills C, Kang D, Thomas PD (2017) PANTHER version 11: expanded annotation data from Gene Ontology and Reactome pathways, and data analysis tool enhancements. Nucleic Acids Research **45:** D183-D189

Mikulski P, Hohenstatt ML, Farrona S, Smaczniak C, Stahl Y, Kalyanikrishna K, Kaufmann K, Angenent GC, Schubert D (2019) The chromatin-associated protein PWO1 interacts with plant nuclear lamin-like components to regulate nuclear size. Plant Cell

Moeder W, Yoshioka K (2008) Lesion mimic mutants: A classical, yet still fundamental approach to study programmed cell death. Plant Signal Behav **3:** 764-767

Nawrath C, Metraux JP (1999) Salicylic acid induction-deficient mutants of Arabidopsis express PR-2 and PR-5 and accumulate high levels of camalexin after pathogen inoculation. Plant Cell **11:** 1393-1404

Peric-Hupkes D, Meuleman W, Pagie L, Bruggeman SWM, Solovei I, Brugman W, Graf S, Flicek P, Kerkhoven RM, van Lohuizen M, Reinders M, Wessels L, van Steensel B (2010) Molecular Maps of the Reorganization of Genome-Nuclear Lamina Interactions during Differentiation. Molecular Cell **38:** 603-613

Pickersgill H, Kalverda B, de Wit E, Talhout W, Fornerod M, van Steensel B (2006) Characterization of the Drosophila melanogaster genome at the nuclear lamina. Nature Genetics **38:** 1005-1014

Poulet A, Duc C, Voisin M, Desset S, Tutois S, Vanrobays E, Benoit M, Evans DE, Probst AV, Tatout C (2017) The LINC complex contributes to heterochromatin organisation and transcriptional gene silencing in plants. Journal of Cell Science **130:** 590-601

Reddy KL, Zullo JM, Bertolino E, Singh H (2008) Transcriptional repression mediated by repositioning of genes to the nuclear lamina. Nature **452:** 243-247

Robert-Seilaniantz A, Grant M, Jones JDG (2011) Hormone Crosstalk in Plant Disease and Defense: More Than Just JASMONATE-SALICYLATE Antagonism. Annual Review of Phytopathology, Vol 49 **49:** 317-343

Sakamoto Y, Takagi S (2013) LITTLE NUCLEI 1 and 4 regulate nuclear morphology in Arabidopsis thaliana. Plant Cell Physiol **54:** 622-633

Scaffidi P, Misteli T (2006) Lamin A-dependent nuclear defects in human aging. Science **312:** 1059-1063

Schreiber KH, Kennedy BK (2013) When Lamins Go Bad: Nuclear Structure and Disease. Cell **152:** 1365-1375

Sequeira-Mendes J, Araguez I, Peiro R, Mendez-Giraldez R, Zhang XY, Jacobsen SE, Bastolla U, Gutierrez C (2014) The Functional Topography of the Arabidopsis Genome Is Organized in a Reduced Number of Linear Motifs of Chromatin States. Plant Cell **26:** 2351-2366

Seyfferth C, Tsuda K (2014) Salicylic acid signal transduction: the initiation of biosynthesis, perception and transcriptional reprogramming. Frontiers in Plant Science **5**

Stingl N, Krischke M, Fekete A, Mueller MJ (2013) Analysis of defense signals in Arabidopsis thaliana leaves by ultra-performance liquid chromatography/tandem mass spectrometry: jasmonates, salicylic acid, abscisic acid. Methods Mol Biol **1009:** 103-113

Stroud H, Greenberg MVC, Feng SH, Bernatavichute YV, Jacobsen SE (2013) Comprehensive Analysis of Silencing Mutants Reveals Complex Regulation of the Arabidopsis Methylome. Cell **152:** 352-364

Tamura K, Fukao Y, Hatsugai N, Katagiri F, Hara-Nishimura I (2017) Nup82 functions redundantly with Nup136 in a salicylic acid-dependent defense response of Arabidopsis thaliana. Nucleus **8:** 301-311

Tapley EC, Starr DA (2013) Connecting the nucleus to the cytoskeleton by SUN-KASH bridges across the nuclear envelope. Current Opinion in Cell Biology **25:** 57-62

Tatout C, Evans DE, Vanrobays E, Probst AV, Graumann K (2014) The plant LINC complex at the nuclear envelope. Chromosome Research **22:** 241-252

Trapnell C, Roberts A, Goff L, Pertea G, Kim D, Kelley DR, Pimentel H, Salzberg SL, Rinn JL, Pachter L (2012) Differential gene and transcript expression analysis of RNA-seq experiments with TopHat and Cufflinks. Nature Protocols **7:** 562-578

Trapnell C, Williams BA, Pertea G, Mortazavi A, Kwan G, van Baren MJ, Salzberg SL, Wold BJ, Pachter L (2010) Transcript assembly and quantification by RNA-Seq reveals unannotated transcripts and isoform switching during cell differentiation. Nature Biotechnology **28:** 511-U174

van Steensel B, Belmont AS (2017) Lamina-Associated Domains: Links with Chromosome Architecture, Heterochromatin, and Gene Repression. Cell **169:** 780-791

van Wees S (2008) Phenotypic analysis of Arabidopsis mutants: trypan blue stain for fungi, oomycetes, and dead plant cells. CSH Protoc **2008:** pdb prot4982

Vicente MRS, Plasencia J (2011) Salicylic acid beyond defence: its role in plant growth and development. Journal of Experimental Botany **62:** 3321-3338

Vlot AC, Dempsey DA, Klessig DF (2009) Salicylic Acid, a Multifaceted Hormone to Combat Disease. Annual Review of Phytopathology **47:** 177-206

Wang H, Dittmer TA, Richards EJ (2013) Arabidopsis CROWDED NUCLEI (CRWN) proteins are required for nuclear size control and heterochromatin organization. BMC Plant Biol **13:** 200

Wang QQ, Liu S, Lu C, La YM, Dai J, Ma HY, Zhou SX, Tan F, Wang XY, Wu YF, Kong WW, La HG (2019) Roles of CRWN-family proteins in protecting genomic DNA against oxidative damage. Journal of Plant Physiology **233:** 20-30

Wildermuth MC, Dewdney J, Wu G, Ausubel FM (2001) Isochorismate synthase is required to synthesize salicylic acid for plant defence. Nature **414:** 562-565

Yamaguchi N, Winter CM, Wu MF, Kwon CS, William DA, Wagner D (2014) PROTOCOLS: Chromatin Immunoprecipitation from Arabidopsis Tissues. Arabidopsis Book **12:** e0170

Zhang XY, Clarenz O, Cokus S, Bernatavichute YV, Pellegrini M, Goodrich J, Jacobsen SE (2007) Whole-genome analysis of histone H3 lysine 27 trimethylation in Arabidopsis. Plos Biology **5:** 1026-1035

Zheng XB, Hu JB, Yue SB, Kristiani L, Kim M, Sauria M, Taylor J, Kim Y, Zheng YX (2018) Lamins Organize the Global Three-Dimensional Genome from the Nuclear Periphery. Molecular Cell **71:** 802-+

Zheng XY, Zhou M, Yoo H, Pruneda-Paz JL, Spivey NW, Kay SA, Dong XNA (2015) Spatial and temporal regulation of biosynthesis of the plant immune signal salicylic acid. Proceedings of the National Academy of Sciences of the United States of America **112:** 9166-9173

Zhou M, Wang W, Karapetyan S, Mwimba M, Marques J, Buchler NE, Dong X (2015) Redox rhythm reinforces the circadian clock to gate immune response. Nature **523:** 472-476

Chapter 3. Additional characterization of defense phenotypes in *crwn* and other nuclear morphology mutants

INTRODUCTION

I demonstrated previously that *crwn* mutations trigger a wide range of transcriptional alterations. In addition, I showed that two double mutants, *crwn1 crwn2* and *crwn1 crwn4*, are lesion mimic mutants (LMMs) that form ectopic cell death lesions. How CRWN proteins are linked to programmed cell death (PCD) remains a fundamental and puzzling question.

Localized PCD is a hallmark of the hypersensitive response, or HR, which is one mechanism that plants use to contain the spread of infectious agents. Many advances in understanding PCD in plants are based on mutants that develop lesions under conditions where wild type does not. One well-documented LMM is *lsd1*,which initiates runaway cell death when grown in a long-day photoperiod (Dietrich et al., 1994). Mateo et al. later found that 45 minutes of strong light illumination can initiate cell death, leading to the conclusion that the amount of light is important in initiating cell death rather than the photoperiod (Mateo et al., 2004). Subsequently, the photosynthetic light harvesting system was scrutinized by this group for possible connections between light and cell death (Mateo et al., 2004). They found that 680nm light absorbed by photosystem II can promote cell death in long-day conditions (Mateo et al., 2004). Incorporation of *chlorophyll a/b binding harvesting-organelle specific* (*cao*) mutations, which reduce PSII activity, into an *lsd1* background ameliorate cell death phenotypes in the resulting *lsd1 cao* double mutants under long-day photoperiods (Mateo et al., 2004). *lsd1* mutants also exhibit low stomatal conductance, causing photorespiration in low CO_2 conditions that further elevate reactive oxygen species (ROS) levels and exacerbate cell death (Mateo et al., 2004; Miller et al., 2010; Carmody et al., 2016).

Insight into the connections among pathogen defense, cell death, ROS and nuclear biology comes from studies in both animals and plants. In animals, ligands of the innate immune

system receptor NKG2d are upregulated by DNA damage agents that hinder DNA replication, suggesting that the DNA damage response (DDR) is involved in pathogen defense response (Gasser et al., 2005). In a study using Arabidopsis, Yan et al. showed that SA induces DNA damage and RAD51 binding to the promoter of the *PR1* gene, indicating that plants also evolved a mechanism activating defense response through DDR (Yan et al., 2013). In human laminopathies, mutations in NL proteins cause genomic instability (Liu et al., 2005). Moreover, multiple studies found that basal ROS levels increase in HGPS individuals (Pekovic et al., 2011; Richards et al., 2011). These observations suggest the involvement of DNA damage and ROS in the pathological manifestations of laminopathies. Because ROS is a well-known cytotoxin that generates DNA damage, an association among laminopathy, DNA damage and ROS is plausible. Thus, if *crwn* mutations can induce DNA damage or ROS production, similar to animal laminopathy, it is conceivable that these changes induce or heighten ectopic defense responses in *crwn* mutants.

In this chapter, I investigate several of unresolved questions concerning how nuclear structure is connected to pathogen defense signaling. First, I demonstrate that a short-day photoperiod can suppress hydrogen peroxide (H_2O_2) production and cell death phenotypes in *crwn1 crwn2* mutants, suggesting the possible involvement of CRWNs in light-stress mediated cell death. Second, I found no evidence that DDR is involved in the induction of pathogen response genes in *crwn* double mutants. Lastly, I also studied whether other Arabidopsis nuclear morphology mutants exhibit altered defense phenotypes.

RESULTS

Short-day growth conditions partially suppress the dwarfism of *crwn1 crwn2* mutants during early vegetative growth

Arabidopsis thaliana is a facultative long-day plant (Langridge, 1957). Short-day growth of Arabidopsis leads to production of more numerous and larger rosette leaves up to the point of flowering compared to plants grown in long-day conditions (Deal et al., 2005). In an effort to generate larger leaves for inoculating plants with pathogen using syringes, I grew a set of *crwn* mutants in short-day photoperiod (8 hours light – 16 hours dark). Unexpectedly, I found that *crwn1 crwn2* mutants grown under these conditions suppressed dwarfism during early vegetative growth (up to 29-days) (Fig. 2.1A). Considering my previous conclusions drawn in Chapter 2 that *crwn1 crwn2* mutants are LMMs and exhibit dwarfing associated with ectopic defense signaling, my finding suggests possible connections between light and *crwn1 crwn2* mutant phenotypes. There are several known LMMs of which the phenotypes can be suppressed by altering light conditions (Yoshioka and Shinozaki, 2009). For example, the dwarfism in *cpr1-1*, *cpr5-1*, *cpr6-1* and *dnd1-1* mutants is suppressed by high light (Mateo et al., 2006). I hypothesize that short-day conditions dampen pathogen defense signaling in *crwn1 crwn2* mutants, leading to suppression of dwarfing. However, later vegetative growth stage (43-day-old plants) showed that *crwn1 crwn2* mutants are still smaller than wild type and *crwn1* single mutants (Fig. 2.1B). This result indicates that the maximum growth capacity in *crwn1 crwn2* mutants in short days is still limited although early growth is suppressed under these conditions. This conclusion is supported by the finding that *sid2 crwn1 crwn2* mutants are intermediate in size between *crwn1 crwn2* mutants and wild type (or *crwn1* single mutants). These observations suggest that SA-dependent pathogen response signaling contributes to photoperiod-dependent dwarfing during early vegetative growth, but that SA-independent mechanisms are also

involved in dwarfing of *crwn1 crwn2* plants, as observed under long-day conditions (see Chapter 2).

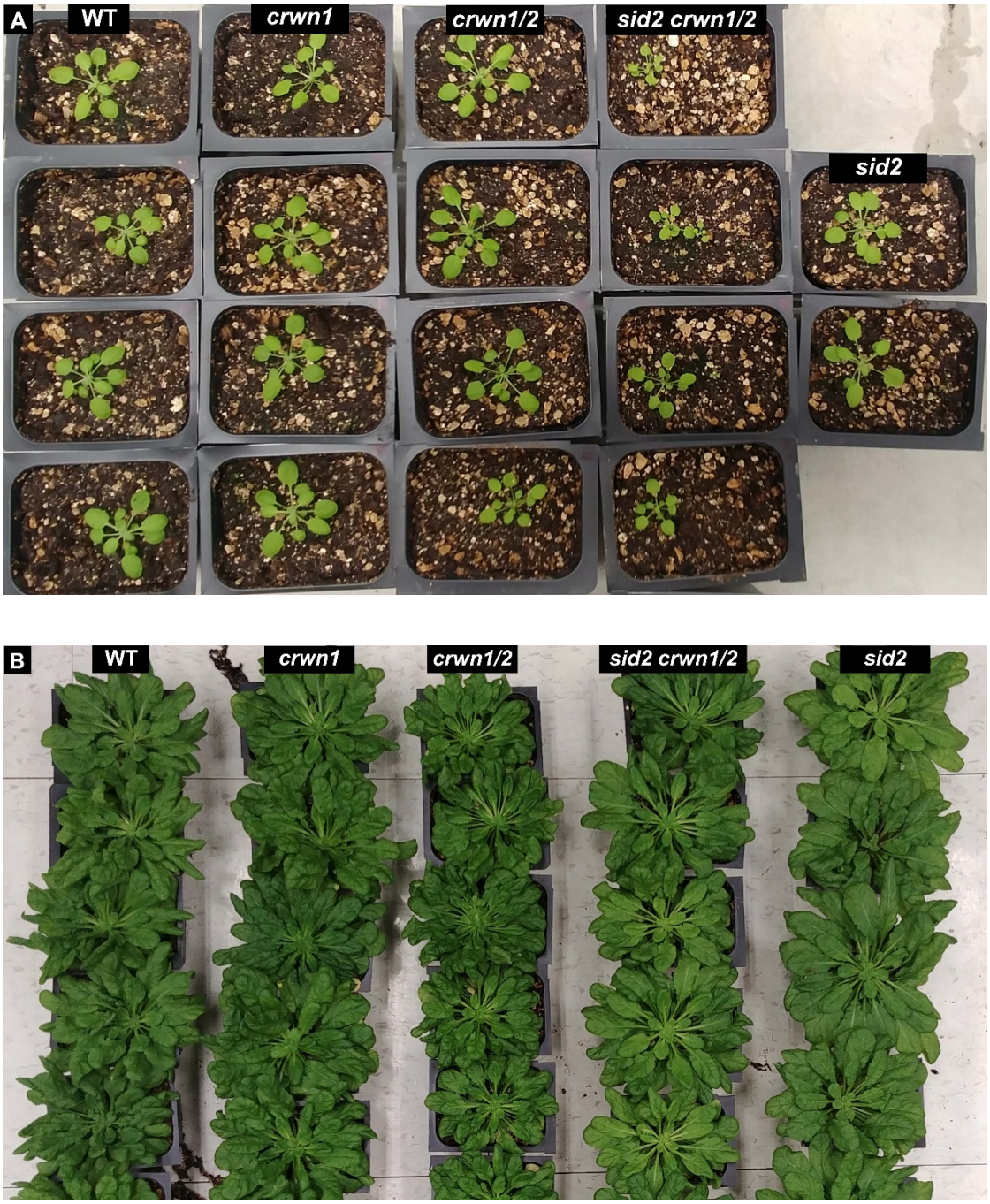

Figure 3.1. Short-day photoperiod suppresses dwarfism in young *crwn1 crwn2* mutants but maximum vegetative growth of rosette leaves is still stunted in older plants; WT, wild-type Col-0. A, 29-day-old plants. Note that *sid2 crwn1 crwn2* mutants had smaller rosettes compared with *crwn1 crwn2* mutants and *sid2* control plants, which might be due to delayed germination or slower initial growth rates. B, 76-day-old plants. Note that *crwn1 crwn2* mutants were smaller at this stage compared to any other plants in the figure.

Short-day growth conditions partially suppress spontaneous cell death in *crwn1 crwn2* mutants but the effects on *PR1* gene expression and *Pst* DC3000 growth are irregular

If short-day photoperiods suppress dwarfism in the initial growth period of *crwn1 crwn2* mutants, what happens to other phenotypes associated with ectopic defense response? Altering the photoperiod can affect cell death which is the key phenotype of LMMs; for example, *lsd1* mutants do not develop lesions under short-day photoperiod (permissive condition) (Dietrich et al., 1994). First, I checked for the presence of lesions in *crwn* mutants. Although the degree of suppression was not complete, short-day photoperiods partially suppressed cell death in 46-day-old *crwn1 crwn2* mutants (Fig. 2.2) compared to long-day grown plants (see Chapter 2). Nonetheless, some lesions were observed in different leaves and individual plants, suggesting

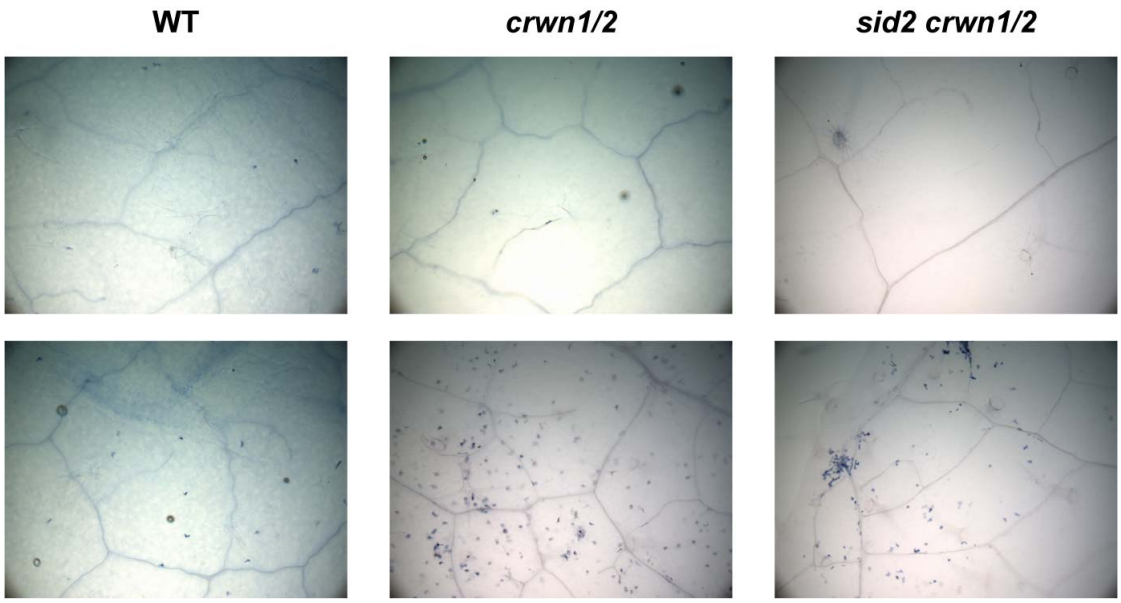

Figure 3.2. Reduced cell death was observed in short-day grown *crwn1 crwn2* mutants; WT, wild-type Col-0. Each picture is taken from different 46-day-old individuals. Note that cell death was suppressed in some individuals but lesions were observed in other plants, suggesting that suppression of cell death by short-day photoperiod is incomplete.

that either short-day photoperiods cannot suppress cell death fully or that lesions can develop in later growth stages in *crwn1 crwn2* mutants, either as a form of senescence or programmed cell death. Interestingly, occasional lesions were also seen in *sid2 crwn1 crwn2* mutants grown in

parallel, arguing that, in these cases, cell death is not dependent on induction of SA production via *SID2*.

Second, I checked, via RT-qPCR, the expression of the *PR1* gene as a marker for an auto-immune response in *crwn1 crwn2* and *crwn1 crwn4* double mutants. In two of the three biological replicates of this experiment, I observed an almost complete abrogation of *PR1* induction (Fig. 2.3A). In the third replicate, *PR1* transcript levels were induced, but the levels (6-to-8-fold) were modest compared to the ca. 100-fold induction observed in *crwn* double mutants under long-day conditions (see Chapter 2). These results suggest that suppression of defense responses occurs in short-day conditions in *crwn* double mutants, but that the suppression is incomplete and variable.

As described in Chapter 2, I previously demonstrated that *crwn* double mutants exhibit an increased resistance against *Pst* DC3000 infection under long-day conditions (Choi et al., 2019). Therefore, I performed a bacterial infection assay using *crwn1 crwn2* mutants and controls grown under short-day conditions. I observed a mixed pattern of resistance in *crwn1 crwn2* mutants (Fig. 2.3B); no differences in bacterial growth were seen 2 days after infection (2dai), but some reduction in bacterial growth was noted in *crwn1 crwn2* mutants 4 days post inoculation. Taken together, these data indicate that it is likely that the short-day photoperiod suppresses cell death and other defense phenotypes, but that this suppression is not complete and might depend on other untested or uncontrolled environmental factors.

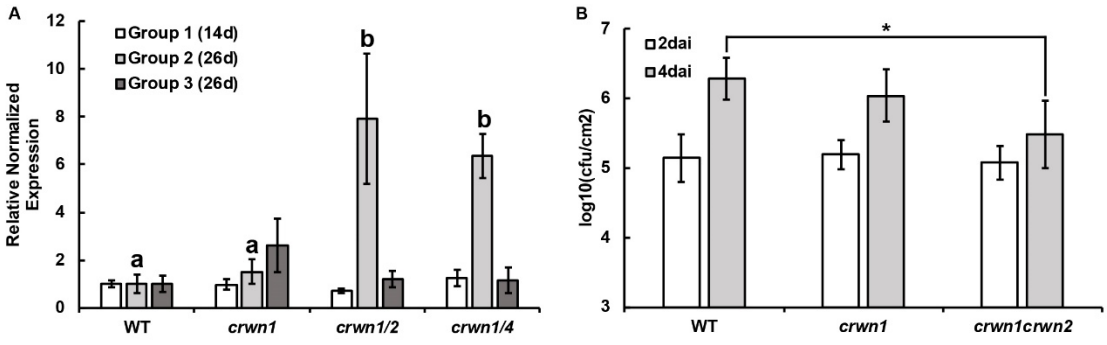

Figure 3.3. Short-day conditions incompletely suppress defense responses in *crwn1 crwn2* mutants. A, two biological samples (group 1 and 3) showed a nearly complete suppression of *PR1* gene induction while group 2 exhibited elevation in transcript levels. One-way ANOVA with post-hoc Tukey HSD test weas performed within each group. There were no significance differences in any comparison in group1 and group3. The three groups were grown in the same condition and the only difference was the age of plants in group1. B, *Pst* DC3000 growth was reduced in *crwn1 crwn2* mutants grown under short-day conditions in the 4dai sample. No differences were seen in the 2dai samples; note that the resistance of *crwn1 crwn2* mutants are apparent 2dai in long-day conditions (see Chapter 2). A Student's *t* test was done between wild type (WT) and mutants in 4dai (*, $P < 0.05$). Error bars indicate SD ($n = 4$).

Short-day growth conditions suppress the accumulation of H_2O_2 observed in *crwn1 crwn2* mutants grown in long-days.

Bursts of ROS can trigger the hypersensitive response (HR) (Zurbriggen et al., 2010). To check if spontaneous lesion formation in *crwn1 crwn2* mutants are associated with ROS, two different types of reactive oxygen compounds, H_2O_2 and the superoxide radical ($O_2^{\bullet-}$), were detected using 3,3'-diaminobenzidine (DAB) and nitro blue tetrazolium (NBT) staining, respectively (Fig. 2.4). Under long-day conditions, *crwn1 crwn2* mutants were stained deeply with the brown color characteristic of the DAB dye, indicating that high H_2O_2 levels were present correlating with the high incidence of cell death in these *crwn* double mutants. In contrast, *sid2 crwn1 crwn2* mutants did not exhibit H_2O_2 accumulation, demonstrating that SA is required for H_2O_2 accumulation. In short-day conditions, the H_2O_2 accumulation observed in long-day grown *crwn1 crwn2* mutants was abolished. This result suggests that long-day conditions are necessary to induce a high level of cell death, which is caused by SA-triggered ROS production.

A very different situation occurs with regards to the second ROS compound monitored. In the long-day photoperiod, $O_2^{\bullet-}$ accumulation was not detected in *crwn1 crwn2* mutants, demonstrating that this reactive oxygen species is not elevated relative to the levels seen in wild-type plants. In contrast, *sid2 crwn1 crwn2* mutants and *sid2* mutants developed higher $O_2^{\bullet-}$ levels, suggesting that the two ROS compounds respond to SA in a different manner. This result is consistent with a previous report showing that *sid2* mutants exhibit high $O_2^{\bullet-}$ levels (Straus et al., 2010). Under short-day conditions, similar levels of NBT staining were observed, indicating that a moderately high level of $O_2^{\bullet-}$ species is present regardless of genotype. These results implicate H_2O_2 as a potential mediator of photoperiod-dependent cell death in *crwn1 crwn2* mutants, while ruling out a significant role for $O_2^{\bullet-}$ species in the programmed cell death process operating in *crwn* double mutants.

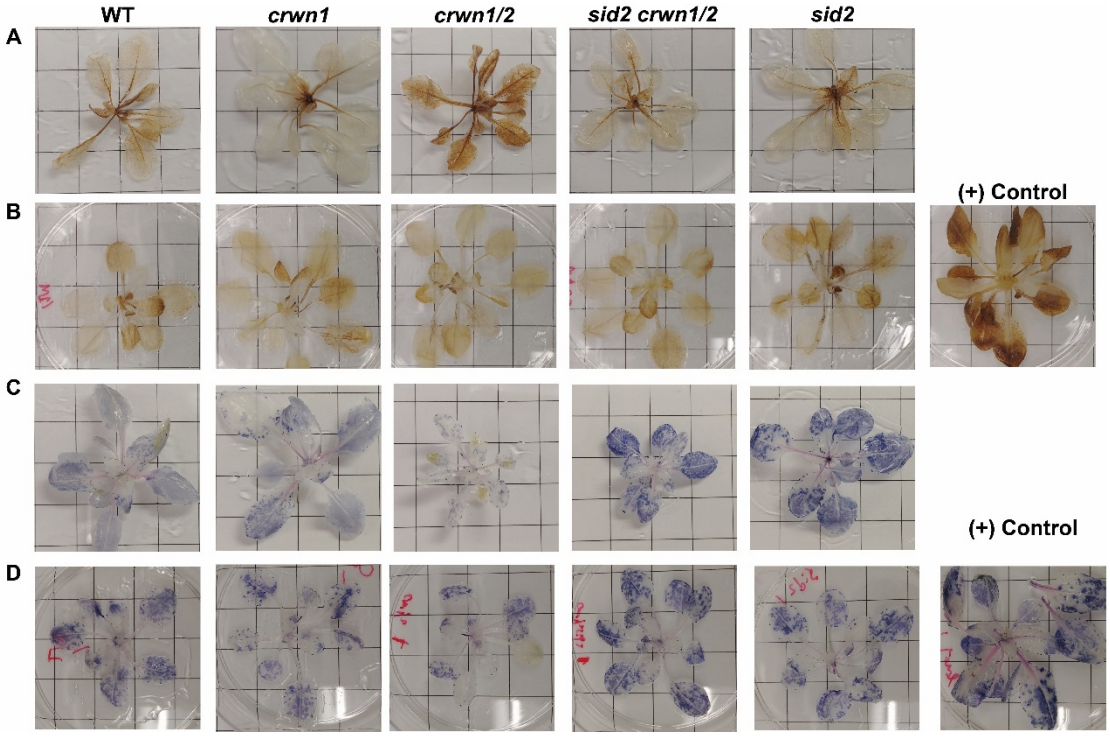

Figure 3.4. *crwn1 crwn2* mutants accumulates excessive hydrogen peroxide in long-day but not short-day conditions (A) while superoxide radical production is wild-type (WT) level (C). The hydrogen peroxide accumulation in long-day grown *crwn1 crwn2* mutants is suppressed in short-day photoperiod (B). A, long-day grown plants were stained with DAB to show H_2O_2 accumulation. B, the same procedure as in A was to short-day grown plants. A long-day-grown *crwn1 crwn2* mutant was used as a positive control. C, long-day grown plants were stained with NBT to check $O_2^{\bullet-}$ production. Note that *sid2* mutations increase $O_2^{\bullet-}$ production, indicating a role of SA in down-regulating this particular ROS compound. D, the same procedure as in C was done to short-day grown plants. A long-day-grown *sid2* mutant was used as a positive control.

DNA damage is not detectable in *crwn* mutants

Nuclear lamina defects in human laminopathies correlate with genomic instability and elevated oxidative stress (Liu et al., 2005; Pekovic et al., 2011; Richards et al., 2011; Sieprath et al., 2012). To test if DNA damage is present in *crwn* mutants, comet assays were performed on isolated nuclei. This assay exploits a characteristic of damaged DNA to make a long smear resembling a flaming tail of comet when isolated nuclei are subjected to an electrophoretic field under denaturing conditions. By contrast, intact DNA within nuclei retains a round shape without much of a tail. A strong tail was seen in the positive controls, comprised of wild-type nuclei treated with H_2O_2, which damages DNA (Fig. 2.5). Untreated wild-type nuclei show an

intermediate configuration, with a brighter focus corresponding to the position of the nucleus and a tail indicative of some DNA damage. Relative to these controls, the *crwn1* and *crwn4* single mutants were similar to wild type, while the *crwn1 crwn2* double mutant had more of the signal concentrated into the nuclear focus. This more compact pattern is also seen in the *sid2 crwn1 crwn2* mutant, indicating that the presence of the *sid2* mutation did not have an effect on halo formation. These results suggest that the DNA packed in the *crwn1 crwn2* nuclei are less damaged. Alternatively, it is possible that the nuclei from *crwn1 crwn2* cells constrain and prohibit tails from forming due to an altered or more compacted nuclear structure.

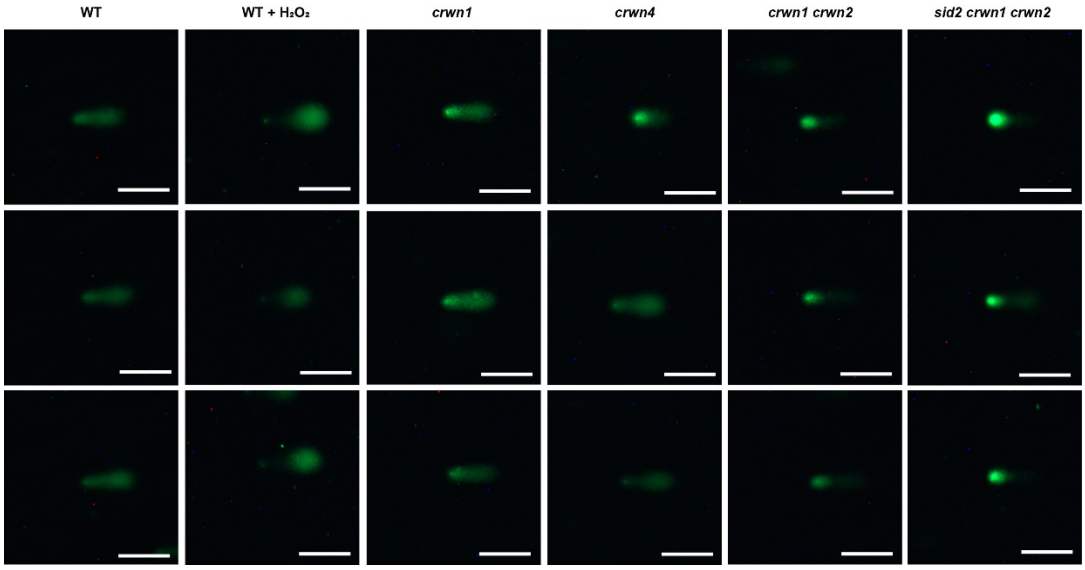

Figure 3.5. The presence of elevated DNA damage in *crwn* mutants is not apparent in comet assays. Alkaline comet assays were performed on *crwn* mutants and SA-deficient *sid2 crwn1 crwn2* mutants. Nuclei extracted from 24-d-old plants were subject to alkaline electrophoresis with 25 V for 40 min. Wild-type (WT) nuclei show narrower tails with bigger comet heads compared with bulged tails and smaller heads from hydrogen peroxide-treated damaged nuclei (positive control). A reduction in tails was observed in *crwn1 crwn2* and *sid2 crwn1 crwn2* mutants. Scale bars represent 100 μm. Images were captured under Leica DM5500 Epifluorescence Microscope with SYBR Gold staining.

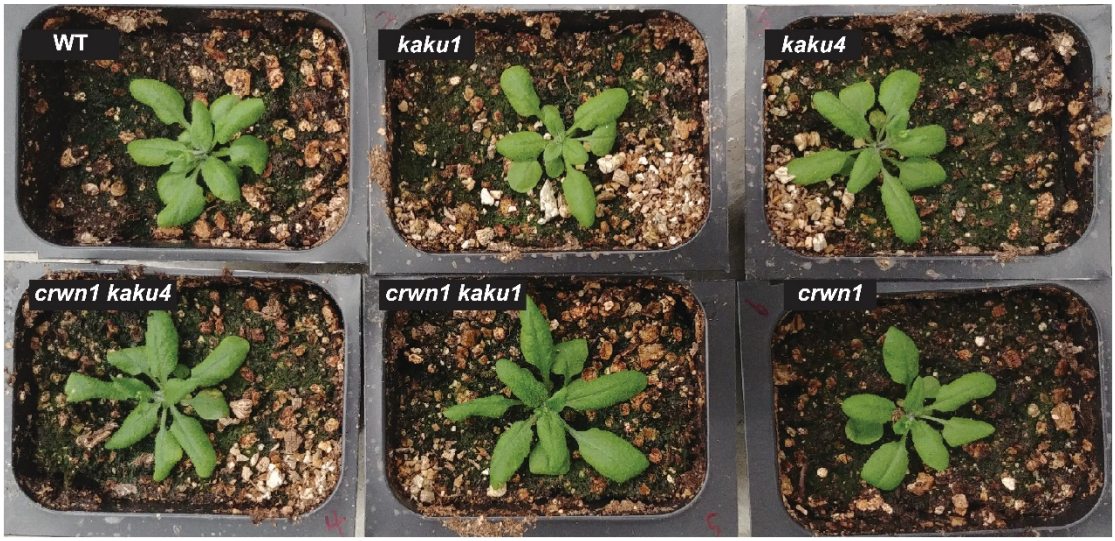

Figure 3.6. *kaku* mutation and combinations between the two *kaku* mutations and a *crwn1* allele do not confer obvious morphological phenotypes. Plants were grown for 24d under long-day conditions.

crwn1 kaku1 and *crwn1 kaku4* do not exhibit defense response

Given my results establishing a connection between nuclear structure and pathogen signaling, I investigated whether or not other nuclear morphology mutants in Arabidopsis have defense-related phenotypes. Specifically, I examined two mutations that affect different structural components of the nucleus. The first mutation tested was *kaku1*, which disrupts a gene encoding a myosin motor that is attached to the nuclear surface and drives nuclear movement (Tamura et al., 2013). The second mutation affects the suspected nuclear lamina protein, KAKU4, that physically interacts with CRWN1 and possibly CRWN4 (Goto et al., 2014). For this analysis, I crossed *kaku1-3* (*myosin xi-i*) and *kaku4-2* mutants to *crwn* mutants, and also studied these *kaku* mutations in the absence of *crwn* mutations. Both of the *kaku* single mutants and the double mutant combinations with *crwn1* grew normally (Fig. 2.6). I then tested for spontaneous cell death lesions by trypan blue staining, and found no evidence for ectopic cell lesions in these genotypes (Fig. 2.7); none of these genotypes should be considered to be a LMM.

To see if *kaku* mutants exhibit altered resistance against bacterial infection, the pathogen, *Pst* DC3000 was infiltrated into leaves of a set of *kaku* mutants (Fig. 2.8), including combinations with multiple *crwn* mutations. The data show that addition of a *kaku4* mutation to a *crwn1 crwn4* mutant background does not change the degree of resistance. Consistently, neither *crwn1 kaku4* mutants nor *crwn1 kaku1* mutants exhibit altered resistance. These findings suggest that neither *kaku1* and *kaku4* has a significant effect on bacterial pathogenesis or pathogen signaling. However, we observed variable defense phenotypes in our *kaku4* mutant line. For example, a high resistance to *Pst* DC3000 infection was observed in our *kaku4* sample, but the presence of *kaku4* did not elevate the partial resistance exhibited by *crwn1 crwn4* mutants (Fig. 2.8). Further, we noted marked variability in the expression of the pathogen response marker gene *PR1* among different biological replicates (Fig. 2.9). These outliers in DC3000 infection and RT-qPCR data suggest that the *kaku4* mutation might affect defense response in an unstable manner.

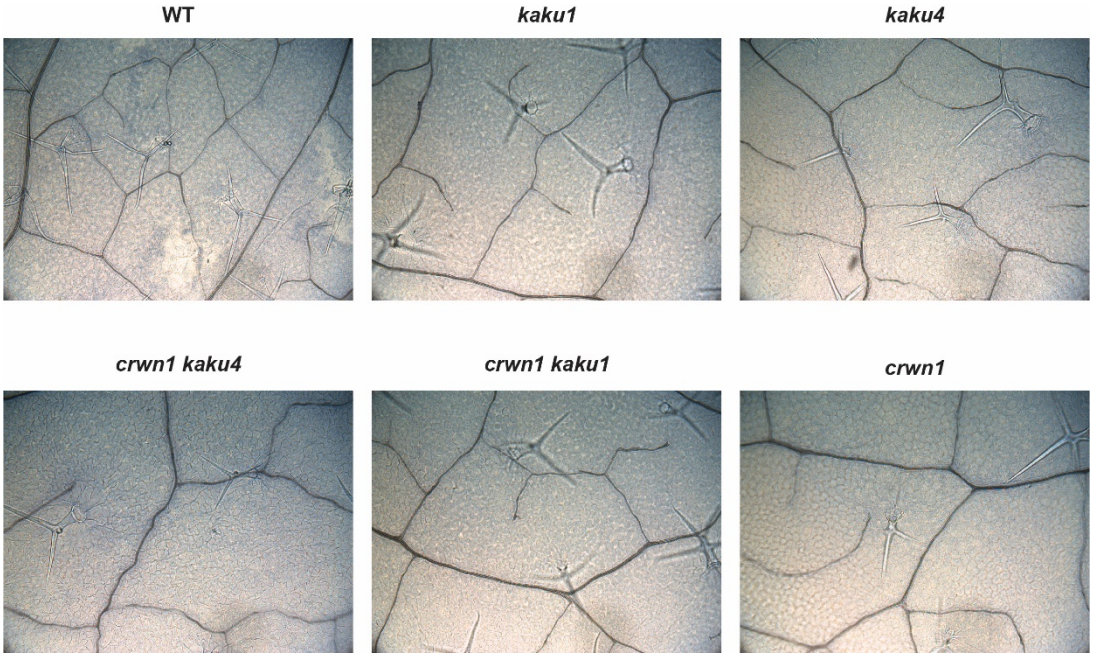

Figure 3.7. *kaku* mutations do not induce cell death. Plants were grown for 24d in long-day photoperiod.

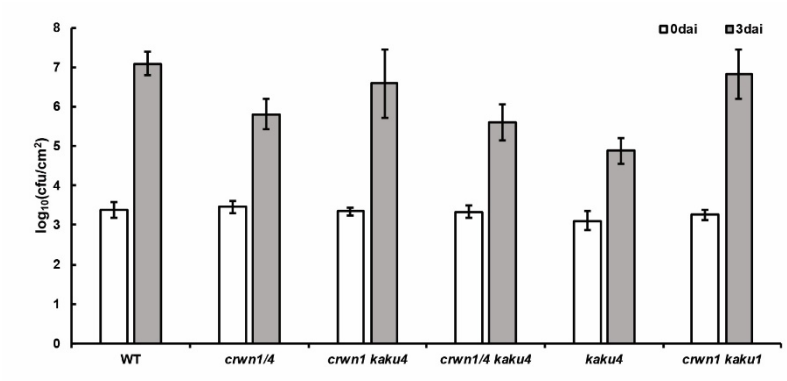

treatments pair	Tukey HSD inferfence
A vs B	** p<0.01
A vs C	insignificant
A vs D	** p<0.01
A vs E	** p<0.01
A vs F	insignificant
B vs C	insignificant
B vs D	insignificant
B vs E	* p<0.05
B vs F	** p<0.01
C vs D	** p<0.01
C vs E	** p<0.01
C vs F	insignificant
D vs E	insignificant
D vs F	** p<0.01
E vs F	** p<0.01

Figure 3.8. *kaku4* and *kaku1* mutations do not affect *Pst* DC3000 resistance in *crwn1 crwn4* and *crwn1* mutants (see *crwn1 kaku4*, crwn1 *crwn4 kaku4* and *crwn1 kaku1*). One-way ANOVA with post-hoc Tukey HSD test was performed among plants 3dai. A, B, C, D, E and F in the table are WT, *crwn1/4*, *crwn1 kaku4*, *crwn1/4 kaku4*, *kaku4* and *crwn1 kaku1* respectively. Error bars indicate SD (n = 4 for 0dai and n = 8 for 3dai).

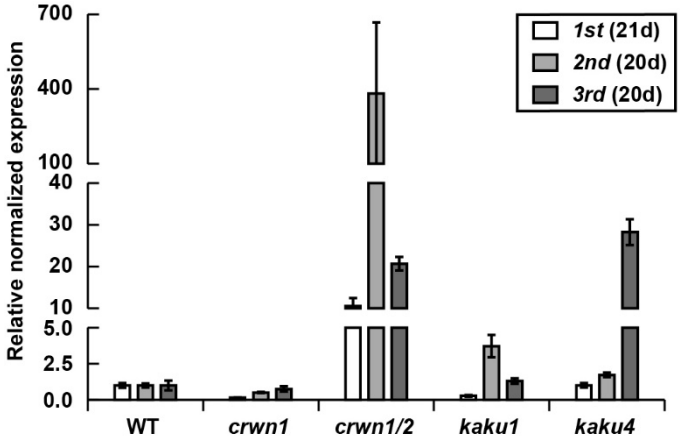

Figure 3.9. *PR1* expression in *crwn* and *kaku* mutants grown in long-day photoperiod was confirmed through RT-qPCR. Each group represents one plant. Note that 3rd group (20d) of *kaku4* mutants exhibited high expression level of the gene. One-way ANOVA with post-hoc Tukey HSD test was performed within each group. A, B, C, D and E in the table are WT, *crwn1*, *crwn1/2*, *kaku1* and *kaku4* respectively.

1st (21d) pair	Tukey HSD Q statistic	Tukey HSD p-value	Tukey HSD inferfence
A vs B	17.4847	0.0010053	** p<0.01
A vs C	9.8283	0.0010053	** p<0.01
A vs D	5.2359	0.0155194	* p<0.05
A vs E	0.1097	0.8999947	insignificant
B vs C	27.313	0.0010053	** p<0.01
B vs D	12.2488	0.0010053	** p<0.01
B vs E	17.5944	0.0010053	** p<0.01
C vs D	15.0642	0.0010053	** p<0.01
C vs E	9.7186	0.0010053	** p<0.01
D vs E	5.3456	0.0133561	* p<0.05

2nd (20d) pair	Tukey HSD Q statistic	Tukey HSD p-value	Tukey HSD inferfence
A vs B	7.4557	0.0025892	** p<0.01
A vs C	65.2863	0.0010053	** p<0.01
A vs D	14.6089	0.0010053	** p<0.01
A vs E	6.0294	0.011217	* p<0.05
B vs C	72.742	0.0010053	** p<0.01
B vs D	22.0647	0.0010053	** p<0.01
B vs E	13.4852	0.0010053	** p<0.01
C vs D	50.6774	0.0010053	** p<0.01
C vs E	59.2569	0.0010053	** p<0.01
D vs E	8.5795	0.0010053	** p<0.01

3rd (20d) pair	Tukey HSD Q statistic	Tukey HSD p-value	Tukey HSD inferfence
A vs B	2.2238	0.5412169	insignificant
A vs C	23.2233	0.0010053	** p<0.01
A vs D	2.3986	0.4779432	insignificant
A vs E	26.4161	0.0010053	** p<0.01
B vs C	25.4472	0.0010053	** p<0.01
B vs D	4.6224	0.0518344	insignificant
B vs E	28.64	0.0010053	** p<0.01
C vs D	20.8247	0.0010053	** p<0.01
C vs E	3.1928	0.2352127	insignificant
D vs E	24.0176	0.0010053	** p<0.01

DISCUSSION

Day-length dependent H_2O_2 generation in *crwn1 crwn2* mutants

In this chapter, I investigated the mechanisms through which CRWN proteins, and perhaps nuclear organization more generally, affect pathogen responses. Unlike animal cells, plants have chloroplasts, which is one of the major sources of ROS along with mitochondria. Although ROS is considered generally harmful, it also serves as a cellular signal. Involvement of chloroplasts in ROS production makes these organelles an important bridge between light and defense response, because ROS bursts are often observed in plant immunity responses.

Excess light energy which surpasses the capacity of light harvesting system is dissipated by reducing oxygen atoms, generating ROS (Song et al., 2006). Thus, mutations which sensitize plants to normally adequate levels of light can lead to perturbation of ROS status. The data shown in Figures 3.1 through 3.4 demonstrate that CRWN proteins are involved in suppressing day-length-dependent H_2O_2 production, which is a likely cause of cell death lesions.

Day-length-dependent LMMs, such as *lsd1* mutants, exhibit cell death in long-day conditions or in high light (Dietrich et al., 1994; Mateo et al., 2004). In contrast, short-day conditions or low light makes permissive conditions in which the mutant does not form lesions (Dietrich et al., 1994; Mateo et al., 2004). In short-day conditions, *crwn1 crwn2* mutants develop reduced cell death coinciding with lower H_2O_2 production, indicating that H_2O_2 production in *crwn1 crwn2* mutants are related to light. Also, the *sid2* mutation suppressed H_2O_2 production of *crwn1 crwn2* mutants in long-day conditions, adding the clue that H_2O_2 production in *crwn1 crwn2* mutants requires SA. However, it is unclear where in the pathway SA acts relative to H_2O_2 generation. This point should be further tested to determine if short-day conditions suppress SA production in *crwn1 crwn2* mutants.

Both Photosystem I and II can produce $O_2^{\bullet-}$(Song et al., 2006; Takagi et al., 2016). However, in *crwn1 crwn2* mutants, there is not enough evidence to establish a correlation

between $O_2^{\bullet-}$ and defense responses. I found that *crwn1 crwn2* mutants in long-day conditions have wild-type levels of $O_2^{\bullet-}$. In contrast, *sid2* and *sid2 crwn1 crwn2* mutants have high levels of $O_2^{\bullet-}$, consistent with previous studies showing that SA can signal dismutasing of $O_2^{\bullet-}$ into H_2O_2, as well as promoting ROS bursts and plant defense in general (Straus et al., 2010). It is noteworthy that SA can also reduce cell death depending on the genetic background, suggesting complex roles for SA in plant immunity (Straus et al., 2010).

One model relevant to my observations is that long-day conditions might generate $O_2^{\bullet-}$, which is maintained at low levels in wild-type plants by basal SA. In this model, increased SA in *crwn1 crwn2* mutants quickly converts $O_2^{\bullet-}$ to H_2O_2, leading to an apparent reduction in $O_2^{\bullet-}$ and increased H_2O_2 as the flux shifts between these two forms of ROS. In short-day conditions, *crwn1 crwn2* mutants develop wild-type levels of $O_2^{\bullet-}$ but not high H_2O_2 compared to long-day grown *crwn1 crwn2* mutants; under this model, less SA and $O_2^{\bullet-}$ generation occur in short-day conditions, leading to less H_2O_2 production.

DNA damage

Multiple lines of the evidence in animals suggests a connection between DNA damage and ROS in situations where the nuclear lamina is damaged, which is plausible because ROS is a well-known cytotoxin generating DNA damage. By extension, if *crwn* mutations induce DNA damage like animal laminopathies, it is conceivable that ectopic defense responses in *crwn* mutants are caused by DNA damage. I included *sid2 crwn1 crwn2* mutants to exclude the effect of SA in mediating DNA damage and ROS bursts when I assessed the effect of *crwn* mutations on DNA damage. I first tested if DNA damage is present in *crwn* mutants by using a single-cell gel electrophoresis procedure known as a comet assay. Contrary to our prediction, I could not detect significant damage in either *crwn1 crwn2* nor *sid2 crwn1 crwn2* mutants. Rather, I found that *crwn1 crwn2* and *sid2 crwn1 crwn2* mutants have less conspicuous tails indicative of DNA

damage. This result demonstrates that genomic instability present in *crwn* mutants might be absent or minimal, and therefore not a likely cause of defense signaling. It is plausible that spontaneous production of SA or genomic instability by loss of CRWNs is tolerated in Arabidopsis plants. Previously, the Richards group showed that *crwn1 crwn2* mutants have few decondensed centromeric 180 bp repeats and denser chromocenter packaging (Wang et al., 2013). Consistent with these findings, (Poulet et al., 2017) showed that chromocenters in *crwn1 crwn2* mutants were more condensed compared to wild type. In animal cells, it was shown that heterochromatin affects both the protection and repair of damaged genomes (Cann and Dellaire, 2011; Takata et al., 2013; Feng et al., 2016). Thus, it is possible that *crwn1 crwn2* mutants could be protected from DNA damage by increased heterochromatin formation (Poulet et al., 2014; Poulet et al., 2017). It is also noteworthy that not every SA accumulation mutant exhibits DNA damage (Rodriguez et al., 2018), indicating that the dose of SA and other factors are involved in inflicting DNA damage.

Other nuclear morphology mutants (*kaku*)

As discussed in Chapter 2, nuclear morphology mutants such as *cpr5* and *nup136* are involved in defense response regulation. Prompted by these observations, I checked to determine if other nuclear morphology mutants – specifically, *kaku1* (*myosin xi-i*) and *kaku4* (another putative nuclear lamina protein mutants) – also have similar immune responses (Tamura et al., 2013; Goto et al., 2014; Haraguchi et al., 2016). I found that neither *kaku1* nor *kaku4* mutants exhibit altered whole-plant phenotypes (Fig. 2.6). Neither did the combination of either *kaku1* or *kaku4* with *crwn1* change the whole-plant growth phenotype. Consistently, there was no cell death in any of these mutants. However, the DC3000 infection test showed that *kaku4* suppressed bacterial growth. Also, one of three biological replicates in RT-qPCR

showed ca. 30-fold transcription of *PR1* in *kaku4* mutants. These results suggest that the *kaku4* mutation affects defense response in an unstable manner with incomplete penetrance.

CONCLUSIONS

In this chapter, I demonstrated how day-length can affect spontaneous defense phenotypes in *crwn1 crwn2* mutants. I found that short-day conditions suppress dwarfism during early growth and, partially, cell death in *crwn1 crwn2* mutants. I further showed that the light condition is correlated with H_2O_2 level, showing that long-day photoperiod is necessary to accumulate H_2O_2 in *crwn1 crwn2* mutants. Collectively, the result suggests that nuclear envelope protein CRWNs are involved in the ROS production pathway, which is dependent on day-length conditions.

Based on the result of Chapter 2 and Chapter 3 that *crwn1 crwn2* mutants accumulate SA and ROS, I also checked to see if *crwn1 crwn2* mutants exhibit DNA damage which can trigger downstream defense responses. Neither *crwn1 crwn2* nor *sid2 crwn1 crwn2* mutants exhibit the genomic breaks, arguing that DNA-damage dependent defense response does not happen in *crwn1 crwn2* mutants regardless of the effect of SA. These results point to the possibility that DNA damage might be suppressed in *crwn1 crwn2* mutants.

MATERIALS AND METHODS

Plant materials

Arabidopsis thaliana were grown on Cornell Mix or MetroMix 360 soil (Sun Gro Horticulture) at 22℃ after 2 d of stratification in a 4℃ cold room. For long-day conditions (16 h of light / 8 h of dark), Conviron growth chamber (Model TC30, BTI Growth chamber #11) at Boyce Thompson Institute green house was used with 60% humidity setting. For short-day conditions (8 h of light / 16 h of dark), Percival growth chamber (Model E41L2, Richards lab) was used without humidity control. *kaku1-3* and *kaku4-2* mutants are from ABRC CS860014 and SALK-076754C, respectively. Other plant material used was described by Wang et al. and Choi et al. (Wang et al., 2013; Choi et al., 2019).

Cell death lesion detection and imaging

Trypan blue staining for detection of cell death was performed as described in Chapter 2 and Choi et al. (2019).

RT-qPCR

RNA Extraction, cDNA synthesis and RT-qPCR were performed as described in Chapter 2 and Choi et al. (2019). *ROC1* was used for housekeeping gene control for RT-qPCR. Primers for *ROC1* are 5'-CGG ATC TCAGTT CTT CAT CTG-3' and 5'-CCT TCT CGA TGG CCT TTA C-3'. Other primers are same as in Chapter 2 and Choi et al. (2019).

Pseudomonas syringae pv. *tomato* DC3000 bacterial growth assays

The assay was performed as described in Chapter 2 and Choi et al. (2019).

Reactive oxygen species detection

Hydrogen peroxide was detected by 3,3'-diaminobenzidine (DAB) (D12384, Aldrich) staining. For 20 mL DAB solution, 10 mg DAB was dissolved in 18 mL of water for a few hours by adjusting pH to 3.0 with 8M HCl. During the procedure, the solution was covered with aluminum foil as DAB is sensitive to light. 10 μL Tween 20 (P9416, Sigma) and 200 μL 0.5M Na_2HPO_4 were added. The solution was filtered through two layers of Miracloth (Calbiochem). Although DAB is not completely soluble even in strong acidic conditions, the filtered solution still has enough DAB in solution to detect H_2O_2. Plant samples were placed in glass vials submerged in the solution. The solution was vacuum-infiltrated for 5 min with piece of cheese cloth added to prevent floating of samples. Samples were left on a shaker in room temperature for 24 h without light. After the incubation, DAB solution was decanted. Vials were filled with bleaching solution (ethanol:acetic acid:glycerol = 3:1:1) and then placed on boiling water bath for 15 min. After the boiling step, the bleaching solution was replaced with a fresh aliquot and further bleached on a shaker in room temperature.

Superoxide anion was detected by nitroblue tetrazolium (NBT) (NBT2.5, Gold Biotechnology) staining. For 100 mL NBT solution, 0.1 g of NBT and 50 μL Tween 20 were dissolved in 100 mL of 50 mM Na_2HPO_4 solution. Vacuum infiltration was conducted for 5 min as described for the DAB staining. Staining took about 2 hr on a shaker in room temperature. Boiling is not necessary for bleaching. Bleaching was done overnight.

Comet assay

DNA damage was assessed using a CometAssay Kit (Trevigen). Alkaline comet assay was performed based on the manufacturer's protocol with slight modifications according to studies of Wang and Liu and Yan et al. (Wang and Liu, 2006; Yan et al., 2013). Throughout the experiment, direct light was avoided. Two to three seedlings were chopped with a razor blade in 1,000 μL of cold 1x PBS (Ca^{2+} and Mg^{2+} free) solutions with 20mM EDTA added. Chopped

samples were filtered with 40 μm nylon mesh. 25 μL of samples were then suspended in 200 μL of molten LMAgarose at 37 ℃. 50 μL of agarose mixtures were then mixed well with a pipette and spread over the Comet Slide area. Slides were placed at 4 ℃ in the dark for 30 min. Slides were then immersed in Lysis Solution at 4 ℃ for 60 min. After removing excess buffer from slides, they were immersed in freshly prepared Alkaline Unwinding Solution, pH>13 (300mM NaOH, 1mM EDTA) at 4 ℃ in the dark for 60 min. Slides were then immersed in Alkaline Electrophoresis Solution, pH > 13 (300 mM NaOH, 1 mM EDTA) and subsequently run in electrophoresis system (Owl Easy Cast B2, Thermo Scientific) at 4 ℃ in the dark for 40 min. Current was kept at approximately 300 mA by adjusting the amount of buffer with the voltage set at 20 to 25 V. After excess buffer was drained, slides were immersed twice in distilled water for 5 min each, then in 70% ethanol for 5 min. Slides were dried at 37 ℃ and stained with 100 μL of 1x SYBR Gold solution. After removing excess SYBR solution, slides were rinsed briefly with distilled water and subject to observation under a confocal microscopy (Leica TCS SP5).

REFERENCES

Cann KL, Dellaire G (2011) Heterochromatin and the DNA damage response: the need to relax. Biochem Cell Biol **89:** 45-60

Carmody M, Waszczak C, Idanheimoa N, Saarinen T, Kangasjarvi J (2016) ROS signalling in a destabilised world: A molecular understanding of climate change. Journal of Plant Physiology **203:** 80-94

Choi J, Strickler SR, Richards EJ (2019) Loss of CRWN Nuclear Proteins Induces Cell Death and Salicylic Acid Defense Signaling. Plant Physiology **179:** 1315-1329

Deal RB, Kandasamy MK, McKinney EC, Meagher RB (2005) The nuclear actin-related protein ARP6 is a pleiotropic developmental regulator required for the maintenance of FLOWERING LOCUS C expression and repression of flowering in Arabidopsis. Plant Cell **17:** 2633-2646

Dietrich RA, Delaney TP, Uknes SJ, Ward ER, Ryals JA, Dangl JL (1994) Arabidopsis mutants simulating disease resistance response. Cell **77:** 565-577

Feng YL, Xiang JF, Kong N, Cai XJ, Xie AY (2016) Buried territories: heterochromatic response to DNA double-strand breaks. Acta Biochim Biophys Sin (Shanghai) **48:** 594-602

Gasser S, Orsulic S, Brown EJ, Raulet DH (2005) The DNA damage pathway regulates innate immune system ligands of the NKG2D receptor. Nature **436:** 1186-1190

Goto C, Tamura K, Fukao Y, Shimada T, Hara-Nishimura I (2014) The Novel Nuclear Envelope Protein KAKU4 Modulates Nuclear Morphology in Arabidopsis. Plant Cell **26:** 2143-2155

Haraguchi T, Tominaga M, Nakano A, Yamamoto K, Ito K (2016) Myosin XI-I is Mechanically and Enzymatically Unique Among Class-XI Myosins in Arabidopsis. Plant Cell Physiol **57:** 1732-1743

Langridge J (1957) Effect of Day-Length and Gibberellic Acid on the Flowering of Arabidopsis. Nature **180:** 36-37

Liu BH, Wang JM, Chan KM, Tjia WM, Deng W, Guan XY, Huang JD, Li KM, Chau PY, Chen DJ, Pei DQ, Pendas AM, Cadinanos J, Lopez-Otin C, Tse HF, Hutchison C, Chen JJ, Cao YH, Cheah KSE, Tryggvason K, Zhou ZJ (2005) Genomic instability in laminopathy-based premature aging. Nature Medicine **11:** 780-785

Mateo A, Funck D, Muhlenbock P, Kular B, Mullineaux PM, Karpinski S (2006) Controlled levels of salicylic acid are required for optimal photosynthesis and redox homeostasis. Journal of Experimental Botany **57:** 1795-1807

Mateo A, Muhlenbock P, Rusterucci C, Chang CC, Miszalski Z, Karpinska B, Parker JE, Mullineaux PM, Karpinski S (2004) LESION SIMULATING DISEASE 1 is required for acclimation to conditions that promote excess excitation energy. Plant Physiol **136:** 2818-2830

Miller G, Suzuki N, Ciftci-Yilmaz S, Mittler R (2010) Reactive oxygen species homeostasis and signalling during drought and salinity stresses. Plant Cell and Environment **33:** 453-467

Pekovic V, Gibbs-Seymour I, Markiewicz E, Alzoghaibi F, Benham AM, Edwards R, Wenhert M, von Zglinicki T, Hutchison CJ (2011) Conserved cysteine residues in the mammalian lamin A tail are essential for cellular responses to ROS generation. Aging Cell **10:** 1067-1079

Poulet A, Arganda-Carreras I, Legland D, Probst AV, Andrey P, Tatout C (2014) NucleusJ: an ImageJ plugin for quantifying 3D images of interphase nuclei. Bioinformatics **31:** 1144-1146

Poulet A, Duc C, Voisin M, Desset S, Tutois S, Vanrobays E, Benoit M, Evans DE, Probst AV, Tatout C (2017) The LINC complex contributes to heterochromatin organisation and transcriptional gene silencing in plants. Journal of Cell Science **130:** 590-601

Richards SA, Muter J, Ritchie P, Lattanzi G, Hutchison CJ (2011) The accumulation of un-repairable DNA damage in laminopathy progeria fibroblasts is caused by ROS generation and is prevented by treatment with N-acetyl cysteine. Human Molecular Genetics **20:** 3997-4004

Rodriguez E, Chevalier J, El Ghoul H, Voldum-Clausen K, Mundy J, Petersen M (2018) DNA damage as a consequence of NLR activation. Plos Genetics **14**

Sieprath T, Darwiche R, De Vos WH (2012) Lamins as mediators of oxidative stress. Biochemical and Biophysical Research Communications **421:** 635-639

Song YG, Liu B, Wang LF, Li MH, Liu Y (2006) Damage to the oxygen-evolving complex by superoxide anion, hydrogen peroxide, and hydroxyl radical in photoinhibition of photosystem II. Photosynthesis Research **90:** 67-78

Straus MR, Rietz S, Ver Loren van Themaat E, Bartsch M, Parker JE (2010) Salicylic acid antagonism of EDS1-driven cell death is important for immune and oxidative stress responses in Arabidopsis. Plant J **62:** 628-640

Takagi D, Takumi S, Hashiguchi M, Sejima T, Miyake C (2016) Superoxide and Singlet Oxygen Produced within the Thylakoid Membranes Both Cause Photosystem I Photoinhibition. Plant Physiology **171:** 1626-1634

Takata H, Hanafusa T, Mori T, Shimura M, Iida Y, Ishikawa K, Yoshikawa K, Yoshikawa Y, Maeshima K (2013) Chromatin Compaction Protects Genomic DNA from Radiation Damage. Plos One **8**

Tamura K, Iwabuchi K, Fukao Y, Kondo M, Okamoto K, Ueda H, Nishimura M, Hara-Nishimura I (2013) Myosin XI-i Links the Nuclear Membrane to the Cytoskeleton to Control Nuclear Movement and Shape in Arabidopsis. Current Biology **23:** 1776-1781

Wang CX, Liu ZC (2006) Arabidopsis ribonucleotide reductases are critical for cell cycle progression, DNA damage repair, and plant development. Plant Cell **18:** 350-365

Wang H, Dittmer TA, Richards EJ (2013) Arabidopsis CROWDED NUCLEI (CRWN) proteins are required for nuclear size control and heterochromatin organization. BMC Plant Biol **13:** 200

Yan SP, Wang W, Marques J, Mohan R, Saleh A, Durrant WE, Song JQ, Dong XN (2013) Salicylic Acid Activates DNA Damage Responses to Potentiate Plant Immunity. Molecular Cell **52:** 602-610

Yoshioka K, Shinozaki K (2009) Signal crosstalk in plant stress responses. Wiley-Blackwell, Ames, Iowa

Zurbriggen MD, Carrillo N, Hajirezaei MR (2010) ROS signaling in the hypersensitive response: when, where and what for? Plant Signal Behav **5:** 393-396

Chapter 4. Characterization of NMCPs in *Solanum lycopersicum* and their roles in plant reproduction

INTRODUCTION

NMCP/CRWN orthologs are present across land plants (Embryophyta) (Ciska and Moreno Diaz de la Espina, 2013; Ciska and de la Espina, 2014), where they partition into two phylogenetically distinct families, NMCP1-like and NMCP2-like, defined by prototypic proteins from carrot. Among the many unresolved questions concerning the biology of NMCP proteins is whether or not these orthologs play similar biological roles in different species. A related question is the extent to which NMCP1-type and NMCP2-type proteins function within a species in distinct versus overlapping roles.

Some insight into the second question came from early cell biological studies in *Apium graveolens* (celery). Using indirect immunofluorescence, Kimura et al. found that NMCP1 and NMCP2 localize differently during mitotic cell division (Kimura et al., 2010). Both AgNMCP1 and AgNMCP2 disassemble from the nuclear periphery at a similar time during prometaphase. AgNMCP1 first concentrates near the spindle at metaphase and then accumulates on segregating chromosomes at anaphase. In contrast, AgNMCP2 scatters across the cytoplasm during metaphase and anaphase. AgNMCP2 subsequently accumulates on segregating chromosomes at telophase, but does so later than NMCP1. These localization studies indicate that the two types of NMCP proteins are regulated, at least partially, in distinct ways. The different dynamics of reassembly at the nuclear rim is interesting in the context of evidence from co-IP studies that NMCP1- and NMCP2-type proteins physically interact, perhaps indirectly, in macromolecular complexes (Goto et al., 2014). Taken together, these findings suggest that NMCP1- and NMCP2-type proteins might be incorporated into different nuclear lamina filament or lattices, but that these structures are nonetheless in physical contact.

The larger question of the conservation or diversity of function of NMCP orthologs across plant taxa requires functional studies, which have been limited to genetic studies in Arabidopsis. These studies have shown that NMCP proteins are required for viability, as well as specification and/or maintenance of nuclear size and shape. In addition, as described in Chapter 2, NMCP proteins are implicated in pathogen defense signaling.

In this chapter, characterization of *Solanum lycopersicum* NMCP1 and NMCP2 mutants is described, providing the first cross-species comparison of the function of these nuclear lamina proteins. The tomato genome encodes two NMCP1-type paralogs, NMCP1A and NMCP1B, and a single NMCP2-like protein, NMCP2. Unlike Arabidopsis *crwn1 crwn2* and *crwn1 crwn4* mutants, consistent SA-related defense phenotypes were not observed in tomato *nmcp1* mutants. However, I discovered unexpectedly male infertility in *NMCP1A/nmcp1a-1; nmcp1b-1/nmcp1b-1* mutants, which produced fragile anther sacs and extremely low levels of mature pollen. Based on the pollen infertility phenotype seen for tomato *nmcp1* mutants, Arabidopsis *crwn* mutants were re-examined for pollen defects. Notably, both *crwn1 crwn2* and *sid2 crwn1 crwn2* mutants produce small siliques with unfertilized and/or aborted seeds, indicating *crwn* mutations inflict reproductive shortage independent of SA effects. Homozygous *nmcp2* single mutants and *nmcp1a nmcp1b* double mutants were not recovered, demonstrating that each class of NMCPs are required for viability in tomato. The differences between the phenotypes of *nmcp* mutants in tomato and Arabidopsis indicate that NMCP proteins, or the nuclear lamina more generally, exert species-specific effects.

RESULTS

Tomato *nmcp1a* and *nmcp1b* single mutants do not exhibit ectopic defense responses

To check if mutations in *NMCP* genes can elicit spontaneous defense responses, I measured transcript levels of *ICS* and *PR1b* genes. Similar to Arabidopsis, *ICS* is an important

gene for SA-biosynthesis and *PR1b* is an SA-dependent gene (Uppalapati et al., 2007). In three *nmcp* mutants tested (carrying either a presumptive null allele of *NMCP1A*, or one of the two predicted null alleles of *NMCP1B*), transcripts of both *ICS* and *PR1b* were not significantly mis-expressed (Fig. 4.1). Next, *Pst* DC3000 was inoculated into tomato leaves by a vacuum infiltration method. While the *nmcp1b-2* mutant showed wild-type levels of DC3000 growth, *nmcp1a-1* and *nmcp1b-1* plants exhibited slight resistance, which was smaller than a unit $\log_{10}$ (cfu/cm^2) (Fig. 4.2). Although the possibility that *nmcp* mutation induced biotic resistance cannot be negated, these data collectively indicate that the degree of the defense response might be low in single *nmcp* mutants. It should be noted that all single *crwn* mutants in Arabidopsis fail to show ectopic defense responses, which are only exhibited by a subset of the possible *crwn* double mutants. Unfortunately, a better comparison using tomato *nmcp1a nmcp1b* double mutants is not possible because deficiency of both *NMCP1A* and *NMCP1B* is lethal in tomato (described below).

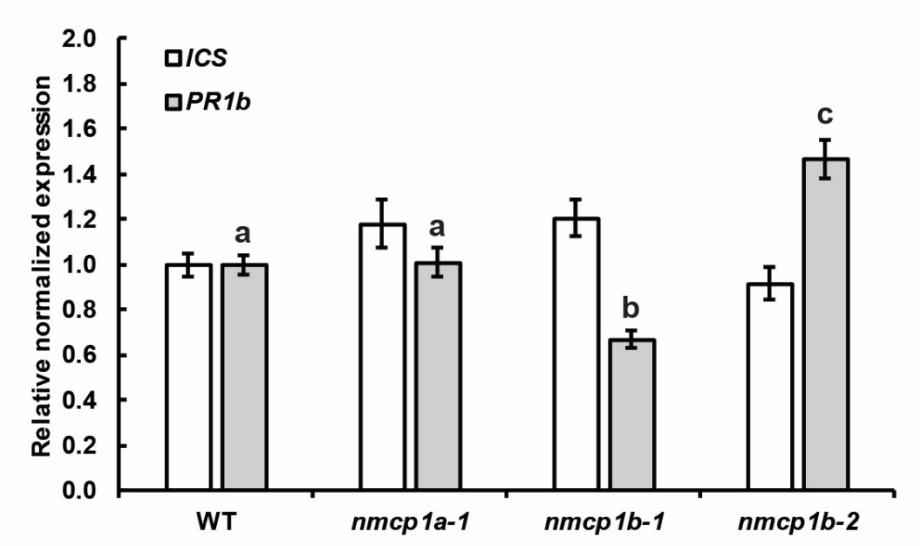

Figure 4.1. *nmcp1a* and *nmcp1b* mutants express wild-type (WT) level *ICS* and *PR1b* genes. One-way ANOVA with post-hoc Tukey HSD test was performed. No comparisons for the *ICS* target are significantly different. Error bars indicate standard error of the mean generated by the Bio-Rad CFX manager software.

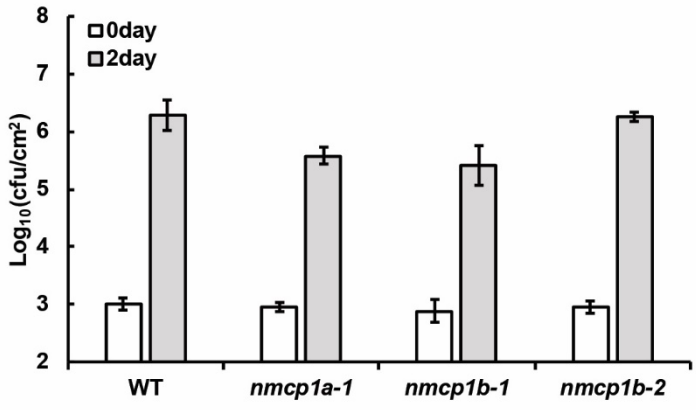

treatments pair	Tukey HSD inferfence
A vs B	* p<0.05
A vs C	** p<0.01
A vs D	insignificant
B vs C	insignificant
B vs D	insignificant
C vs D	* p<0.05

Figure 4.2. *nmcp1a-1* and *nmcp1b-1* mutants exhibit weak resistance to *Pst* DC3000. DC3000 was vacuum infiltrated to second leaf of plants of indicated genotypes. Error bars are *SD* (*n* = 3). One-way ANOVA test with post-hoc Tukey HSD test was performed. A, B, C and D in the table are WT, *nmcp1a-1*, *nmcp1b-1* and *nmcp1b-2*, respectively.

Tomato *NMCP1A/nmcp1a-a; nmcp1b-1/nmcp1b-1* mutants fail to produce pollen

Our lab found that *nmcp1a nmcp1b* double mutants were not recovered in populations segregating both *nmcp1* and *nmcp2* alleles. This result indicates that NMCP1-type proteins are essential in tomato and their function cannot be replaced by NMCP2. Further, *NMCP1A/nmcp1a-1; nmcp1b-1/nmcp1b-1* mutants (specifically, individuals S18-35/12 and S18-35/16 – collectively referred to as S18-35) did not bear fruit, while *nmcp1a-1/nmcp1a-1; NMCP1B/nmcp1b-1* mutants and homozygotes for either *nmcp1a-1* or *nmcp1b-1* were viable and bore fruit containing seed. To investigate the infertility of S18-35, I first checked the phenotypes of the flowers and pollen. Although the overall morphology of S18-35 flowers looks normal, anther sacs from these plants were often less bulged compared to wild type, suggesting a possible failure in anther sac and/or pollen development (Fig. 4.3A and B). These slender anther sacs were fragile and easily fragmented into several pieces (Fig. 4.3C). Notably, S18-35/12 and S18-35/16 contained little pollen compared with the other genotypes shown (Fig. 4.3C). To check viability of pollen in S18-35 mutants, Alexander staining (Alexander, 1969) was applied to the pollen of each mutant. Wild-type flowers produce copious amounts of pollen with a high percentage staining as viable (Fig. 4.4). *nmcp1a-1* mutants and

nmcp1b-1 mutants also exhibit large amount of viable pollen, suggesting that the *nmcp1* paralog mutations singly do not induce male sterility (Fig. 4.4). However, S18-35/12 and S18-35/16 produced little pollen and most of grains produced were stained as inviable (Fig. 4.4). The absence of viable pollen was confirmed by my inability to recover fruits after manual self-pollination. However, outcrossing male wild-type pollen to S18-38 mutants as females yielded fruit with seeds, indicating that infertility of S18-35 stemmed from male sterility.

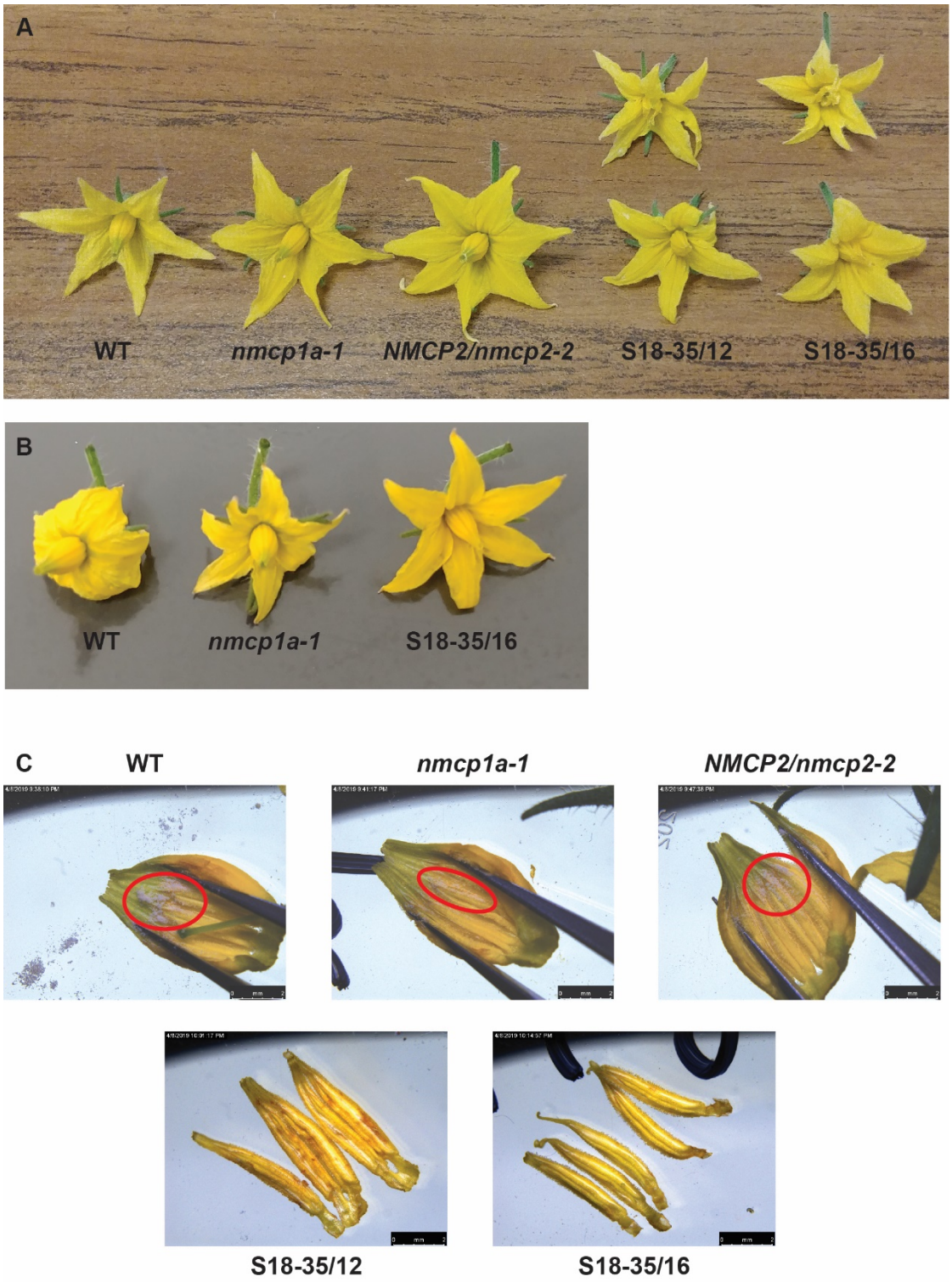

Figure 4.3. S18-35/12 and S18-35/16 mutants (*NMCP1A/nmcp1a-1; nmcp1b-1/nmcp1b-1*) have fragile anthers with little pollen compared to other genotypes. Panels A and B shows the overall morphology of the flowers from different genotypes. Panel C shows anther sacs dissected to expose pollen, which are visible in some genotypes (inside the red circles). Note that anther sacs of S18-35/12 and S18-35/16 could not be pinned down by forceps as they readily shredded. Images in C were taken using a Leica M205 stereomicroscope.

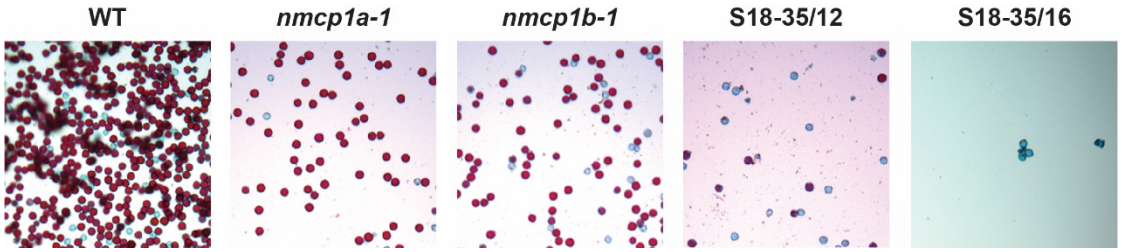

Figure 4.4. A high incidence of pollen inviability in S18-35/12 and S18-35/16. Alexander's staining of pollen collected from different genotypes; WT, wild-type M82. Magenta indicates viable pollen and blue indicates aborted ones. Note that the amount of pollen shown in the figure does not represent the actual amount of pollen production. Images were taken under Leica DM5500B microscope at the same magnification.

Pollen from Arabidopsis *crwn* mutants is viable

In the light of the observed male sterility of tomato *NMCP1A/nmcp1a-1; nmcp1b-1/nmcp1b-1* mutants, I investigated seed production in Arabidopsis *crwn* mutants. Because *crwn1 crwn2* mutants are smaller in size than wild-type plants, which is at least partially due to high level of SA, I included *sid2 crwn1 crwn2* mutants in my analysis to control for the effect of excess SA. I first checked pollen viability by Alexander staining (Fig. 4.5) and found that pollen in anther sacs of an array of Arabidopsis *crwn* mutants were stained as magenta, indicating a high proportion of viable pollen. This result is consistent with the fact that tested mutants can all bear siliques with viable seeds.

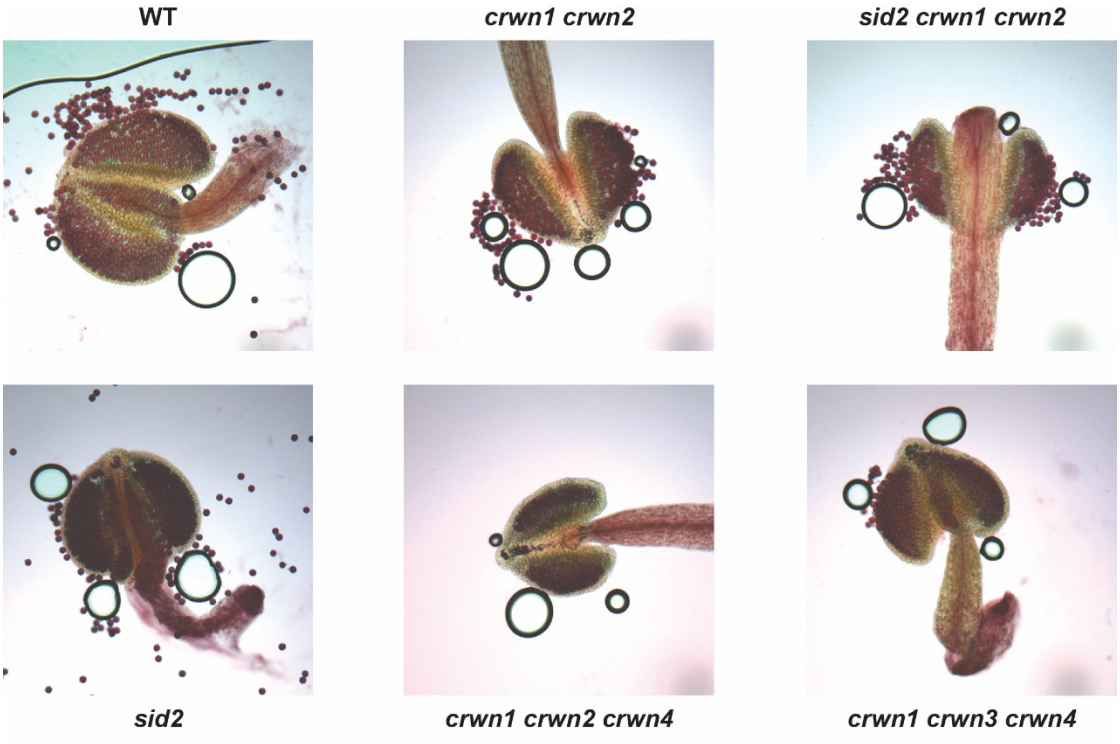

Figure 4.5. Pollen from Arabidopsis *crwn* mutants is viable regardless of SA accumulation. Anther sacs of different genotypes of Arabidopsis were stained with Alexander's staining solution. Images were taken using a Leica DM5500B microscope.

Reduced seed yield in Arabidopsis *crwn1 crwn2* mutants

Previously, I found that an excess level of SA is responsible for rosette dwarfism in *crwn1 crwn2* mutants (see Chapters 2 and 3). However, shorter bolt height, smaller silique length, and shriveled seeds observed in *crwn1 crwn2* mutants are also seen in *sid2 crwn1 crwn2* mutants (Fig. 4.6A and B). The result demonstrates that these phenotypes are the result of the *crwn* mutations and are not caused by elevated SA. I further checked to see if smaller siliques were correlated with reduced seed production. I found that the total number of ovules (sum of unfertilized ovules, aborted seeds and viable seeds) are similar between wild type and *crwn1 crwn2* mutants (Fig. 4.6C). However, the number of viable seeds are significantly reduced in *crwn1 crwn2* mutants and *sid2 crwn1 crwn2* mutants, compared to wild type (Fig. 4.6D). Similar to silique size, the *sid2* mutation did not alter the number of viable seeds in *crwn1 crwn2*

mutants. Collectively, these results indicate that *crwn1 crwn2* mutants have stunted reproductive capability, which is independent from the effect of elevated SA.

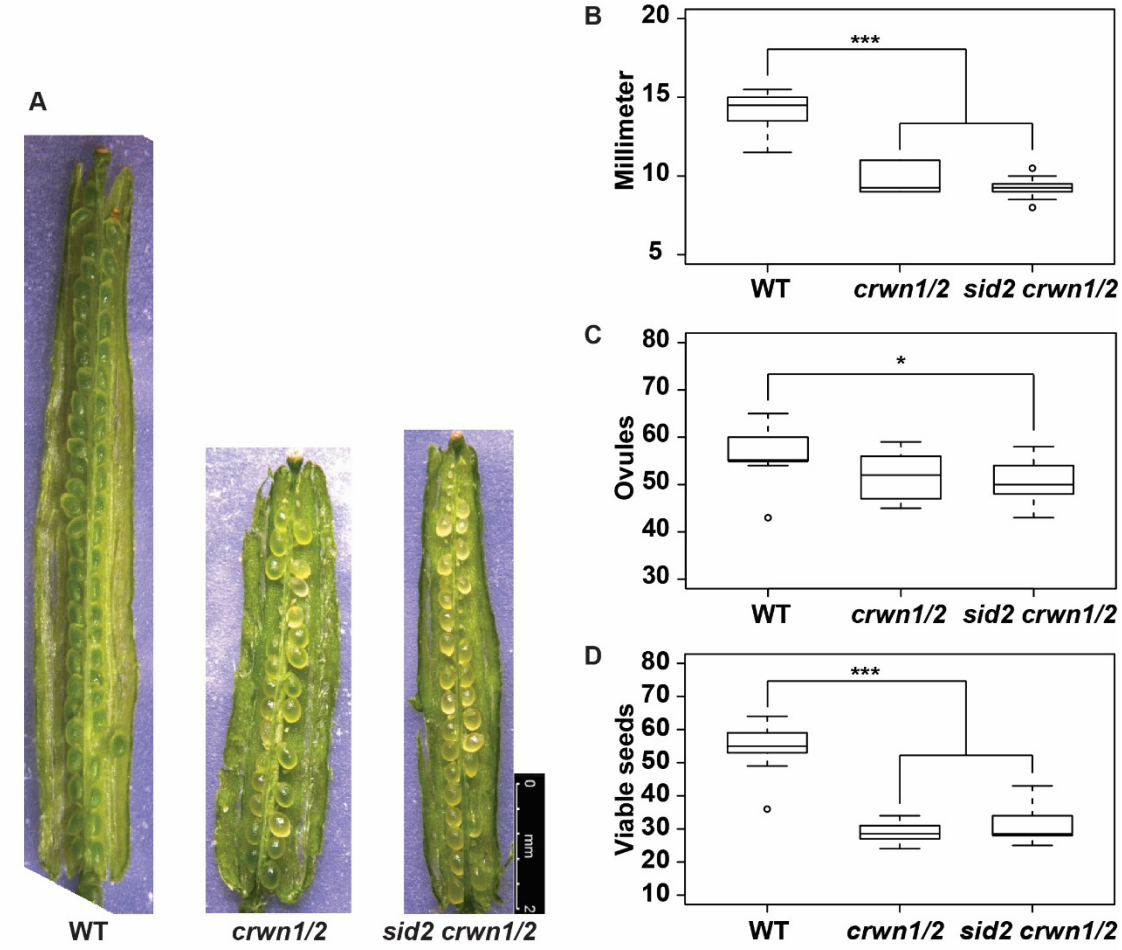

Figure 4.6. Arabidopsis *crwn1 crwn2* mutants produce short siliques with fewer viable seeds compared to wild type (WT). These phenotypes are not suppressed by *sid2* mutations. A, siliques from indicated genotypes. Images were taken using a Leica M205 stereomicroscope. B, sizes of siliques in indicated genotypes in millimeter. C, the number of ovules in the indicated genotypes. D, the number of viable seeds in the indicated genotypes. $n = 10$ for B, C and D. Student's *t* tests were performed for B, C and D (*, $P < 0.05$ and ***, $P < 0.001$). Note that there is no significant difference between *crwn1 crwn2* mutants and *sid2 crwn1 crwn2* mutants in B, C and D.

DISCUSSION

To determine if the functions of NMCP proteins are conserved in different plant species, I studied tomato *nmcp* mutants. Initially, I checked to see if these tomato mutants exhibit ectopic defense phenotypes similar to those exhibited by Arabidopsis *crwn1 crwn2* and *crwn1 crwn4* mutants. Although there was no significant difference in transcript level of several SA responsive genes between tomato wild type and *nmcp* single mutants, weak *Pst* DC3000 resistance was observed in *nmcp1a-1* and *nmcp1b-1* but not *nmcp1b-2* mutants. It should be further verified if this mild effect is reproducible. Given that *crwn* single mutants in Arabidopsis did not show defense responses, the possibility that tomato mutants with more compromised NMCP function needs to be considered. However, attempts to isolate *nmcp1a nmcp1b* mutants were unsuccessful, indicating that the desired *nmcp1* double mutant is inviable. Thus, lethality of *nmcp* double mutants precludes making a proper comparison to the situation in Arabidopsis where gradients in NMCP function can be more easily established using viable *crwn* double and triple mutants. One approach worth pursuing is to study double mutants that are homozygous for hypomorphic (leaky) alleles. Another option is to see if the null *nmcp1* alleles are haploinsufficient (see below) as *NMCP1A/nmcp1a-1; nmcp1b-1/nmcp1b-1* and *nmcp1a-1/nmcp1a-1; NMCP1B/nmcp1b-1* mutants are viable. Alternative approaches to elucidate molecular mechanisms, including determining protein-protein interactions and effects on transcriptional circuits, might be required in tomato to overcome this lack of a clear phenotype in defense response.

I found that *NMCP1A/nmcp1a-1; nmcp1b-1/nmcp1b-1* mutants (S18-35/12 and S18-35/16) showed pollen defects. Based on previous studies about the involvement of the nuclear envelope and lamins in meiosis in mice (Ding et al., 2007; Link et al., 2013; Zeng et al., 2018), I checked tomato *nmcp* for pollen viability. The result showed that mature pollen in tomato *NMCP1A/nmcp1a-1; nmcp1b-1/nmcp1b-1* mutants are largely aborted but neither *nmcp1a* nor

nmcp1b homozygotes show pollen defects. One theory to explain the inviability of pollen in *NMCP1A/nmcp1a-1; nmcp1b-1/nmcp1b-1* mutants is haploinsufficiency of *NMCP* genes. Based on the expression level of *NMCP* genes retrieved from the TomExpress, a public RNA expression resource (Zouine et al., 2017), *NMCP1B* is more highly expressed compared to the other two paralogs in meristems, leaves and flowers (Fig. 4.7). We reasoned that the loss of a single wild-type *NMCP1B* might results in a significant reduction of *NMCP1* transcript. *NMCP1A/nmcp1a-1; nmcp1b-1/nmcp1b-1* mutants are therefore predicted might have less *NMCP1* products for pollen viability compared to either *nmcp1b-1/nmcp1b-1* or *nmcp1a/nmcp1a* single mutants, or the male fertile *nmcp1a-1/nmcp1a-1; NMCP1B/nmcp1b-1* mutant.

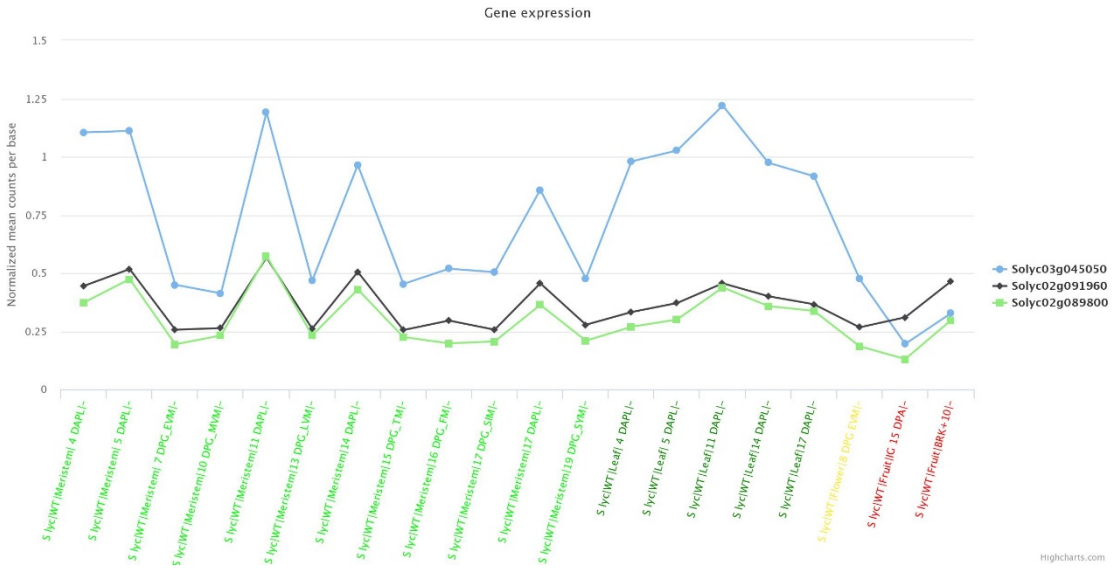

Figure 4.7. *Solanum lycopersicum NMCP1B* (Solyc03g045050, skyblue) is expressed highly in wild-type M82. The graph was generated by TomExpress database. *NMCP1A*, Solyc02g089800, light green; *NMCP2*, Solyc02g091960, black.

How does a reduction in NMCP1 function causes pollen lethality? In Arabidopsis *crwn* mutants, pollen is not aborted. However, I found that *crwn1 crwn2* mutants have fewer viable seeds compared to wild-type siliques but the number of ovule is not significantly affected. These findings suggest that there is a defect in fertilization. In 2014, Zhou and Meier showed that the Arabidopsis nuclear envelope proteins WITs and WIPs are required for the mobility of vegetative nuclei and efficient delivery of sperm cell nuclei to ovules (Zhou and Meier, 2014). In wild-type pollen, a vegetative nucleus moves along the length of the pollen tube, leading the two sperm cell nuclei. These three nuclei maintain in close proximity to the elongating tip of the pollen tube. In *wit1 wit2* mutants, however, the two sperm nuclei enter the tube first and then the vegetative nucleus follows them. In addition, the timing of all three nuclei entering the pollen tube is so delayed that the nuclei are far apart from the growing tip of the pollen tube (Zhou and Meier, 2014). Thus, there is a possibility that *crwn* mutations affect fertilizations by altering movement of sperm cell nuclei and/or the coordination of movement among the three nuclei.

MATERIALS AND METHODS

Plant materials

Solanum lycopersicum mutants used in this chapter were generated from M82 by CRISPR/Cas9. For the detailed loci information and methods to generate mutants, see the dissertation of E. Blunt (2018). Seeds were first sowed on wet filter paper and then transferred to Cornell osmocote soil after germination.

RNA extraction, cDNA synthesis and RT-qPCR

RNA was extracted from leaflets of the 2nd or 3rd compound leaf of the tomato mutants or wild-type control (cultivar M82). The remainder of procedure is same as described in Chapter

2 (Choi et al., 2019). For qPCR, *ARD2* (Sl01g104170) was used as a housekeeping gene and normalization control. Primers used for qPCR are as follows: *ARD2*, 5'-TTC AAG GTG CAG CAG TGG AA-3' and 5'-CCG CTC AGC CAT GGT CAT AA-3'; *ICS* (Sl06g071030), 5'-CTC CCT CGC TGC TTC TTC TC-3' and 5'-TGA ACC GAC ACC AGC TAC AC-3'; *PR1b* (Sl09g007010), 5'-CTT GCG GTT CAC AAC GAT GC-3' and 5'-ATC ACC CGC TCT TGA GTT GG-3'.

Pseudomona syringae pv. *tomato* DC3000 infection

DC3000 was grown as previously described (Choi et al., 2019). The concentration of the bacteria in inoculum was approximately 10^4 cfu mL^{-1}. The plants were infected approximately one month after sowing. The entire aerial part of the plants was infiltrated with the inoculum by vacuum infiltration with intensity of 25 kPa. Inoculated leaves were harvested at 0-day-after inoculation and 2-day-after inoculation. The remainder of the procedure was same as previously described (Choi et al., 2019).

Alexander staining

Alexander staining was performed as described by Alexander (Alexander, 1969). The final concentration of glacial acetic acid was 4 %. Flowers were fixed in 10 % ethanol overnight before staining.

REFERENCES

Alexander MP (1969) Differential Staining of Aborted and Nonaborted Pollen. Stain Technology **44:** 117-+

Choi J, Strickler SR, Richards EJ (2019) Loss of CRWN Nuclear Proteins Induces Cell Death and Salicylic Acid Defense Signaling. Plant Physiology **179:** 1315-1329

Ciska M, de la Espina SMD (2014) The intriguing plant nuclear lamina. Frontiers in Plant Science **5**

Ciska M, Moreno Diaz de la Espina S (2013) NMCP/LINC proteins: putative lamin analogs in plants? Plant Signal Behav **8:** e26669

Ding X, Xu R, Yu JH, Xu T, Zhuang Y, Han M (2007) SUN1 is required for telomere attachment to nuclear envelope and gametogenesis in mice. Developmental Cell **12:** 863-872

Goto C, Tamura K, Fukao Y, Shimada T, Hara-Nishimura I (2014) The Novel Nuclear Envelope Protein KAKU4 Modulates Nuclear Morphology in Arabidopsis. Plant Cell **26:** 2143-2155

Kimura Y, Kuroda C, Masuda K (2010) Differential nuclear envelope assembly at the end of mitosis in suspension-cultured Apium graveolens cells. Chromosoma **119:** 195-204

Link J, Jahn D, Schmitt J, Gob E, Baar J, Ortega S, Benavente R, Alsheimer M (2013) The Meiotic Nuclear Lamina Regulates Chromosome Dynamics and Promotes Efficient Homologous Recombination in the Mouse. Plos Genetics **9**

Uppalapati SR, Ishiga Y, Wangdi T, Kunkel BN, Anand A, Mysore KS, Bender CL (2007) The phytotoxin coronatine contributes to pathogen fitness and is required for suppression of salicylic acid accumulation in tomato inoculated with Pseudomonas syringae pv. tomato DC3000. Molecular Plant-Microbe Interactions **20:** 955-965

Zeng XH, Li KQ, Yuan R, Gao HF, Luo JL, Liu F, Wu YH, Wu G, Yan XH (2018) Nuclear Envelope-Associated Chromosome Dynamics during Meiotic Prophase I. Frontiers in Cell and Developmental Biology **5**

Zhou X, Meier I (2014) Efficient plant male fertility depends on vegetative nuclear movement mediated by two families of plant outer nuclear membrane proteins. Proceedings of the National Academy of Sciences of the United States of America **111:** 11900-11905

Zouine M, Maza E, Djari A, Lauvernier M, Frasse P, Smouni A, Pirrello J, Bouzayen M (2017) TomExpress, a unified tomato RNA-Seq platform for visualization of expression data, clustering and correlation networks. Plant Journal **92:** 727-735

Chapter 5. Plant lamina as a platform for dynamic regulation

Work published during the last 5 years in the field demonstrates that the plant nuclear lamina has various roles in plant physiology and signaling, in addition to its expected role in structural support and morphological maintenance of nuclei. Although each of these recent studies is not exclusive from each other, the topics they address can be divided into three areas. First and foremost, the plant lamina regulates defense responses. My work showed that a loss of Arabidopsis nuclear lamina proteins induces SA-triggered defense responses (Choi et al., 2019). Guo et al. also showed that CRWN1 interacts with NTL9 to suppress *PR1* expression (Guo et al., 2017). Both studies revealed that *crwn1 crwn2* mutants exhibit enhanced resistance against bacterial pathogen *Pseudomonas syringae*. However, there remains the important question of how mechanistically CRWNs regulate defense responses. While the Richards group has demonstrated that *crwn* mutations lead to SA accumulation, how nuclear lamina defects lead to SA production is not fully understood. In contrast, Guo et al. invoke a specific gene expression mechanism, based on the physical interaction between CRWN1 and NTL9. Regardless of the strength of the conclusion that CRWN1's activity as a co-repressor explains *PR1* gene induction in *crwn* mutants, it does not explain the wholesale SA signaling that occurs. In addition, the Guo et al. study is contrary to my results in that they argue that SA response is not observed in *crwn* mutants. These considerations suggest that it will be important in the future to determine if NTL9 plays a more extensive role in inducing SA responses. NTL9 is a positive regulator of *SID2* (Zheng et al., 2015) and *ntl9 crwn1 crwn2* mutants down-regulate *SID2* compared to *crwn1 crwn2* mutants (Guo et al., 2017). Thus, it is possible that NTL9 acts as a hyper-activator of *SID2* in the absence of CRWN1, but that needs to be reconciled with the negative role for NTL9 on *PR1* when interaction between NTL9 and CRWNs is absent. In the future, it would be interesting to determine if SA induction is altered in *ntl9 crwn1 crwn2* mutants compared to *crwn1 crwn2* mutants. It is also necessary to check if NTL9 binding targets

on which NTL9 acts as a positive regulator are up-regulated in *crwn1 crwn2* mutants. These experiments would help clarify the role of the reported NTL9-CRWN1 interaction in SA signaling.

The second topic is epigenetic regulation by the plant nuclear lamina. Recent studies in epigenetic regulation involving CRWNs indicate that CRWN1 interacts with both chromatin and the PRC2 complex (Hu et al., 2019; Mikulski et al., 2019). We also showed that combining *crwn1* and *crwn2* mutations leads to down-regulation of H3K27me3 on the *PR1* locus (Choi et al., 2019). To crosscheck these data arguing that loss of CRWN leads to a reduction in H3K27me3 leading to gene de-repression, H3K27me levels across the genome of *crwn1* mutants and other higher *crwn* mutants need to be quantified using ChIP-seq. In addition, the PLAD map from Hu et al., H3K27me3 maps from both WT and *crwn* mutants, and gene expression data from *crwn* mutants needs to be crosschecked. It is also necessary to perform RNA-seq in *sid2 crwn1 crwn2* mutants to determine the transcriptomic effects caused by combining *crwn1* and *crwn2* mutants in the absence of SA. The RNA-seq data of *sid2 crwn1 crwn2* would also help to determine if transcriptomic alterations in *sid2 crwn1 crwn2* mutants are tied to changes in H3K27me3 levels, when cross-referenced with H3K27me3 ChIP-seq data.

Finally, the nuclear envelope and nuclear lamina appear to be involved in the male reproduction in plants. Zhou and Meier showed that nuclear envelope proteins, and the organelle movement that they drive, are necessary for efficient delivery of male gametophyte nuclei to ovules (Zhou and Meier, 2014). In Chapter 4, I showed that both *crwn1 crwn2* and *sid2 crwn1 crwn2* mutants in Arabidopsis produce a reduced number of viable seeds. Moreover, *NMCP1A/nmcp1a-1; nmcp1b-1/nmcp1b-1* mutants in tomato do not produce viable pollen. It is unclear if Arabidopsis *crwn* mutants and tomato *nmcp* mutants also have problems in pollen nuclei movement as in Zhou and Meier's study. Thus one obvious future direction is to check pollen nuclei movement of *nmcp/crwn* mutants. Tagging vegetative nuclei and sperm cell nuclei to track the movement of the nuclei in mutant background is required. Pollen competition assay

between WT and *nmcp/crwn* mutants can also test viability of pollen. Furthermore, it would be of interest to check if meiosis in *nmcp/crwn* mutants are affected, which might be an additional cause of pollen abortion.

Possible coordination between the nuclear lamina and NPCs

Clues regarding spontaneous immunity in *crwn1 crwn2* mutants also come from results concerning other components of nuclear envelope. The *cpr5* mutant is a well-known LMM that has been studied for decades. Only recently, however, it was it shown that CPR5 is a nucleoporin and that its loss changes nuclear shape (Gu et al., 2016). Other work on nuclear pore complexes also determined that some NUPs can regulate both plant immune responses and nuclear shape (Tamura et al., 2010; Tamura et al., 2017). Moreover, cytoskeletal integrity can affect nuclear shape and nuclear transport in animal studies, as shown by Larrieu et al. (Larrieu et al., 2014; Larrieu et al., 2018). These results bring me to the possibility that *crwn/nmcp* mutations affect NPC functions and/or nuclear transport. One way to validate how *crwn/nmcp* mutations would physically alter distribution of nuclear pore complexes is to observe NPC distribution in different genetic backgrounds. This localization might be achieved by electron microscopy after isolating nuclei, or be assessed by following the distribution of fluorescently tagged nucleoporins in transgenic lines. Quantifying transcriptional and translational levels of NPCs would also provide information for monitoring how NPCs are affected in *crwn* mutants. Tracking tagged nuclear transport cargoes in *crwn/nmcp* mutants is another important step to take to examine the possibility that these mutations alter stress-gated nuclear transport of gene regulatory factors (Gu et al., 2016).

Roles of CRWN2 and CRWN3 paralogs

In almost all genetic studies published to date, the redundancy of CRWN paralogs left open questions regarding how the four CRWNs interact with each other and share their functions.

Most reports concerning molecular mechanisms - involving ChIP, protein-protein interaction and protein degradation - focused on one of the four CRWNs. Nonetheless, clear phenotypes are mostly demonstrated in double and triple mutants, suggesting that CRWN proteins work together. For example, anticipated phenotypes from the loss of CRWN1 are reduced H3K7me3 marks and increased transcription of *PR1* due to interactions between CRWN1 and PWO1 or NTL9, respectively. However, these two phenotypes are shown in *crwn1 crwn2* mutants but in *crwn1* mutants. Thus, it is necessary to define the roles of CRWN2 and CRWN3 proteins and determine how they co-operate with CRWN1 or CRWN4. Possible things to check include testing interactions between CRWN2/CRWN3 and known interactors of CRWN1/CRWN4, or the possible interaction between CRWN2/CRWN3 and CRWN1/CRWN4. Genomic and epigenomic analysis of CRWN2 and CRWN3 mutants would be another avenue to pursue, especially concerning H3K27me3 landscapes. It is noteworthy that several groups study CRWN3 focusing on the ABA pathway and seed germination (Zhao et al., 2016; Wang et al., 2019). Again, strong phenotypes, for example hypersensitivity to ABA, were found in *crwn1 crwn3* mutants, but not in *crwn3* single mutants. These observations that CRWNs are involved in both SA and ABA response pathway argue that the plant nuclear lamina regulates stress pathway in general. Thus, it is necessary to dissect how these two stress pathways are related by analyzing transcriptomic and molecular data. For example, *crwn1 crwn3* mutant transcriptomic data can be compared to *crwn1 crwn2* and *crwn1 crwn4* mutants, which will help determine the effect of *crwn2*, *crwn3* and *crwn4* mutations when each of them is introduced into a *crwn1* mutant background.

In a similar manner, it is necessary to think holistically about seemingly discrete phenotypes, which could be linked to each other. For example, CRWN1 is known to be involved in SA responses (from our *crwn1 crwn2* mutant data), PLAD interaction (CRWN1 protein), PWO1 interaction (CRWN1 protein) and ABA pathway (in *crwn1 crwn3* mutants). However,

it is still in question how PLADs released in *crwn1 crwn2* mutants contribute to SA responses or chromocenter organization. Are these two read-outs two largely independent phenomena? Or is one of them preceded by the other? Is gene expression in *crwn1 crwn2* mutants mostly from SA? Or does the loss of *CRWN1* primarily trigger down-regulation of H3K27me to express some key genes in defense responses? Thus, the goal is to understand CRWNs in a holistic manner, as evidence from various mutant phenotypes and mechanistic studies accumulate.

REFERENCES

Choi J, Strickler SR, Richards EJ (2019) Loss of CRWN Nuclear Proteins Induces Cell Death and Salicylic Acid Defense Signaling. Plant Physiology **179:** 1315-1329

Gu YN, Zebell SG, Liang ZZ, Wang S, Kang BH, Dong XN (2016) Nuclear Pore Permeabilization Is a Convergent Signaling Event in Effector-Triggered Immunity. Cell **166:** 1526-+

Guo TT, Mao XG, Zhang H, Zhang Y, Fu MD, Sun ZF, Kuai P, Lou YG, Fang YD (2017) Lamin-like Proteins Negatively Regulate Plant Immunity through NAC WITH TRANSMEMBRANE MOTIF1-LIKE9 and NONEXPRESSOR OF PR GENES1 in Arabidopsis thaliana. Molecular Plant **10:** 1334-1348

Hu B, Wang N, Bi X, Karaaslan ES, Weber AL, Zhu W, Berendzen KW, Liu C (2019) Plant lamin-like proteins mediate chromatin tethering at the nuclear periphery. Genome Biol **20:** 87

Larrieu D, Britton S, Demir M, Rodriguez R, Jackson SP (2014) Chemical inhibition of NAT10 corrects defects of laminopathic cells. Science **344:** 527-532

Larrieu D, Vire E, Robson S, Breusegem SY, Kouzarides T, Jackson SP (2018) Inhibition of the acetyltransferase NAT10 normalizes progeric and aging cells by rebalancing the Transportin-1 nuclear import pathway. Sci Signal **11**

Mikulski P, Hohenstatt ML, Farrona S, Smaczniak C, Stahl Y, Kalyanikrishna K, Kaufmann K, Angenent GC, Schubert D (2019) The chromatin-associated protein PWO1 interacts with plant nuclear lamin-like components to regulate nuclear size. Plant Cell

Tamura K, Fukao Y, Hatsugai N, Katagiri F, Hara-Nishimura I (2017) Nup82 functions redundantly with Nup136 in a salicylic acid-dependent defense response of Arabidopsis thaliana. Nucleus **8:** 301-311

Tamura K, Fukao Y, Iwamoto M, Haraguchi T, Hara-Nishimura I (2010) Identification and Characterization of Nuclear Pore Complex Components in Arabidopsis thaliana. Plant Cell **22:** 4084-4097

Wang QQ, Liu S, Lu C, La YM, Dai J, Ma HY, Zhou SX, Tan F, Wang XY, Wu YF, Kong WW, La HG (2019) Roles of CRWN-family proteins in protecting genomic DNA against oxidative damage. Journal of Plant Physiology **233:** 20-30

Zhao WM, Guan CM, Feng J, Liang Y, Zhan N, Zuo JR, Ren B (2016) The Arabidopsis CROWDED NUCLEI genes regulate seed germination by modulating degradation of ABI5 protein. Journal of Integrative Plant Biology **58:** 669-678

Zheng XY, Zhou M, Yoo H, Pruneda-Paz JL, Spivey NW, Kay SA, Dong XNA (2015) Spatial and temporal regulation of biosynthesis of the plant immune signal salicylic acid. Proceedings of the National Academy of Sciences of the United States of America **112:** 9166-9173

Zhou X, Meier I (2014) Efficient plant male fertility depends on vegetative nuclear movement mediated by two families of plant outer nuclear membrane proteins. Proceedings of the National Academy of Sciences of the United States of America **111:** 11900-11905